The Control of Flexible Structure Vibrations Using A Cantilevered Adaptive Truss

by

Robert H. Wynn, Jr.

Dissertation submitted to the Faculty of the

Virginia Polytechnic Institute and State University

in partial fulfillment of the requirements for the degree of

Doctor of Philosophy

in

Mechanical Engineering

APPROVED:

Harry H. Robertshaw, Chairman

Robert G. Leonard

Charles F. Reinholtz

Alfred L. Wicks

Douglas K. Lindner

September, 1990
Blacksburg, Virginia

The Control of Flexible Structure Vibrations Using A Cantilevered Adaptive Truss

by

Robert H. Wynn, Jr.

Committee Chairman: Harry H. Robertshaw

Mechanical Engineering

Abstract

This study presents analytical and experimental procedures and design tools for the control of flexible structure vibrations using a cantilevered adaptive truss. A specific six-actuator, octahedral-octahedral truss effects the control of different flexible structures. These structures could represent space structures or robotic manipulators or a variety of other flexible structures where unwanted structural vibration could reduce the performance of the system. Three of these structures; a slender beam, a single curved beam, and two curved beams are controlled both in simulation and with an experimental test article. The test article, comprised of the flexible structure, the adaptive truss, and the actuators shows excellent agreement between simulated and experimental responses to initial conditions in both open-loop and (LQR) closed-loop control. As a example of the ability of the truss to control the slender beam, a first mode simulated frequency of 3.11Hz (3.09Hz experimental) and damping ratio of 0.0044 (0.0044) are controlled to produce a 3.20Hz (3.14Hz) frequency and a damping ratio of 0.2876 (0.2746). This 6000% increase in damping without a significant change in the modal frequency shows the potential of the adaptive truss in vibration control. The agreement between simulated and experimental data shows the validity of the modeling and experimental procedures. From the information gained, conclusions are drawn about the uses of an adaptive truss in the control of flexible structure vibrations.

Acknowledgements

I would like to thank those who have helped me in this endeavor, first my advisor, Dr. Harry Robertshaw, without whom this project would not have been and without whom I probably would have gone to another school. His advice in and out of school has been greatly appreciated. Also thanks to my other committee members, Dr. R. G. Leonard, Dr. A. L. Wicks, Dr. C. F. Reinholtz and Dr. D. K. Lindner for their support.

Thanks go to NASA Langley Research Center , Spacecraft Structures Branch for their financial support, under grant NAG-1-933 and Dr. C. G. Horner of NASA for his support.

Thanks to everybody in the office, Will, Buddy, Bob, Paul, Ken and others for their assistance.

Thanks go to my parents for their love and support in this undertaking.

Most of all thanks go to my wife, Carol, forever and ever Amen.

Contents

List of Figures

List of Tables

Nomenclature

Symbol	Definition	Unit
$b_1,\ b_2,\ b_3$	body-fixed unit vectors	
B_m	motor input matrix	N/V
C_m	motor damping matrix	$N/(m/sec^2)$
g	gravitational constant	m/sec^2
G_g	gearhead gain	rad_{in}/rad_{out}
G_{ls}	lead screw gain	m/rad
E	Young's Modulus	P_a
I	area moment of inertia	m^4
I_a	motor armature current	A
I_{in}	inertia as seen from the gearhead	Kg/m^2
I_{ls}	lead screw inertia	Kg/m^2
I_m	motor inertia	Kg/m^2
I_{out}	inertia as seen by the gearhead	Kg/m^2
I_θ	inertia seen by the motor	Kg/m^2
$J_x,\ J_y,\ J_z$	mass moments of inertia about x, y, z axis	Kg/m^2
K	general stiffness matrix	N/m
K_b	motor back emf coefficient	$V/rad-sec$
K_t	motor torque constant	$N-m/A$
l	active batten length	m
L_a	motor armature inductance	Henry, H
M	general mass matrix	Kg
M_m	motor mass matrix	Kg
$n_1,\ n_2,\ n_3$	unit vectors in the Newtonian coordinate frame.	
P_r	primitive coordinates ($x,\ y,\ z,\ \alpha,\ \beta,\ \gamma$)	
r	position vector	m
R_a	motor armature resistance	Ohms, Ω
$R_x,\ R_y,\ R_z$	position vectors in x, y, z directions	

Symbol	Definition	Unit
T_l	kinematic transformation	$m/m,\ rad/m$
T_m	motor torque	$N-m$
V_m	motor input voltage	V
$w(s,t)$	time and position dependent modal amplitudes	m
$w_x\ w_y\ w_z$	modal amplitudes in x, y, z directions	m
q	modal coefficients	
$\dot{}$	first time derivative	
$\ddot{}$	second time derivative	
T	transpose of a matrix or a vector	

Greek Letters

$\alpha\ \beta\ \gamma$	Euler rotation angles	rad
δ	translations and rotations of nodal points	$m,\ rad$
θ_m	motor angular position	rad
θ_l	lead screw angular position	m
θ_{in}	angular position, input to the gearhead	rad
θ_{out}	angular position, output of of the gearhead	rad
ϕ	modal matrix	
ϕ_i	mode shape weighting coefficients	
ϵ	linear density	kg/m
ε	strain	m/m

Chapter 1

Introduction

One of the continuing challenges the scientists in the space program have had is the great cost of sending an object into space. With the recent thrust towards larger space vehicles, a major undertaking has been the use of lighter weight materials to reduce the cost. These lighter materials, which are for the most part inherently lightly damped, have opened a new field with particular new problems that must be addressed. One of the problems that these space structures have is in vibration damping. These flexible, lightly damped structures will need to be "damped" either actively or passively.

Vibration damping can play an important role in the success of space missions. For example, the Hubble space telescope is currently not performing up to expectations, due in part, to a vibration caused by thermal cycling (Aviation Week, 1990). As the telescope orbits it experiences a 50°F temperature gradient that produces a 25 cm tip deflection in the 12.1 m solar panels. This motion keeps the telescope from being accurately positioned for approximately 6 min until the vibration naturally decays. If some type of active or passive vibration control system were used, the time required to reduce the motion could be shortened.

Another problem that is foreseen by NASA engineers is maintaining accuracy for future missions such as an orbiting interferometer telescope (Laskin, 1989). The interferometer works by precisely positioning small aperture telescopes, that are separated by a large distance, thereby synthesizing a larger effective aperture. In order for the telescope to work, the distances must be maintained to within a small fraction of the wavelength of light being observed (Fanson, 1989). Thus, vibrations in the telescope may render it useless.

The number of vibration control problems for space applications is copious. The author believes there is a natural break in the type of problems that fall into the category of vibration control: "large motion" and "small motion". The orbiting interferometer falls into the "small" category. This category pertains to structures where precision is of primary importance and any unwanted motion will be catastrophic, or at least will cause mission success to be greatly affected. The Hubble vibration problem is in the "large" category. These motions, although unwanted, do not completely disable the experiment in progress.

This work concentrates on the control of "large" motions of flexible structures. In this presentation, the motions are generated by initial conditions and controlled with an adaptive truss. We define an adaptive truss as a structure comprised of extensible links. When extended, the links cause the truss to change its shape (or configuration) thus applying a force or motion to an attached flexible structure. When the force or motion is applied correctly, the unwanted vibration can be reduced.

The goal of this dissertation is to present an analytical and experimental procedure

for the control of flexible structures using a cantilevered adaptive truss. Included in the procedure are two modeling approaches for flexible structures, a modeling procedure for the adaptive truss, and a modeling procedure for the actuators. Chapter 3 presents this formulation, along with simulation and experimental considerations. Chapter 4 discusses some issues that apply to the experimental setup at VPI&SU. Beginning in Chapter 5, a specific six-actuator, octahedral-octahedral adaptive truss is modeled. This truss is used in Chapters 6 and 7 to control specific flexible structures. Chapter 6 discusses a slender beam where both a variational model and a finite-element are compared for consistency. The variational model is used to produce simulated results for comparison to experimental data. Chapter 7 presents analyses of a curved beam, two curved beams, and four curved beams. Each of these cases is modeled with the finite-element approach. The simulated results of the one-beam and two-beam cases are compared to experimental data. The model for the four-beam case is presented. From the information gained by controlling these cases conclusions are drawn about the uses of the adaptive truss in the control of flexible structure vibrations in Chapter 8. Before the formulation is presented, a review of the current and pertinent literature will be presented.

Chapter 2

Literature Review

This discussion presents some of the issues concerned with adaptive structures and their ability to control flexible structure vibrations. Adaptive structures are defined by Wada (1989) as *a structural system whose geometric and inherent structural characteristics can be beneficially changed to meet mission requirements either through remote commands and/or automatically in response to external stimulations.* In this presentation an adaptive truss, whose geometric orientation can be changed by moving active links, is used to control structural vibrations in a series of increasingly complex flexible structures. These structural vibrations are generated by initial condition disturbances.

In the literature there seems to be a natural break in the type of vibration control problems that are discussed. The problems seem to fall in one of two categories, "small motion" control and "large motion" control. Small motion systems are generally those systems that require precise positioning and any unwanted vibration will greatly reduce system capabilities. Most of the literature seems to be in this area. Large motion systems, the ones considered here, are generally not concerned with high accuracy precision, but instead deal with slewing/pointing or "gross" vibration

of the structure, and any unwanted vibration that does not limit system performance. For each type of motion there is a variety of different type of actuators that can be used to control vibration.

Different types of actuators address the different types of control issues. Some of these actuators include piezoelectric, proof mass, reaction wheel, reaction jets motor/lead screw and ball screw combinations. The actuator that seems to receive the most attention is the piezoelectric, and most applications are in the "small motion" category. One person that has worked with piezoelectric actuators is Fanson (1989).

Fanson has investigated using piezoelectric active-members to control the flexible motion of a precision truss. His work is directed towards the orbiting interferometer telescope (Laskin 1989) in which very precise tolerances, a few nanometers, are to be maintained in a large flexible structure, tens of meters wide. The system was *designed to exhibit many of the salient features of truss structures that will form key components of next generation spacecraft.* Specifically the truss is comprised of piezoelectric active-members in a stiff and statically indeterminate truss structure. The active-members are integral parts of the structure with maximum motion of the actuator limited to 106 microns at a force of 97 lb. In Fanson's paper, single-input single-output (SISO) control laws were designed using Bode and root locus analysis. Four control designs were implemented; three non-collocated actuator/sensor pairs and one collocated actuator/sensor pair. The experimental results were consistent with the root locus analysis. Fanson along with Preumont (1990), and Lu (1990) present methods for optimal placement of the actuators in structures.

Other types of actuators have been used for "small motion" control. Hallauer (1989) presented work that deals with air-jet thrusters and reaction-mass actuators. His work uses these two actuators to increase the effective bandwidth of the controller. The air-jets are only good for low frequencies, due to mechanical time delays. The reaction mass is good for high frequencies but has no effect on lower frequencies. Velocity feedback was used with the collocated sensors and actuators. Good control was achieved. Only experimental data was provided.

Others have worked with reaction type actuators. These actuators move a mass, either linear or rotary which induce a force or moment on the structure. The reaction type actuators are good for high frequencies, but the added mass is expensive to put in orbit. Other types of actuators are good for "large motion" vibration control; included are DC motors used either for directly slewing the structure, or for driving a rotary/linear actuator.

Slewing experiments have been presented by Juang (1986). A mathematical model of the slewed structure is developed by deriving the kinetic and potential energies of the structure and applying the generalized Hamiltonian principle. The actuator dynamics are modeled and combined with the structure dynamics to produce the entire system equations. A reduced-order model with three bending modes was used in the evaluation of the optimal control law. Two different test models were used for experimental validation, a steel beam and a scale-model of a solar panel. Satisfactory agreement was achieved between experimental measurements and theoretical predictions. The continuous time control was implemented on an analog computer. Slewing the base of the beam about a rotary axis is one approach; it is also desirable

to slew in more than one direction, that is where an adaptive truss comes in.

Much work has been done at VPI&SU in the area of adaptive trusses. Reinholtz (1990) states, *Adaptive trusses offer the greatest stiffness and strength for a given weight of any articulated structure or mechanism.* An adaptive truss is a statically determinate structure comprised of appropriate joints and extensible links that can cause the truss to change its orientation and therefore interact actively with any other structures attached to it. Potential uses for adaptive trusses are as actuators to perform a variety of tasks that require (possibly) high-degrees of freedom. Some of these tasks are: spatial pointing, positioning, reflecting, docking, and, in long chains, robotic tasks. Additionally, active trusses can be utilized to effect the desired dynamics during these tasks.

One of the first uses of an adaptive truss to control a beam continuum is presented by Lovejoy (1987). Lovejoy derives the equations of motion for the planar adaptive truss and attached beam. His approach was to model the planar actuator using a lumped mass approach where a expression for the kinetic energy is first written and the Lagrangian formed. Next the potential and kinetic energies for the beam are developed using a three-mode Ritz approximation. Lagrange's equation is applied to form a set of governing equations. The truss and beam equations are combined by equating forces, and the overall set of system equations is produced. A Linear Quadratic Regulator (LQR) optimal control law is implemented in a simulation. Good control was achieved. Other work has been done with this planar adaptive truss configuration.

Clark (1988, 1989, 1990) performed a parametric study of the planar vibration control of a cantilevered truss beam in which he showed that an adaptive truss actuator has significant advantages over inertia-type actuators (proof masses and reaction wheels), including lower weight. Additionally, adaptive trusses have the potential of simultaneously performing other tasks. The adaptive truss in Clark's work was in a cantilevered configuration; we study this configuration for the adaptive truss, but in a spatial form.

Adaptive trusses can be formed with a variety of basic unit cells that increase in complexity from the tetrahedron with six struts and four vertices to the dodecahedran with eighteen struts and eight vertices, Reinholtz (1990). More complex unit cells are possible, but these have not yet found practical application.

The octahedral configuration with twelve struts and six vertices in the unit cell is the adaptive truss utilized for this work. The truss is a two-bay, so-called, octahedral-octahedral structure, with six active members. There are actually two unit cells in each bay. The unit cells share some vertices and struts forming a short chain-like structure. These trusses can have variable aspect ratio's depending on the relative lengths of the fixed battens and longerons. The variable-length battens can approximately double their length using internal lead screw designs.

The experimental system studied is at VPI&SU on loan from NASA Langley Research Center, and described by Rhodes (1985). He studied the octahedral configuration for its deployment capabilities – the truss can be folded almost flat. Changing the lengths of the active battens causes the truss to change its orientation, thus af-

fecting any attached flexible structures. The active battens consist of a motor, gearhead, and lead screw combination. Much work has been done with this particular spatial adaptive truss.

Kung (1988) first presented work with the spatial adaptive truss used to control an attached beam. The equations of motion for the flexible beam were presented and a first attempt to control the system was performed. The work was continued by Robertshaw (1989). Warrington (1990) presented similar results for a different truss configuration. A study to determine the optimum number of actuators in a six degree-of-freedom active truss was presented by Wynn (1990).

The goal of this work is to develop a process for modeling and controlling a cantilevered adaptive truss that has an attached flexible structure. What follows presents the methods for modeling the three structures utilized, the method for modeling the adaptive truss, and the control approach for the vibration reduction task. These are then applied to the three experiments and the results discussed.

Chapter 3

A General Analysis

This study presents a general formulation of the control of flexible structure vibration using a cantilevered adaptive truss. In this chapter general procedures are derived for developing equations of motion for a flexible structure, for the kinematics of an adaptive truss, and for the actuators that drive the truss. Some control issues are discussed that pertain to the control of flexible structure vibrations. First, flexible structure modeling is discussed.

3.1 Flexible Structure Modeling

Two procedures are followed to model the flexible structures attached to the adaptive truss: the variational approach and the finite-element approach. The variational approach, using the open-loop modal description for the Ritz discretizations, is the preferred method because of the resulting lower-order approximations and their attractive parametric form. However, the method can become cumbersome with even a small amount of structural complexity. The finite element method works well for many structures and also can be posed in a modal sense. For each of these approaches, discussed below, it is assumed that the truss supplies a kinematic (motion) input to the structure. This is equivalent to the, so-called, stiff-actuator assumption.

3.1.1 Variational Method

This variational approach for a spatial flexible beam attached to the adaptive truss at VPI&SU has been presented by Kung (1988) and expanded by Robertshaw (1989) and Warrington (1990). Each of these authors present the same general formulation that is to follow.

In the variational approach the equations of motion are derived from Lagrange's equation using the potential and kinetic energies of the continuum. The first step is to locate a differential mass of the beam in the Newtonian coordinate frame. Then, differential expressions for the potential and kinetic energies of the beam are written and integrated spatially to form the total energies. These energies are functions of beam physical parameters, the motion of the base of the beam attached to the truss (geometric terms), and the (deflection) coefficients of the Ritz discretization of the beam displacement field (modal terms).

Figure 3.1 shows a schematic of an adaptive truss with a slender beam attached and coordinates defined. A vector $\bar{\mathbf{r}}$, Eq. (3.1), is needed to describe the location of the continuum, or a differential mass in it, in the Newtonian coordinate system. R_x, R_y, and R_z describe the global position of the base of the structure, this is the point where the active truss attaches. α, β, and γ are the Euler rotation angles that describe the orientation of the base of the structure. The physical geometry of the structure is described through the uses of x, y, and z. Modal deflections are included in w_x, w_y, and w_z. In the development the n coordinates are Newtonian,

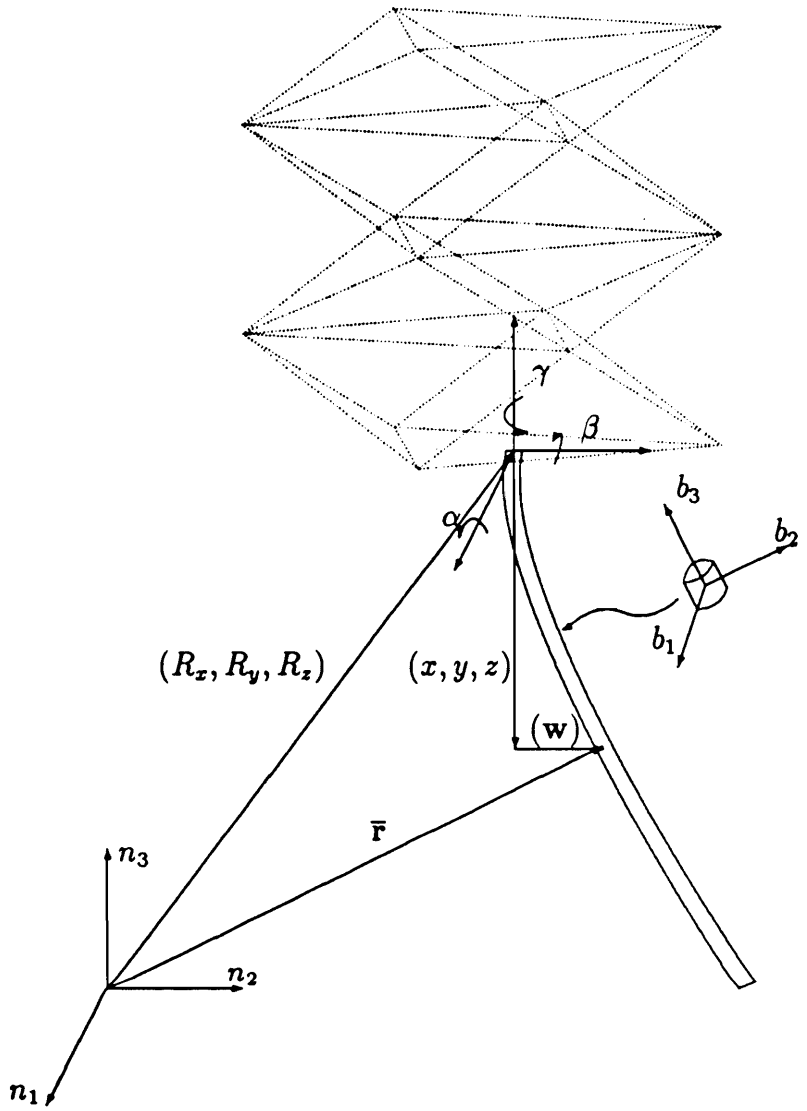

Figure 3.1: Attached Flexible Structure Coordinate System

and the b coordinates are flexible-body-fixed coordinates.

$$\bar{r} = R_x n_1 + R_y n_2 + R_z n_3 + f(x, y, z, w_x, w_y, w_z)_{b_1,b_2,b_3} \tag{3.1}$$

This equation is transformed entirely to the Newtonian coordinate frame, producing

$$\bar{r} = R_x n_1 + R_y n_2 + R_z n_3 + f(x, y, z, w_x, w_y, w_z, \alpha, \beta, \gamma)_{n_1,n_2,n_3}, \tag{3.2}$$

where:

R_x, R_y, R_z locate the position of the base of the structure
α, β, γ describe the rotation of the base of the structure
x, y, z locate a position along the structure from the base
w_x, w_y, w_z are modal displacements.

The $\bar{r}$ vector is used in the calculation of the kinetic and potential energies of the structure. The kinetic energy is found in terms of translations, Eq. (3.3), and rotations, Eq. (3.4).

$$KE_t = \frac{\epsilon}{2} \int_0^l \dot{\bar{r}} \cdot \dot{\bar{r}} \, ds, \tag{3.3}$$

where:

ϵ is the mass per unit length of the structure
l is the length of the structure.

$$KE_r = \frac{1}{2} \int_0^l \begin{bmatrix} \dot{\alpha} & \dot{\beta} & \dot{\gamma} \end{bmatrix} \begin{bmatrix} \frac{J_x}{l} & 0 & 0 \\ 0 & \frac{J_y}{l} & 0 \\ 0 & 0 & \frac{J_z}{l} \end{bmatrix} \begin{bmatrix} \dot{\alpha} \\ \dot{\beta} \\ \dot{\gamma} \end{bmatrix} ds, \tag{3.4}$$

where:

J_x J_y J_z are the mass moments of inertia about x, y, z axis.

Next, the potential energy of the flexible structure must be derived. Two forms of

potential energy included in the model are strain energy and gravitational potential. The form of the potential energy from strain energy is due to bending and/or torsion and is

$$PE_s = \frac{EI}{2} \int_0^l [w_x''(s)]^2 + [w_y''(s)]^2 + [w_z''(s)]^2 ds, \tag{3.5}$$

where:

E is Young's Modulus of the material
I is the area moment of inertia of the structure
$w_x''(s)$, $w_y''(s)$, $w_z''(s)$ are the spatial second
derivative of the transverse deflection in the x, y, z directions.

This equation is derived from the fact that strain energy is proportional to beam curvature, i.e. the second derivative of transverse deflection; this will be explained in Section 4.2.1.

The gravitational potential is

$$PE_g = g\epsilon \int_0^l \bar{r} \cdot n_3 \, ds. \tag{3.6}$$

Once all of the potential and kinetic energies are calculated, the Lagrangian is formed.

$$L = \sum KE's - \sum PE's \tag{3.7}$$

This seemingly simple task is actually quite complicated due to the continuous structure having an infinite number of modal amplitudes. One approach, to the problem, is to approximate the modes of the structure with a summation of assumed

mode shapes for a subset of the infinite number of modes. This approach is referred to as the Ritz or Rayleigh-Ritz (Hurty, 1964) method, Eq. (3.8) .

$$\mathbf{w}(s,t) = \sum_{i=1}^{n} \phi_i(s) q_i(t), \tag{3.8}$$

where:

$\mathbf{w}(s,t)$	are the transverse deflections of the structure
$\phi(s)$	are the open-loop mode shapes of the structure
$\mathbf{q}(t)$	are the time-dependent modal amplitudes
n	is the number of modes of interest.

After the Ritz approximation has been applied the Lagrangian is reduced by keeping terms up to and including second order. When Lagrange's equation, Eq. (3.9), is applied a linear set of system equations, Eq. (3.10), is produced.

$$\frac{\partial}{\partial t}\left(\frac{\partial L}{\partial \dot{q}_i} - \frac{\partial L}{\partial q_i}\right) = 0, \tag{3.9}$$

$$\mathbf{M}\ddot{\mathbf{q}} + \mathbf{K}\mathbf{q} = \mathbf{B_a}\ddot{\mathbf{p}}_\mathbf{r} + \mathbf{B_p}\mathbf{p_r}, \tag{3.10}$$

where:

$\mathbf{M}$	is the system mass matrix
$\mathbf{K}$	is the system stiffness matrix
$\mathbf{B_a}$	is the acceleration input matrix
$\mathbf{B_p}$	is the position and rotation input matrix
$\mathbf{p_r}$	is the position and rotation of the base of the structure
$\ddot{\mathbf{p}}_\mathbf{r}$	is the acceleration of the base of the structure
$\mathbf{q}$	is the modal amplitudes
$\ddot{\mathbf{q}}$	is the acceleration of the modal amplitudes.

The variational method is a very good way of developing mathematical models but, the Ritz approach to the solution is difficult when the structure is not a simple one. As an alternative for modeling the flexible structure, a finite-element method

is presented.

3.1.2 Finite Element Method

Reddy (1984) states, *The finite-element method overcomes the difficulty of the variational method because it provides a systematic procedure for the derivation of the approximation functions.* The finite-element approach discretizes the system into a set of simple subdomains called finite-elements. Over each element an approximation function is used that is a linear combination of algebraic polynomials. These approximation functions are similar to the Ritz approximations, but are only used over a small element of the structure; they are also not as complex. A series of approximation functions is combined to form the model of the entire structure.

When a system is described in a finite-element sense, a set of equations is produced that describes the dynamic relationship between the nodes, the boundaries of the elements, of the structure. From these "discretized" equations mass and stiffness matrices, **M** and **K**, can be extracted. For a unforced system Eq. (3.11) is produced.

$$[\mathbf{M}]\,\ddot{\mathbf{\Delta}} + [\mathbf{K}]\,\mathbf{\Delta} = 0, \tag{3.11}$$

where:

$\mathbf{\Delta}'s$ are translations and rotations of the nodal points
$\ddot{\mathbf{\Delta}}'s$ are translational and rotational accelerations of the nodal points.

This equation is for a structure with no boundary conditions applied; with the imposition of the boundary conditions we can obtain a solution. This is done by specifying the boundary conditions. Eq. (3.11) can then be partitioned into known and unknown portions.

$$\begin{bmatrix} \mathbf{M_1} & \mathbf{M_2} \\ \mathbf{M_3} & \mathbf{M_4} \end{bmatrix} \begin{Bmatrix} \ddot{\mathbf{\Delta}}_1 \\ \ddot{\mathbf{\Delta}}_2 \end{Bmatrix} + \begin{bmatrix} \mathbf{K_1} & \mathbf{K_2} \\ \mathbf{K_3} & \mathbf{K_4} \end{bmatrix} \begin{Bmatrix} \mathbf{\Delta}_1 \\ \mathbf{\Delta}_2 \end{Bmatrix} = 0, \tag{3.12}$$

where:

$\mathbf{\Delta_1}, \ddot{\mathbf{\Delta}}_1$ are known boundary conditions
$\mathbf{\Delta_2}, \ddot{\mathbf{\Delta}}_2$ are unknown.

Expanding this equations yields two sets of equations.

$$\mathbf{M_2}\ddot{\mathbf{\Delta}}_2 + \mathbf{K_2}\mathbf{\Delta_2} = -\mathbf{M_1}\ddot{\mathbf{\Delta}}_1 - \mathbf{K_1}\mathbf{\Delta_1} \tag{3.13}$$

$$\mathbf{M_4}\ddot{\mathbf{\Delta}}_2 + \mathbf{K_4}\mathbf{\Delta_2} = -\mathbf{M_3}\ddot{\mathbf{\Delta}}_1 - \mathbf{K_3}\mathbf{\Delta_1} \tag{3.14}$$

Equation (3.14) has N_2 equations and N_2 unknowns; Eq. (3.13) has N_1 equations and N_2 unknowns; where N_2, N_1 are the length of the Δ_2 and Δ_1 vectors respectively.

Equation (3.13) and Eq. (3.14) relate the knowns of the system to the unknowns of the system. In this case the finite element knowns and unknowns are positions and rotations of the nodes. If we have a planar beam with input at the base then we know x_1, θ_1 ($\mathbf{\Delta_1}$) and the unknowns are $x_2, \cdots x_6, \theta_2, \cdots \theta_6$ ($\mathbf{\Delta_2}$), as shown in Figure 3.2. In spatial problems we would have six knowns or unknowns for each node.

The finite-element equations can be used for system control if we can measure or estimate the absolute positions and rotations of the nodal points, in order to use

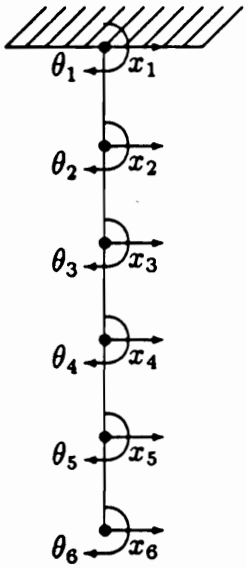

Figure 3.2: Finite-Element Beam with Base Input

them as system states. In most cases the measurement of the nodal positions and rotations is not possible. However, modal displacement is one property that could be used. To this end, just as we did in the variational approach (as in the $\overline{r}$ vector of Eq.(3.1)), we could describe the location of each point with a geometric term and a modal term.

If we look at the steady-state (zero velocity and acceleration) part of Eq. (3.14) we can define the relationship between the known displacements and the unknown displacements of the structure.

$$\mathbf{K_4 \Delta_2 = -K_3 \Delta_1} \tag{3.15}$$

$$\mathbf{\Delta_2 = -K_4{}^{-1} K_3 \Delta_1} \tag{3.16}$$

This give us a geometric relationship between the knowns and the unknowns. If we add a modal term to this we have a relation just like the varational model.

$$\mathbf{\Delta_2} = \underbrace{\mathbf{-K_4{}^{-1} K_3 \Delta_1}}_{\text{Geometric Part}} + \underbrace{\phi \mathbf{q}}_{\text{Modal Part}} \tag{3.17}$$

$$\mathbf{\ddot{\Delta}_2 = -K_4{}^{-1} K_3 \ddot{\Delta}_1} + \phi \ddot{\mathbf{q}} \tag{3.18}$$

therefore

$$\mathbf{M_4}(-\mathbf{K_4}^{-1}\mathbf{K_3}\ddot{\mathbf{\Delta}}_1 + \phi\ddot{\mathbf{q}}) + \mathbf{K_4}(-\mathbf{K_4}^{-1}\mathbf{K_3}\mathbf{\Delta}_1 + \phi\mathbf{q}) = -\mathbf{M_3}\ddot{\mathbf{\Delta}}_1 - \mathbf{K_3}\mathbf{\Delta}_1 \quad (3.19)$$

$$\mathbf{M_4}\phi\ddot{\mathbf{q}} + \mathbf{K_4}\phi\mathbf{q} = (\mathbf{M_4}\mathbf{K_4}^{-1}\mathbf{K_3} - \mathbf{M_3})\ddot{\mathbf{\Delta}}_1 \quad (3.20)$$

For normalized mass and stiffness

$$\phi^T\mathbf{M_4}\phi\ddot{\mathbf{q}} + \phi^T\mathbf{K_4}\phi\mathbf{q} = \phi^T(\mathbf{M_4}\mathbf{K_4}^{-1}\mathbf{K_3} - \mathbf{M_3})\ddot{\mathbf{\Delta}}_1. \quad (3.21)$$

Once the system is in this normalized form, the modes of interest can be kept, thus allowing reduction of the size of the problem. Equation (3.21) relates to Eq. (3.10) in that the vector $\ddot{\mathbf{\Delta}}_1$ is equivalent to $\ddot{\mathbf{p}}_r$. Equation (3.21) does not contain terms that are multiplied by $\mathbf{p}_r$ ($\mathbf{\Delta}_1$); this due to the manner in which the modal displacements were incorperated in the model.

Gravity and FEM

In the variational approach gravity was included in the potential energy term. Gravity enters the equation of motion as a term that modifies the stiffness matrix, $\mathbf{K}$, and as a term that modifies the input $\mathbf{B_p}$. This is shown later. As stated above the equivilant $\mathbf{B_p}$ matrix for the finite-element method was eleminated; therefore an alternative method of introducing the modal displacements into the finite-element development is needed.

In the finite-element method gravity enters the problem as a constant force.

$$[\mathrm{M}]\,\ddot{\mathbf{\Delta}} + [\mathrm{K}]\,\mathbf{\Delta} = g\mathrm{M}\cdot\mathbf{n_3} \tag{3.22}$$

The problem is how to get the gravitational term to enter into the stiffness matrix $\mathbf{K}$, and into the input matrix $\mathbf{B_p}$, in the finite-element method. This other method is unclear to the author and further work is needed in order to develop the procedure. It is believed by the author that two problems need to be addressed; how to include the gravitational term in the finite-element matricies and how to transform the nodal position and rotation matricies to modal matricies while maintaing the added gravitational term.

The finite-element approach does produce models equivalent to those produced by the variational approach save the terms due to gravity.

Now that we have a model for the flexible structure, the next piece of our flexible structure vibration control problem to be modeled is the adaptive truss.

3.2 Adaptive Truss Model

This section presents a method for describing the kinematic transformation that exists from the active links of the adaptive truss to the base coordinates of the flexible structure.

Adaptive trusses are comprised of non-actuated and actuated members that, when extended, cause the truss to change its orientation, thus applying a displacement or force on any structure attached to it. In this work, the truss is treated as a

kinematic mechanism, i.e. the truss dynamics (other than active batten dynamics) are not included. The truss kinematics are of the form of a linear kinematic transformation (an analytically derived Jacobian) from change in active link length to a change in coordinates of the base of the flexible structure. In order to develop this transformation some basic knowledge of adaptive trusses is needed.

All adaptive trusses are comprised of basic units called cells. There are many different types of cells, the smallest of these, the tetrahedron, possesses six struts and four vertices (nodes of connecting joint locations) (Reinholtz,1990). A schematic diagram of the tetrahedron is shown in Figure 3.3. Another basic cell is the octahedral, shown in Figure 3.4, it possesses twelve struts and six vertices.

There has been much work devoted to the development of equations that describe the relationship between the length of each strut of an adaptive truss and the global position of the vertices. There are two types of kinematic problems associated with these relationships, the forward problem and the inverse problem. The forward problem is to find the relative position of all the vertices of the truss given the lengths of all the members. The inverse problem is to find the link lengths given the nodal points. From the standpoint of using the adaptive truss as a controller of a flexible structure the forward problem is the one of interest. The relationship between the active link lengths and the flexible structure base coordinates must be known; this is the input to the flexible structure (see Eq.(3.10)).

The solution of the forward problem is always nonlinear and may not be possible in closed form (Reinholtz,1990). In general, kinematic constraint equations are

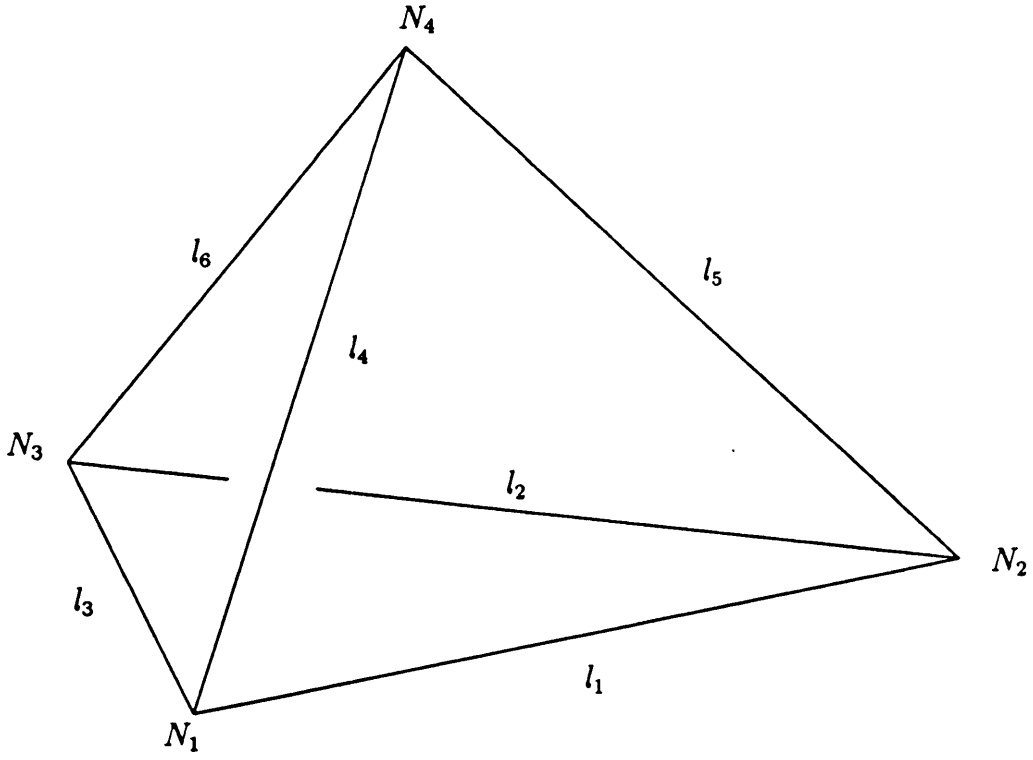

Figure 3.3: Tetrahedral Truss Schematic and Notation

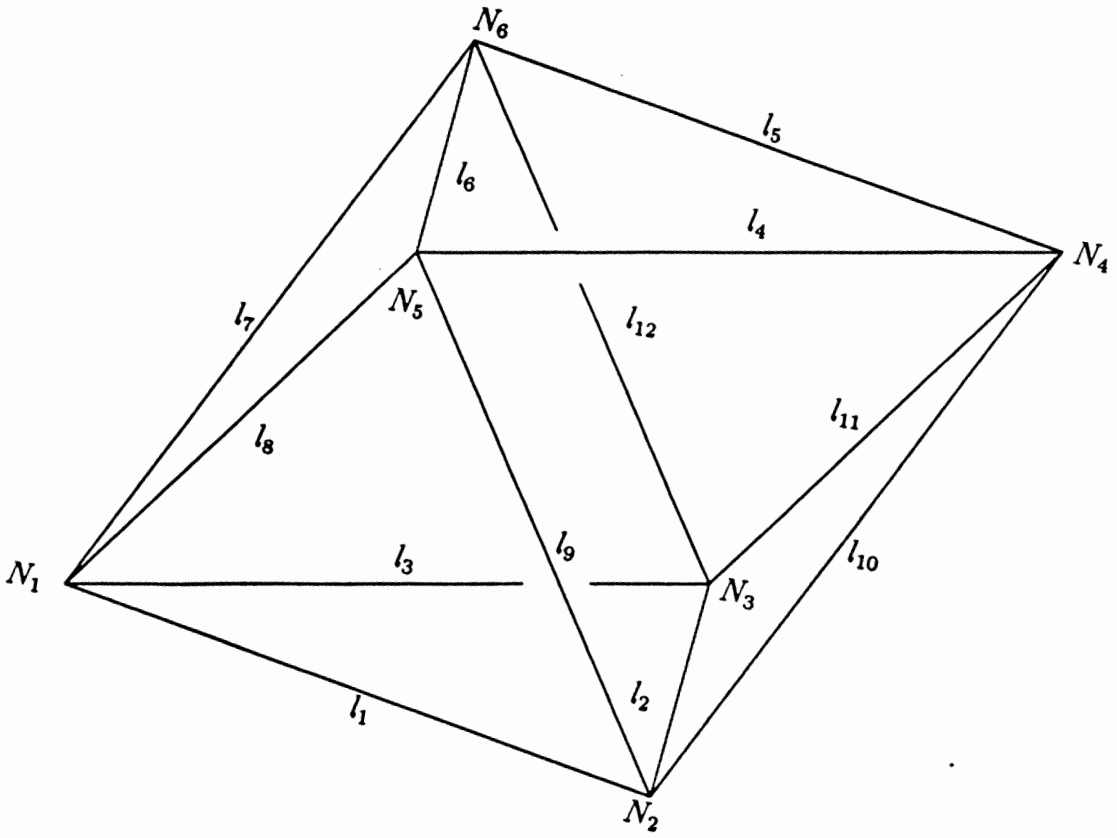

Figure 3.4: Octahedral Truss Schematic and Notation

written for each member of the basic cell. These constraint equations are then solved simultaneously, usually by some type of iteration method. Once the constraints are known basic, cells can be added together to produce a truss assemblage. For example, the tetrahedral truss, Figure 3.3 has kinematic constraint equations as follows:

$$\begin{aligned}
l_1^2 &= (N_{1x} - N_{2x})^2 + (N_{1y} - N_{2y})^2 + (N_{1z} - N_{2z})^2 \\
l_2^2 &= (N_{2x} - N_{3x})^2 + (N_{2y} - N_{3y})^2 + (N_{2z} - N_{3z})^2 \\
l_3^2 &= (N_{1x} - N_{3x})^2 + (N_{1y} - N_{3y})^2 + (N_{1z} - N_{3z})^2 \\
l_4^2 &= (N_{1x} - N_{4x})^2 + (N_{1y} - N_{4y})^2 + (N_{1z} - N_{4z})^2 \\
l_5^2 &= (N_{2x} - N_{4x})^2 + (N_{2y} - N_{4y})^2 + (N_{2z} - N_{4z})^2 \\
l_6^2 &= (N_{3x} - N_{4x})^2 + (N_{3y} - N_{4y})^2 + (N_{3z} - N_{4z})^2
\end{aligned} \tag{3.23}$$

where:

$l_i's$ are the i_{th} link length
N_{ij} is the i_{th} vertex in the j_{th} direction.

Given the link lengths, l's, and the location of two of the vertices, the location of the remainder of the vertices can be found. Once a single unit cell has been defined other unit cells can be stacked together forming a complete truss assemby. This approach is a brute-force attack of the problem; Reinholtz (1990) has developed other methods of defining the forward kinematic analysis.

Once the kinematic equations are derived the Jacobian is formed. In some cases the Jacobian can be found in closed form, but in most cases it is formed by analytically moving one link, (with all others fixed) and recording the changes in R_x, R_y, R_z α, β, and γ. The Jacobian transforms change in active link lengths to change in base coordinates of the flexible structure. The Jacobian is a function of the link lengths and will change for different operating locations.

$$\mathbf{p}_r = \mathbf{T}_l \mathbf{l} \tag{3.24}$$

It has been shown (Warrington, 1990) that the linearity of the transformation is valid for the velocities and accelerations at the nominal, symmetric, positions of the truss (i.e. the operating point that we have chosen). Therefore,

$$\dot{\mathbf{p}}_r = \mathbf{T}_l \dot{\mathbf{l}}, \; ; \; \ddot{\mathbf{p}}_r = \mathbf{T}_l \ddot{\mathbf{l}} \tag{3.25}$$

Where l is the motion of the variable-length battens

$$\mathbf{l} = \begin{bmatrix} l_1 & l_2 & l_3 & l_4 & l_5 & l_6 \end{bmatrix}^T. \tag{3.26}$$

These Equations are combined with Eq. (3.10) or Eq. (3.21), depending on which modeling approach was used, to give a relation between active batten length and flexible structure modal amplitudes.

Next, a relation between motor input voltage and active batten length is needed in order for the truss/flexible structure equations to be complete.

3.3 Active Batten Model

For this study the actuator, the active batten in the truss, is modeled in two parts; the motor, and the gearhead and lead screw combination. The governing equation for a dc armature-controlled motor is derived by applying Kirchoff's loop law to the equivalent motor circuit (see, for example Electro-Craft, 1980), Figure 3.5 shows the circuit.

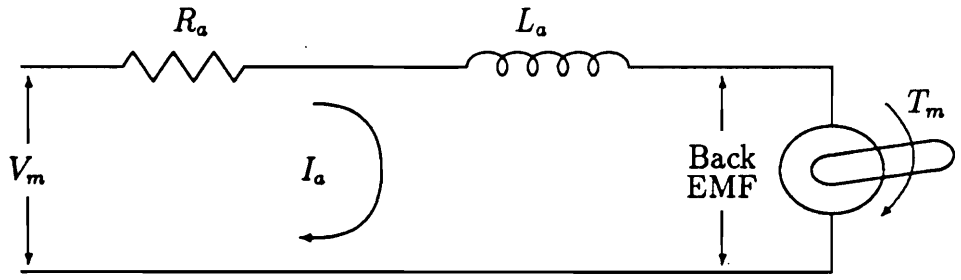

Figure 3.5: Motor Equivalent Circuit

$$V_m = L_a \dot{I}_a + R_a I_a + K_b \dot{\theta}_m, \tag{3.27}$$

where:

V_m = the motor input voltage
L_a = the motor inductance
I_a = the motor current
R_a = the motor armature resistance
K_b = the motor back emf coefficient
$\dot{\theta}_m$ = the motor shaft velocity.

The motor torque, T_m, is defined by the product of the current and the torque constant, K_t, and is equal to the inertia, I_θ, times the motor acceleration, $\ddot{\theta}_m$, assuming no losses. Some loss is due to friction and is ignored in the model, but included in the simulation.

$$T_m = I_a K_t = I_\theta \ddot{\theta}_m \tag{3.28}$$

If the electrical time constant, produced by the inductance, is small compared to the mechanical time constant, resulting from the inertia term, the motor Eq. (3.27) becomes,

$$V_m = \frac{R_a I_\theta \ddot{\theta}_m}{K_t} + K_b \dot{\theta}_m. \tag{3.29}$$

A justification for the elimination of the inductance can be shown by examining actual motor parameters. Figure 3.6 shows the transfer function magnitude for an actual motor, (one of the ones used in this experiment) with inductance modeled and without it. There is a difference between the two models only at frequencies higher than 1000 $\frac{rad}{sec}$. This means that if the flexible structure to be controlled is

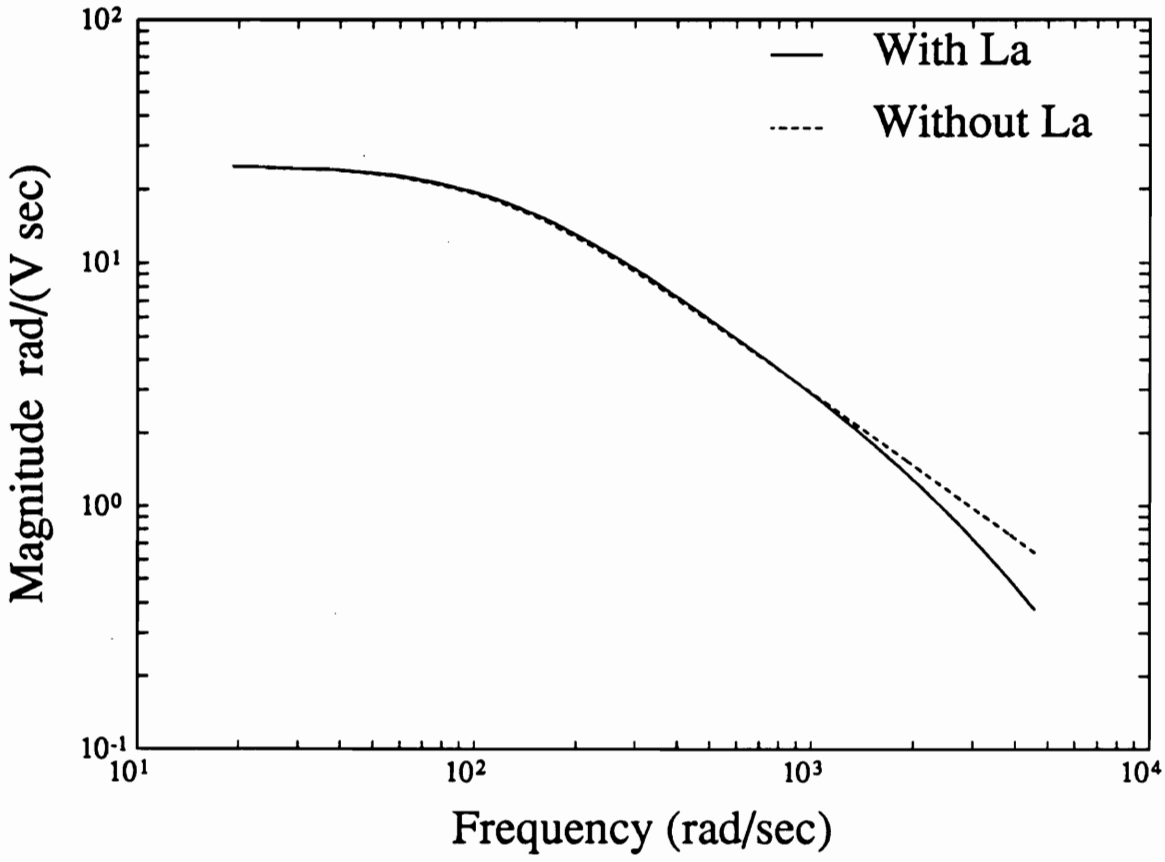

Figure 3.6: Motor Transfer Function, With and Without Modeled Inductance

slower that the break frequency caused by the inductor then the elimination of the inductor is justified.

In Eq. (3.29) I_θ is the effective inertia seen by the motor. Included in this inertia term is the armature/gearhead inertia, and the lead screw inertia. The motor gearhead affects the driven structure as follows: the effect of a motor gearhead with θ_{in} going in and θ_{out} coming out, Figure 3.7, can be modeled by equating kinetic energy as seen from each side of the gearhead

$$\frac{1}{2} I_{in} \dot{\theta}_{in}^2 = \frac{1}{2} I_{out} \dot{\theta}_{out}^2 \tag{3.30}$$

but, due to the gearhead

$$\theta_{out} = \frac{\theta_{in}}{G_r}, \; \dot{\theta}_{out} = \frac{\dot{\theta}_{in}}{G_r} \tag{3.31}$$

so

$$I_{in} = \frac{I_{out}}{G_r{}^2}. \tag{3.32}$$

Therefore, the effective inertia, I_θ, of Eq. (3.29) which is turning a lead screw through a gearhead is

$$I_\theta = I_m + \frac{I_{ls}}{G_r{}^2}, \tag{3.33}$$

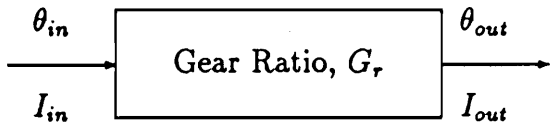

Figure 3.7: Motor Block Diagram

where:

I_m is the motor and gearhead inertia
I_{ls} is the lead screw inertia
G_r is the gearhead gain.

Another inertia term that one might want to include is the effective mass that the lead screw is driving. In this development this mass is assumed negligible due to the high ratio gearhead and to the so-called stiff actuator assumption. This means that the motor is modeled as if it applies a displacement to the active batten and that the load of the active batten does not affect the motor.

The rotary motion, θ_m, of the motor is related to the linear motion of the active batten, l, by

$$\theta_m = \frac{G_r}{G_{ls}} l. \tag{3.34}$$

Thus the final equation of motion for the motor, lead screw combination is

$$V_m = \frac{R_a I_\theta G_r \ddot{l}}{K_t G_{ls}} + \frac{K_b G_r \dot{l}}{G_{ls}}. \tag{3.35}$$

The actuator equations, truss equations, and flexible structure equations are now assembled.

3.4 Combined System Representation

The flexible structure equations, truss transformation, and actuator equations are assembled into a state-space representation so that closed loop control can be performed.

Substituting the truss transformation, Eq. (3.24) into the beam equation Eq. (3.10) or Eq. (3.21) produces

$$\mathbf{M_{b1}\ddot{q} + K_{b1}q = B_{ba}T_l\ddot{l} + B_{bp}T_l l}. \tag{3.36}$$

Multiplying by $\mathbf{M_{b1}^{-1}}$ and including $\mathbf{C_b\dot{q}}$ to model the effects of experimentally determined modal damping yields

$$\ddot{\mathbf{q}} + \mathbf{C_b\dot{q} + K_b q = M_l\ddot{l} + K_l l}, \tag{3.37}$$

where:

$$\begin{aligned} \mathbf{C_b} &= 2[\zeta\omega]_i\mathbf{I} \\ \mathbf{K_b} &= \mathbf{M_{b1}^{-1}K_{b1}} \\ \mathbf{M_l} &= \mathbf{M_{b1}^{-1}B_{ba}T_l} \\ \mathbf{K_l} &= \mathbf{M_{b1}^{-1}B_{bp}T_l}. \end{aligned}$$

The inclusion of modal damping enables the model to match the open-loop characteristics of the flexible structures.

This equation is used with the actuator equation, Eq. (3.35) in order to assemble the entire system.

$$\ddot{\mathbf{q}} + \mathbf{C_b\dot{q} + K_b q = M_l\ddot{l} + K_l l} \tag{3.38}$$

$$\mathbf{M_m\ddot{l} + C_m\dot{l} = B_m v_m} \tag{3.39}$$

with: $\mathbf{z} = \begin{Bmatrix} l \\ q \end{Bmatrix}$.

Equations (3.38) and (3.39) combined to form

$$\mathbf{M_t\ddot{z} + C_t\dot{z} + K_t z = B_t v_m}, \tag{3.40}$$

where:

$$\mathbf{M_t} = \begin{bmatrix} \mathbf{M_m} & \mathbf{0} \\ \mathbf{-M_l} & \mathbf{I} \end{bmatrix}$$

$$\mathbf{C_t} = \begin{bmatrix} \mathbf{C_m} & \mathbf{0} \\ \mathbf{0} & \mathbf{C_b} \end{bmatrix}$$

$$\mathbf{K_t} = \begin{bmatrix} \mathbf{0} & \mathbf{0} \\ \mathbf{-K_l} & \mathbf{K_b} \end{bmatrix}$$

$$\mathbf{B_t} = \begin{bmatrix} \mathbf{B_m} \\ \mathbf{0} \end{bmatrix}.$$

Define $\mathbf{y = \dot{z}}$

$$\mathbf{M_t\dot{y} + C_t y + K_t z = B_t v_m} \tag{3.41}$$

to form the state-space representation of the adaptive truss system.

$$\begin{Bmatrix} \dot{\mathbf{z}} \\ \dot{\mathbf{y}} \end{Bmatrix} = \begin{bmatrix} \mathbf{0} & \mathbf{I} \\ \mathbf{-M_t^{-1}K_t} & \mathbf{-M_t^{-1}C_t} \end{bmatrix} \begin{Bmatrix} \mathbf{z} \\ \mathbf{y} \end{Bmatrix} + \begin{bmatrix} \mathbf{0} \\ \mathbf{-M_t^{-1}B_t} \end{bmatrix} \mathbf{v_m} \tag{3.42}$$

Which is of the form

$$\mathbf{\dot{x} = Ax + Bu} \tag{3.43}$$

where:

$$\mathbf{x} = \begin{Bmatrix} \mathbf{l} \\ \mathbf{q} \\ \dot{\mathbf{l}} \\ \dot{\mathbf{q}} \end{Bmatrix} \tag{3.44}$$

and

$$\mathbf{u} = \left\{ \mathbf{v_m} \right\}. \tag{3.45}$$

Now we can apply control to the system model.

3.5 Control

One objective of this work was to demonstrate the control of flexible structure vibrations using the adaptive truss; with emphasis on agreement between simulated and experimental results (model verification). There are different methods for determining suitable gain sets for this multiple-input-multiple-output (MIMO) system. The control approach chosen was the discrete linear quadratic regulator (LQR) optimal control design, another possible scheme is pole placement.

Pole placement involves specifying all of the closed-loop eigenvalues of the system. Because (MIMO) systems with state feedback have more gains than eigenvalues, an algorithm (one such algorithm is discussed in Little, 1986) that minimizes the sensitivity of the poles to perturbations in the closed-loop system is used. With pole placement designs it is very easy to demand pole locations that produce very large gains, so caution must be used when implementing this method.

The LQR method was chosen due to its ease of implementation. The selection of the parameters to specify LQR gains and what these parameters do to the gain set is more straightforward to the author than the selection of the poles for pole placement.

No matter what control design is used the first step is to discretize the system, because digital control is to be implemented. This is done by assuming a zero-order hold on the system inputs and a sampling time of T, using

$$\mathbf{\Phi} = e^{\mathbf{A}T} \tag{3.46}$$

$$\mathbf{\Gamma} = \int_0^T e^{\mathbf{A}v} dv \mathbf{B} \tag{3.47}$$

which provides for

$$\mathbf{x[k+1]} = \mathbf{\Phi x[k]} + \mathbf{\Gamma u[k]}. \tag{3.48}$$

$\mathbf{\Phi}$ and $\mathbf{\Gamma}$ are now used in the LQR design to determine the gain set.

3.5.1 LQR Design Methodology

This design (Little, 1986) calculates an optimal feedback gain set $\mathbf{K}$ such that the control law

$$\mathbf{u}[k] = -\mathbf{K}\mathbf{x}[k] \tag{3.49}$$

minimizes the cost function

$$J = \sum_{i=0}^{n} (\mathbf{x}^T[i]\mathbf{Q}\mathbf{x}[i] + \mathbf{u}^T[i]\mathbf{R}\mathbf{u}[i]) \tag{3.50}$$

subject to the constraint equation

$$\mathbf{x}[k+1] = \mathbf{\Phi}\mathbf{x}[k] + \mathbf{\Gamma}\mathbf{u}[k]. \tag{3.51}$$

Where $\mathbf{Q}$ and $\mathbf{R}$ are weighting matrices $\mathbf{Q}$ weights the error between the desired states and the actual states (in our case the desired states are zero) and $\mathbf{R}$ weights the actuator forces. $\mathbf{Q}$ and $\mathbf{R}$ are square matrices with the size of $\mathbf{Q}$ being equal to the number of states and the size of $\mathbf{R}$ equal to the number of control inputs.

The choice of $\mathbf{Q}$ and $\mathbf{R}$ in the LQR control law development is somewhat arbitrary. In this problem a comparatively large $\mathbf{Q}$ will cause the control to emphasize the vibration reduction task with resulting large control efforts, a comparatively large $\mathbf{R}$ will emphasize reducing the control effort with a less effective vibration reduction. Through experimental trial and error the author has devised a procedure to help determine the values of $\mathbf{Q}$ and $\mathbf{R}$, this procedure is presented next.

Expermental Insight into LQR

From experimental insight the author has developed a method of determining practical ranges of $\mathbf{Q}$ and $\mathbf{R}$ that seems to take the guesswork out of the selection of $\mathbf{Q}$ and $\mathbf{R}$ in the LQR control design.

The selection of the **Q** and **R** matrices in the LQR control design is a somewhat arbitrary task. The **Q** matrix is positive semi-definite and usually all the off diagonal terms are set to zero, this is the case in this discussion. The **R** matrix is positive definite and usually all the off diagonal terms are set to zero. Therefore the problem at hand is to select the diaognal elements of the **Q** and **R** matrices.

This approach tries to maximize the control effort while minimizing the effects of saturation of the physical system. Saturation is "bad", but if the controller does not drive the system to near saturation it is "overdesigned" in that the capibility of the actuator is not being utilized. For example the experimental apparatus used in this dissertation has a physical constraint that only 25 volts can be supplied to each actuator. The goal is then to determine an LQR gain set that will produce control voltages that are approximately 25 volts for the expected values of the states (the system error when the reference is non-zero). This is done by considering experimental knowledge of the system, (i.e. maximum expected values of each of the states).

The first step in this method is to rank the states in order of importance. For the flexible structure control problem this ranking was chosen to be modal amplitude, actuator position, modal velocity, and actuator velocity. This is a statement of the fact that we are more concerned with the vibraton reduction task and not with the position of the truss. (The velocities were not measured so they were ranked low.)

After the ranking has been determined actual values for **Q** and **R** need to be determined and an initial gain matrix calculated. Two points are considered in order

to pick a first choice of **Q** and **R**. First if a state cannot be measured or is of little significance, set its coresponding **Q** entry to zero. This is the lowest penalty that can be put on a state and should produce a low gain for that state. For the flexible control problem discussed here these correspond to the modal velocity (we can not measure it) and actuator velocity (we do not care about it). Next choose the remainder of the **Q** entries based on the relative ranking, the highest ranking the largest entry the lowest ranking the lowest entry.

Before an *LQR* gain set can be calculated a value for **R** must be determined. **R** weights the control effort, but the relative magnitude between **Q** and **R** is of importance. In this method each actuator is treated as equal to any other, so each **R** diagonal entry is the same. Since the ratio of **Q** and **R** is important, the actual value of **R** can be set to one without loss of generality.

Once the initial guesses of **Q** and **R** have been determined an initial gain matrix is produced. This is an optimal gain set for the chosen values of **Q** and **R**, but it may not be optimal based upon our actuator limitations. This is determined by examining the control effort generated by a change in our most valued state. For example in our problem we said that the modal amplitudes were the most important states. If the first mode is given the highest values of these states then we use it to determine if our gain set is reasonable. This is done be calculating the control effort required using this state as a worst case test. If we then calculate a control voltage that is 0.1 volts (maximum is 25) then our gain set is too small, if we calculate 2500 volts then our gain set is too high. A new gain set is calculated by adjusting the relative magnitude of **Q**, a higher **Q** will produce a larger gain set. The larger

gain set will increase the speed at which the system is controlled. This iterative process seems to take some of the guesswork out of the LQR design procedure and help provide an easy means of selecting a gain set. These gain sets are now used in simulations and in the experimental setup.

Chapter 4

Simulation and Experimental Considerations

In order to verify the analytical model, open-loop and closed-loop simulation data was compared to experimental data. The model verification was based upon an experimental configuration at VPI&SU consisting of a six active-link truss and three flexible structures. In order for the simulation to more closely resemble the experimental data some non-linear effects were added to the simulation of the linear plant; these were amplifier saturation and lead screw friction. Experimental considerations pertain to the conversion of strain to modal amplitude, calibration, and the computer code.

4.1 Simulation Considerations

In order for the simulation of the linear plant to more closely resemble the actual experimental setup two non-linear effects were included; amplifier saturation and lead screw friction.

4.1.1 Saturation

Saturation occurs when the control signal computed is greater than can be delivered to the system. This can be characterized by a predetermined, system-dependent, maximum value, usually a maximum voltage. In this case the value is 25 volts. In the simulation the control has a hard saturation for inputs greater than the maximum. Saturation should be included in all structural control simulations. Saturation effects will have a large influence on all practical structural control systems, especially in response to transient loadings.

4.1.2 Friction

Friction in the adaptive links can cause system performance to be degraded. In all cases friction will absorb control energy that would dampen low-amplitude vibrations, thus these low amplitude vibrations are not controlled. Friction was simulated as Coulomb type, constant-offset opposing the velocity; a characteristic friction plot is shown in Figure 4.1. In the application of friction in our model a corresponding friction "voltage" was calculated and subtracted from the control voltage. This voltage is constant except when the velocity of the batten is nearly zero, then the friction voltage is set equal to the input voltage so that the friction voltage does not drive the system. Friction occurs in all lead screw configurations, if it is not modeled the resulting simulated control will be better than the experimental control (small amplitude vibrations will be damped). Figure 4.2 shows simulated and experimental active batten velocity plots for a low frequency triangular wave. The experimental plot shows the effect friction has on the system.

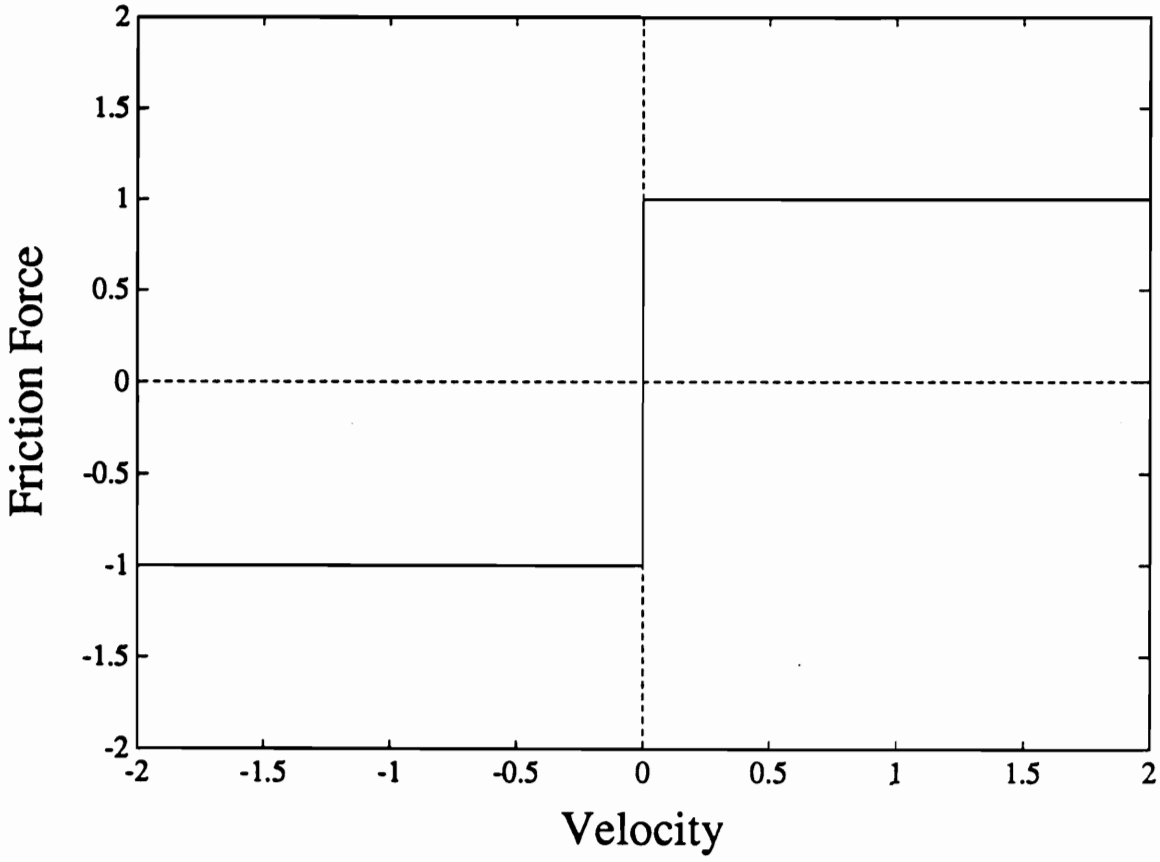

Figure 4.1: Characteristic Friction Plot

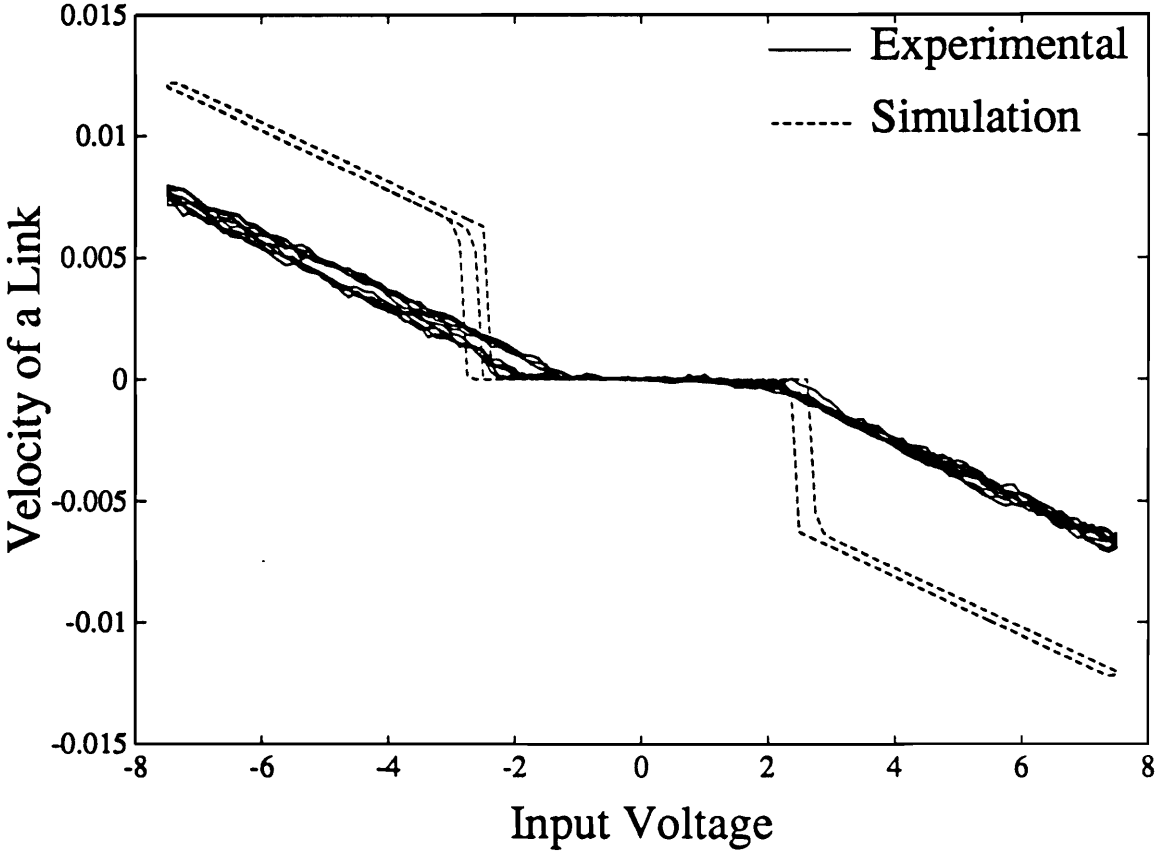

Figure 4.2: Link Friction Plots

4.2 Experimental Considerations

In the development of the state-space form of the adaptive truss model the states are active batten lengths, l's, and modal amplitudes, q's. In order to measure the active batten length a linear potentiometer is used. Actual position is calculated by applying calibration constants to the voltage generated by the potentiometer. Measuring modal amplitudes is not as straightforward; there is not a device that directly measures them. The approach used was to measure strain in the flexible structure and then transform it into modal amplitudes. This transformation is described below.

4.2.1 Strain and Modal Amplitude

The relationship between modal amplitude and strain can be found by from the definition of strain for a beam subject to a pure bending moment, (Popov, 1976).

$$\varepsilon = \frac{MC}{EI} \tag{4.1}$$

The moment is also defined from curvature, (Popov, 1976)

$$\frac{1}{\rho} = \frac{\frac{d^2v}{dx^2}}{[1 + \frac{dv}{dx}^2]^{\frac{3}{2}}} = \frac{M}{EI}, \tag{4.2}$$

where:

M is the moment in the beam
C is the distance form the neutral axis
EI is the rigidity of the beam
ρ is the curvature of the beam
x is the distance along the curve
v is the deflection at x.

For most engineering applications the deflection is small so the slope $\frac{dv}{dx}$ is also small.

Therefore the square of the slope is negligible as compared to one; thus Eq. (4.2) becomes

$$\frac{d^2v}{dx^2} = \frac{M}{EI}. \tag{4.3}$$

This is the governing spatial differential equation for the deflection of an elastic beam. Therefore rearranging Eq. (4.1) and Eq. (4.3) gives,

$$\varepsilon = \frac{d^2v}{dx^2}C \tag{4.4}$$

or the strain can be found by differentiating the displacement twice.

In our development the deflection of the structure is defined by Eq. (3.8), therefore the strain in the structure is

$$\varepsilon(s,t) = \sum_{i=1}^{n} \phi_i''(s) q_i(t). \tag{4.5}$$

With this relationship between modal amplitude and strain we can form a matrix expression, S_t, that relates the strain, at a given set of points along a structure, to the modal amplitudes of the structure.

$$\begin{Bmatrix} \varepsilon_1 \\ \varepsilon_2 \\ \varepsilon_3 \end{Bmatrix} = \mathbf{S} \begin{Bmatrix} q_1 \\ q_2 \\ q_3 \end{Bmatrix}, \tag{4.6}$$

where:

$$\mathbf{S} = \begin{bmatrix} \varepsilon_{1,1} & \varepsilon_{2,1} & \varepsilon_{3,1} \\ \varepsilon_{1,2} & \varepsilon_{2,2} & \varepsilon_{3,2} \\ \varepsilon_{1,3} & \varepsilon_{2,3} & \varepsilon_{3,3} \end{bmatrix}. \tag{4.7}$$

We actually need to go from strain to modal amplitude not the other way, so

$$\begin{Bmatrix} q_1 \\ q_2 \\ q_3 \end{Bmatrix} = \mathbf{S_t} \begin{Bmatrix} \varepsilon_1 \\ \varepsilon_2 \\ \varepsilon_3 \end{Bmatrix}, \tag{4.8}$$

where:

$$\mathbf{S_t} = \mathbf{S}^{-1}. \tag{4.9}$$

Therefore when $\mathbf{S_t}$ is multiplied by the strain vector the resulting three modal amplitudes are calculated.

4.3 Specific Experimental Setup

In the experimental setup, show schematically in Figure 4.3, position of the truss and strain in the flexible structure are digitized with an analog to digital converter (ADC) and converted to system states (q's and l's). The active batten length changes, l's, were transduced with 12 inch-stroke, film-resistive potentiometers. The beam motions, q,s, were measured with strain gage bridges placed at locations along the beam. The control voltage is then output through a digital to analog converter (DAC) and amplified. The amplified signal drives the motors, gearheads, and lead screws, which move the truss and effect the flexible structure.

The experiments were performed using a 20 MHz, 80386-based computer with a commercially available A/D and D/A system. All the algorithms were coded in C. A block diagram of the control algorithm is shown in Figure 4.4. The ten to fourteen-input, six-output control algorithms were calculated at rates from 190 Hz

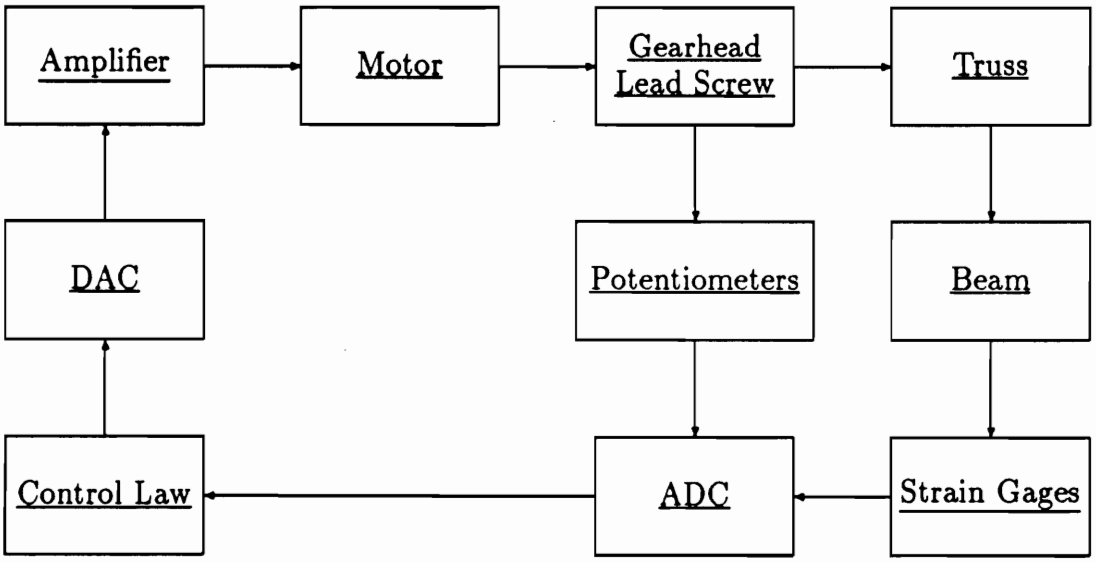

Figure 4.3: Experimental Setup Block Diagram

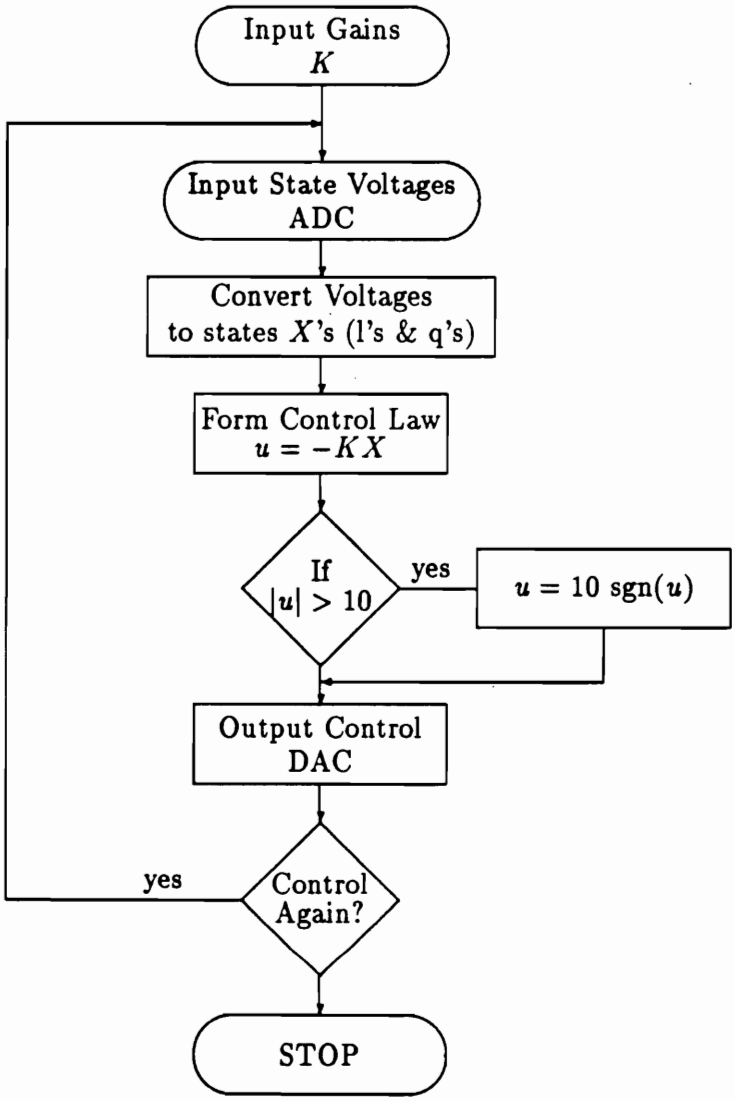

Figure 4.4: Computer Code Block Diagram

to 260 Hz, depending on the application. The first step in the control code is to input the gain matrix. Control begins by digitizing the inputs and converting them to actual states. Next the control law is formed. Since the digital to analog converter can output only up to 10 volts the control value must be clipped and then output to the system. The control is now returned to step one.

4.3.1 Specific Experimental Considerations

Experimental control of system requires consideration of many issues that are generally not considered in simulated control; the biggest of these is calibration. Calibration, in this sense, involves converting measured values into usable states. For example, consider a simple problem of moving one active batten of the truss. A linear potentiometer outputs a voltage that is proportional to displacement, with 0 volts output in the center, 10 volts at 6 inches, and -10 volts at -6 inches. This value is converted to a digital value by the analog to digital converter (ADC). The digital value is a twelve bit integer with 0 corresponding to minus full-scale voltage and 4095 corresponding to plus full-scale voltage. The full-scale voltage value can be 1.25, 2.5, 5.0, or 10.0 volts. In addition to the ADC calibration, the value must be converted to meters to be compatible with the model.

Therefore:

$$P = \frac{(V - 2047)}{2047} F_s \frac{12}{20} 0.0254, \tag{4.10}$$

where:

P is the position in meters
V is the digital voltage
F_s is full-scale ADC voltage.

This position value, along with the other states, is used in the control law

$$\mathbf{u} = -\mathbf{K}\mathbf{x} \tag{4.11}$$

and is sent out of the controller by a digital-to-analog converter (DAC) to the amplifier and then to the motor. The DAC requires a integer value of 0 for -10 volts and 4095 for 10 volts. The amplifier inverts the signal and multiplies it by 2.5. therefore the analog value is

$$\mathbf{u_{analog}} = \frac{\mathbf{K}}{2.5}\mathbf{x} \tag{4.12}$$

and the digital value is

$$\mathbf{u} = int\ \frac{10\mathbf{u_{analog}} + 2047}{204.7}. \tag{4.13}$$

This seemingly simple idea of experimentally controlling one active batten of the truss shows that it is actually not very simple.

Other problems occur while implementing experimental control and some insight into the experimental control of flexible structures has been gained at VPI&SU. For example, how to determine why a simulated control problem is stable and the experimental case is unstable. This type of problem many times results from some type

of calibration factor that was lost or forgotten, and as shown earlier there can be many of these calibration factors. The problem is how to find the culprit. Assuming that the plant is inherently open-loop stable, (ours is), then one can examine the control of each state independently.

For example, if the experimental closed-loop system is unstable (and open-loop stable), we would expect that the problem is in the control law implementation (i.e. instrumentation, calibration, software). For our specific problem, first, check to see if the position control of the truss works; the truss will try to maintain the zero position with no other input than the link positions. One approach for doing this is to zero all of the modal amplitudes in the control program. This new controller should drive the active battens to the zero position, if it does not then there is probably a sign wrong in the calibration factor(s). Once the position control problem has been corrected try the entire control problem again. If it still does not work, look at the control of one mode of the structure. Check to see if a positive modal deflection produces a positive modal value in the program. Concentrate on the control of this one mode by exciting only that mode with small amplitude vibrations. As a debugging tool a lower gain set might be used, (a lower Q matrix in the LQR design.) this slows down the response of the system and allows the operator to more closely observe the experiment.

Now that the we have discussed the procedures, modeling, simulating, and controlling, it is time to discuss a specific adaptive truss and three flexible structures to be controlled.

Chapter 5

A Specific Adaptive Truss

This chapter presents the adaptive truss at VPI&SU. Specific kinematic analysis and actuator analysis are applied to this truss, as developed in Sections 3.2 and 3.3.

The truss, a two bay octahedral-octahedral structure, originally built by Rhodes (1985) at NASA Langley Research Center and later modified at VPI&SU has six active battens. Each active batten consists of a motor and lead-screw actuator with a nominal length of 45 inches. The fixed battens are approximately 48 inches long and the cross-longerons approximately 34 inches long, these dimensions produce a truss about 8 feet tall. A schematic diagram of the adaptive truss studied is shown in Figure 5.1.

5.1 Truss Model

As stated in the general development the truss is modeled in two parts, the kinematic equations and the actuator equations.

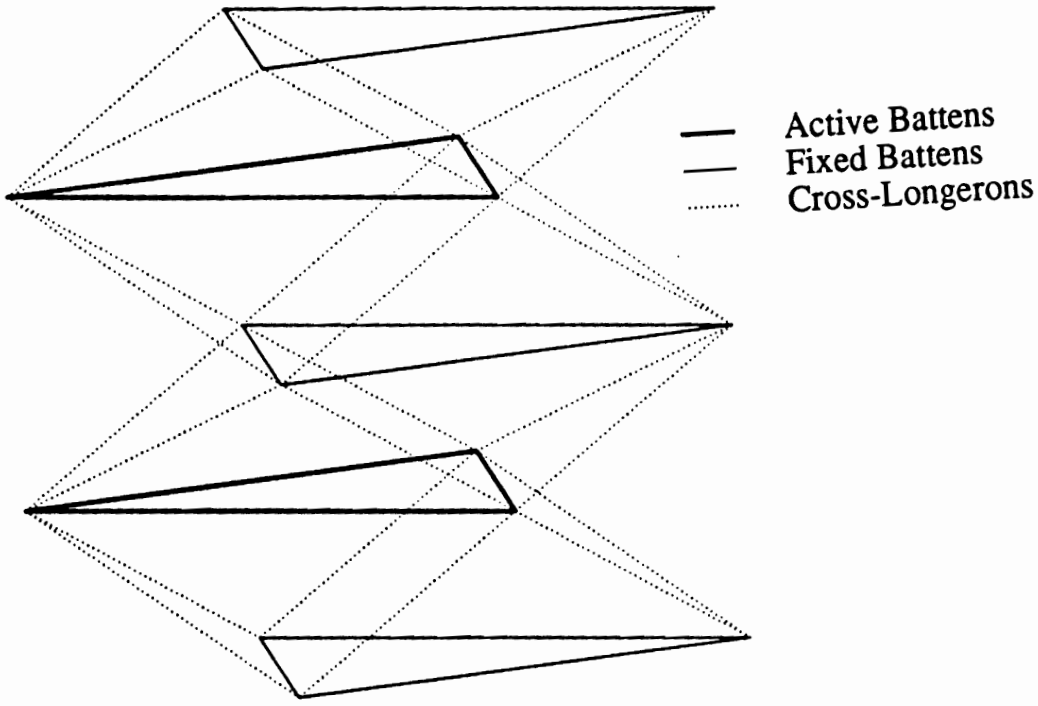

Figure 5.1: A Schematic Diagram of an Adaptive Truss

5.1.1 Kinematic Equations

The truss is modeled as a "stiff" actuator; that is, the truss affects the attached flexible structure, but the structure does not affect the truss, since the lead screws in the active battens can not be back-driven. This truss input is modeled by means of a linear transformation which is the Jacobian of the kinematic equations of the truss (Craig, 1986). The Jacobian is formed by moving one batten, (with all others fixed) and analytically determining the changes in $R_x, R_y, R_z, \alpha, \beta$ and γ. See Section 3.2 for details. The Jacobian is a function of the operating point and will change if that operating point is moved. The Jacobian of interest transforms the change in active batten lengths to a change in base coordinates of the attached flexible structure. The transformation is of the form

$$\mathbf{p_r} = \mathbf{T_l l}, \tag{5.1}$$

where:

$$\mathbf{l} = \begin{bmatrix} l_1 & l_2 & l_3 & l_4 & l_5 & l_6 \end{bmatrix}^T \tag{5.2}$$

$$\mathbf{p_r} = \begin{bmatrix} R_x & R_y & R_z & \alpha & \beta & \gamma \end{bmatrix}^T. \tag{5.3}$$

For the octahedral-octahedral truss configuration at VPI&SU the Jacobian is

$$\mathbf{T_l} = \begin{bmatrix} 0.6300 & 0 & -0.6300 & 1.8830 & 0 & -1.8830 \\ 0.3700 & -0.7400 & 0.3700 & 1.0900 & -2.1800 & 1.0900 \\ 0.2600 & 0.2600 & 0.2600 & 0.2600 & 0.2600 & 0.2600 \\ -1.0600 & 0 & 1.0600 & -1.0600 & 0 & 1.0600 \\ 0.6300 & -1.2600 & 0.6300 & 0.6300 & -1.2600 & 0.6300 \\ 0.0000 & 0.0000 & 0.0000 & 0.0000 & 0.0000 & 0.0000 \end{bmatrix}. \quad (5.4)$$

This Jacobian is for the operating point used with all the active battens at 45 inches. Notice that for this configuration the last row is all zero this indicates that the truss will not provide rotation about the γ axis for this operating point.

The kinematic transformation is combined with the actuator description to produce the truss model. The actuator description for the truss at VPI&SU is developed in the next section.

5.1.2 Actuator Equations

The actuators in the VPI&SU adaptive truss are off-the-shelf DC motors that drive a lead screw through a gearhead. Table 5.1 lists the physical parameters of the motor.

The equation of motion for the motor, lead screw combination as defined in section 3.3 is

$$V_m = \frac{R_a I_\theta G_r \ddot{l}}{K_t G_{ls}} + \frac{K_b G_r \dot{l}}{G_{ls}}. \quad (5.5)$$

Table 5.1: Maxon DC Motor Parameters

Maxon DC Motor Parameters		
Part # 43.034.000 2200 011		
Symbol	Value	Unit
L_a	0.00062	H
R_a	2	Ohms
I_a	6.76E-6	Kg-m^2
K_b	0.0398	V/(rad-s)
K_t	0.0398	N-m/A
G_r	5.2	
G_{ls}	2.5266E-11	m / rad
I_{ls}	6.8823E-7	Kg-m^2

For our truss there are six motor, lead-screw pairs and each has to be included in the overall truss equation. Thus the motor equation is

$$\mathbf{M_m}\ddot{\mathbf{l}} + \mathbf{C_m}\dot{\mathbf{l}} = \mathbf{B_m}\mathbf{v_m}, \tag{5.6}$$

where:

$$\mathbf{M_m} = \begin{bmatrix} 1 & 0 & 0 & 0 & 0 & 0 \\ 0 & 1 & 0 & 0 & 0 & 0 \\ 0 & 0 & 1 & 0 & 0 & 0 \\ 0 & 0 & 0 & 1 & 0 & 0 \\ 0 & 0 & 0 & 0 & 1 & 0 \\ 0 & 0 & 0 & 0 & 0 & 1 \end{bmatrix} \frac{I_\theta R_a G_r}{K_t G_{ls}}$$

$$\mathbf{C_m} = \begin{bmatrix} 1 & 0 & 0 & 0 & 0 & 0 \\ 0 & 1 & 0 & 0 & 0 & 0 \\ 0 & 0 & 1 & 0 & 0 & 0 \\ 0 & 0 & 0 & 1 & 0 & 0 \\ 0 & 0 & 0 & 0 & 1 & 0 \\ 0 & 0 & 0 & 0 & 0 & 1 \end{bmatrix} \frac{K_b G_r}{G_{ls}}$$

$$\mathbf{B_m} = \begin{bmatrix} 1 & 0 & 0 & 0 & 0 & 0 \\ 0 & 1 & 0 & 0 & 0 & 0 \\ 0 & 0 & 1 & 0 & 0 & 0 \\ 0 & 0 & 0 & 1 & 0 & 0 \\ 0 & 0 & 0 & 0 & 1 & 0 \\ 0 & 0 & 0 & 0 & 0 & 1 \end{bmatrix}.$$

In the development of the motor equations an assumption about inductance was made; it stated that if the electrical time constant is small compared to the mechanical one then the inductance can be ignored. Figure 5.2 shows an experimental and simulated plot of the motor transfer function. The experimental transfer function magnitude was obtained by exciting the motor with random noise. The velocity of the motor, due to the random input, was recorded along with the random input and an experimental transfer function magnitude calculated for the frequency range of interest. The simulated result does not include the inductance term; thus validating the assumption.

These equations, truss and actuators, are now combined with the equations of three different flexible structures in order to perform specific control tasks. The first flexible structure, a slender beam, is presented in the next Chapter.

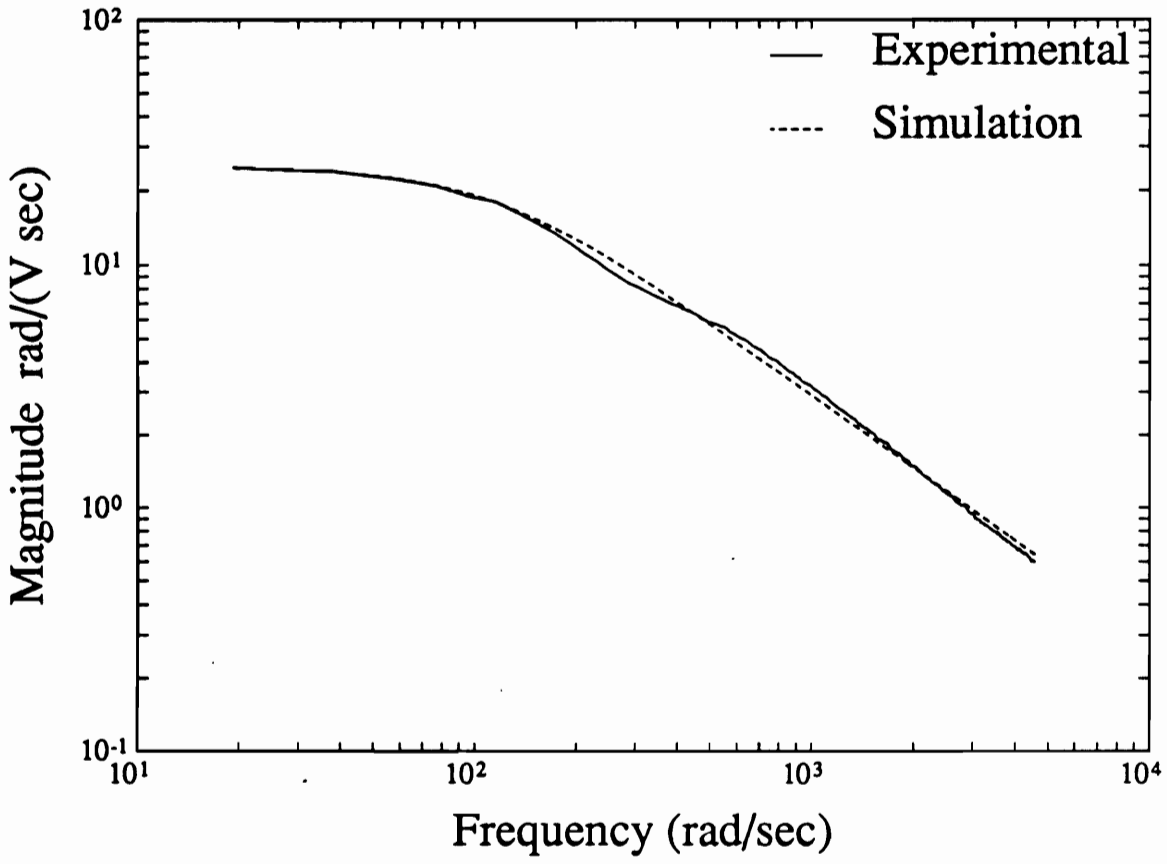

Figure 5.2: Motor Transfer Function

Chapter 6

Specific Flexible Structure, A Slender Beam

This chapter presents the first structure that was controlled with the octahedral-octahedral adaptive truss at VPI&SU, a $\frac{1}{8}$" diameter, 75" long brass beam. A schematic diagram of the truss is shown in Figure 6.1. Two beam models are derived, one using a variational approach and the other a finite-element approach. The inclusion of the finite-element model was to verify that the developed procedure is correct, so it can be applied to structures that do not lend themselves to the variational method. The structure model is combined with the actuator equations and kinematic transformation and a overall system is determined. A discrete linear quadratic gain set is derived and partial state-feedback implemented. Simulated and experimental results are then compared in order to validate the modeling methods and experimental procedures.

6.1 Variational Approach

The equations of motion for the slender beam attached to the truss are developed using the potential and kinetic energies of the beam as discussed in Section 3.1.1. A three-term Ritz approximation for the beam deflections is assumed for each of

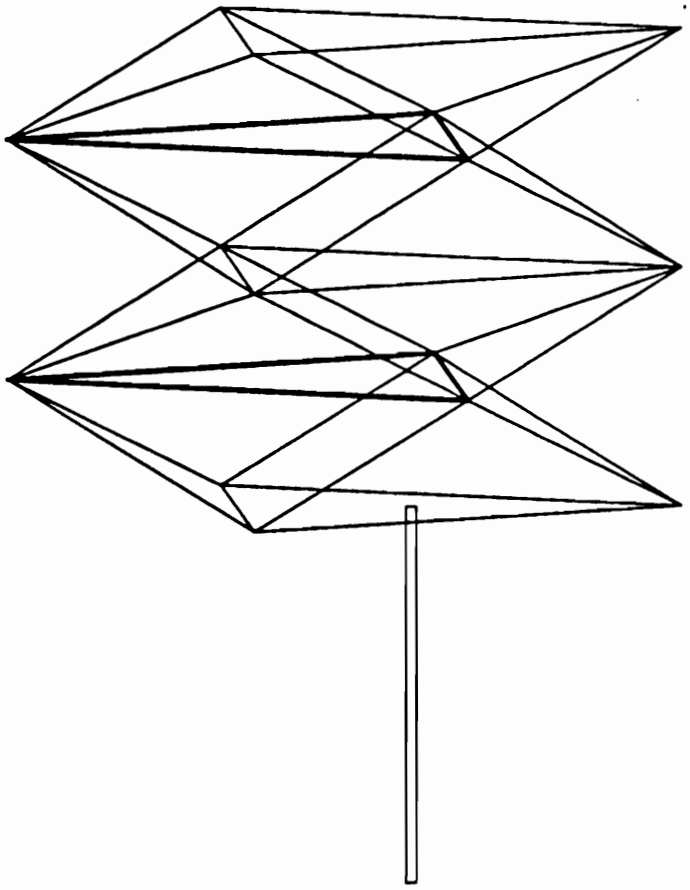

Figure 6.1: Adaptive Truss with A Slender Beam Attached

the deflections in the x and y coordinate axes (i.e. perpendicular to the beam axis). The Ritz approximations are:

$$w_x(s,t) = \sum_{i=1}^{n} \phi_i(s) q_i(t) \tag{6.1}$$

$$w_y(s,t) = \sum_{j=1}^{n} \phi_j(s) q_j(t) \tag{6.2}$$

where $q_i's, q_j's$ are the modal coefficients and $\phi_i's, \phi_j's$ are the open-loop mode shapes of the beam in the x and y directions. The mode shapes used are those of a clamped-free beam and are defined as

$$\phi_i = A_i[\cosh \beta_i x - \gamma_i \sinh \beta_i x - \cos \beta_i x + \gamma_i \sin \beta_i x]. \tag{6.3}$$

The coefficients for the first three modes are defined in Table 6.1 (Thomson, 1981).

Table 6.1: Clamped-free Ritz Coefficients

i	A_i	γ_i	$L\beta_i$
1	0.5	0.7341	1.8751
2	−0.5	1.0185	4.6941
3	0.5	0.9992	7.8547

The beam equation of motion in Eq. (6.4), which was developed in section 3.1.1, results from applying Lagrange's equations to the beam energy statement comprised of kinetic energy resulting from translational motion transverse to the beam axis, and potential energy resulting from beam bending and gravity.

$$\mathbf{M_{b1}\ddot{q} + K_{b1}q = B_{ba}\ddot{p}_r + B_{bp}p_r} \tag{6.4}$$

$\mathbf{q}$ is defined by three (open-loop) modal deflections in the x and y directions, respectively.

$$\mathbf{q} = \begin{bmatrix} q_{1x} & q_{2x} & q_{3x} & q_{1y} & q_{2y} & q_{3y} \end{bmatrix}^T \tag{6.5}$$

$\mathbf{p_r}$ is the kinematic motion input to the base of the beam from the active truss.

$$\mathbf{p_r} = \begin{bmatrix} R_x & R_y & R_z & \alpha & \beta & \gamma \end{bmatrix} \tag{6.6}$$

R_x, R_y and R_z are the translational motions in the x, y and z directions of the active truss; α, β and γ are rotations of the active truss around orthogonal axes (in the x, y and z directions) perpendicular to the beam axis at the base of the beam. Eq. (6.4) shows that the active truss couples to the beam through both motion and acceleration of the base. In the absence of gravity, only the acceleration coupling would remain.

$\mathbf{M_{b1}}$ is the mass matrix of the beam,

$$\mathbf{M_{b1}} = \begin{bmatrix} I_1 & I_7 & I_9 & 0 & 0 & 0 \\ I_7 & I_2 & I_8 & 0 & 0 & 0 \\ I_9 & I_8 & I_3 & 0 & 0 & 0 \\ 0 & 0 & 0 & I_4 & I_{10} & I_{12} \\ 0 & 0 & 0 & I_{10} & I_5 & I_{11} \\ 0 & 0 & 0 & I_{12} & I_{11} & I_6 \end{bmatrix} \tag{6.7}$$

where the $I's$ are integrals of the mode shapes and are defined in Appendix A.

$\mathbf{K_{b1}}$, in Eq. (6.4), is the beam stiffness matrix which is comprised of $\mathbf{K_1}$, from the strain energy, and $\mathbf{K_2}$, from the gravitational potential,

$$\mathbf{K_{b1}} = \mathbf{K_1} + \mathbf{K_2} \tag{6.8}$$

$$\mathbf{K_1} = \begin{bmatrix} I_{34} & I_{40} & I_{42} & 0 & 0 & 0 \\ I_{40} & I_{35} & I_{41} & 0 & 0 & 0 \\ I_{42} & I_{41} & I_{36} & 0 & 0 & 0 \\ 0 & 0 & 0 & I_{37} & I_{43} & I_{45} \\ 0 & 0 & 0 & I_{43} & I_{38} & I_{44} \\ 0 & 0 & 0 & I_{45} & I_{44} & I_{39} \end{bmatrix} \frac{EI}{\varepsilon} \tag{6.9}$$

$$\mathbf{K_2} = \begin{bmatrix} I_{46} & I_{52} & I_{54} & 0 & 0 & 0 \\ I_{52} & I_{47} & I_{53} & 0 & 0 & 0 \\ I_{54} & I_{53} & I_{48} & 0 & 0 & 0 \\ 0 & 0 & 0 & I_{49} & I_{55} & I_{57} \\ 0 & 0 & 0 & I_{55} & I_{50} & I_{56} \\ 0 & 0 & 0 & I_{57} & I_{56} & I_{51} \end{bmatrix} g. \tag{6.10}$$

The input to the base of the beam is affected by the position matrix $\mathbf{B_{bp}}$ and the acceleration matrix $\mathbf{B_{ba}}$,

$$\mathbf{B_{ba}} = \begin{bmatrix} -I_{13} & 0 & 0 & I_{19} & 0 & 0 \\ -I_{14} & 0 & 0 & I_{20} & 0 & 0 \\ -I_{15} & 0 & 0 & I_{21} & 0 & 0 \\ 0 & -I_{16} & 0 & 0 & -I_{22} & 0 \\ 0 & -I_{17} & 0 & 0 & -I_{23} & 0 \\ 0 & -I_{18} & 0 & 0 & -I_{24} & 0 \end{bmatrix} \tag{6.11}$$

$$\mathbf{B_{bp}} = \begin{bmatrix} 0 & 0 & 0 & I_{13} & 0 & 0 \\ 0 & 0 & 0 & I_{14} & 0 & 0 \\ 0 & 0 & 0 & I_{15} & 0 & 0 \\ 0 & 0 & 0 & 0 & -I_{16} & 0 \\ 0 & 0 & 0 & 0 & -I_{17} & 0 \\ 0 & 0 & 0 & 0 & -I_{18} & 0 \end{bmatrix} g\varepsilon. \tag{6.12}$$

The variational approach can be very difficult for a complex structure. Another approach is to model the structure using the finite-element method. The next section presents the finite-element model for the slender beam, as developed in Section 3.1.2, and shows that the procedure is a viable alternative to the variational approach.

6.2 Finite Element Approach

A finite element model of the free-free configuration of the slender beam was generated using PAL, a personal-computer-based, finite-element program. The mass and stiffness matrices were extracted and manipulated as described in Section 3.1.2. In order to compare the variational approach and the finite element approach the resulting matrices are shown.

$$\mathbf{M^{-1}K} = \begin{bmatrix} 9.729 & 0 & 0 & 0 & 0 & 0 \\ 0 & 382.1 & 0 & 0 & 0 & 0 \\ 0 & 0 & 2995.7 & 0 & 0 & 0 \\ 0 & 0 & 0 & 9.729 & 0 & 0 \\ 0 & 0 & 0 & 0 & 382.1 & 0 \\ 0 & 0 & 0 & 0 & 0 & 2995.7 \end{bmatrix} \tag{6.13}$$

$$\mathbf{M_{FEM}^{-1}K_{FEM}} = \begin{bmatrix} 9.7319 & -3.2e-14 & -4.6e-13 & 0 & 0 & 0 \\ 2.7e-13 & 382.90 & 8.0e-13 & 0 & 0 & 0 \\ -1.5e-13 & -8.8e-13 & 3035.4 & 0 & 0 & 0 \\ 0 & 0 & 0 & 9.7319 & -3.2e-14 & -4.6e-13 \\ 0 & 0 & 0 & 2.7e-13 & 382.90 & 8.0e-13 \\ 0 & 0 & 0 & -1.5e-13 & -8.8e-13 & 3035.4 \end{bmatrix} \tag{6.14}$$

$$\mathbf{M^{-1}B_a} = \begin{bmatrix} -1.5657 & 0 & 2.0226 & 0 \\ 0.8669 & 0 & -0.3217 & 0 \\ -0.5091 & 0 & 0.1161 & 0 \\ 0 & -1.5657 & 0 & -2.0226 \\ 0 & 0.8669 & 0 & 0.3217 \\ 0 & -0.5091 & 0 & -0.1161 \end{bmatrix} \tag{6.15}$$

$$\mathbf{M_{FEM}^{-1}B_{a\,FEM}} = \begin{bmatrix} -1.5659 & 0 & 2.0226 & 0 \\ 0.8691 & 0 & -0.3232 & 0 \\ -0.5123 & 0 & 0.1163 & 0 \\ 0 & -1.5659 & 0 & -2.0226 \\ 0 & 0.8691 & 0 & 0.3232 \\ 0 & -0.5123 & 0 & -0.1163 \end{bmatrix} \tag{6.16}$$

In each case gravity not included, see the discussion in Section 3.1.2 for an explanation.

These results show that finite-element and variational approach give the same system matrices for the slender beam problem. This helps to verify our finite-element approach, so that we can trust the finite-element method for future structures. The variational model is now combined with truss equations and the actuator equations to produce the system equations.

6.3 System Equations and Control Law Implementation

Whether the energy or the FEM approach is used a mathematical model for the beam continuum is produced. The beam model, truss equation and actuator equations are combined into state-space model, as described in Eq. (3.42), that describe the entire system.

In order to apply closed-loop vibration control to this multi-input, multi-output

system, the system equations are combined into a compatible state-variable form, discretized for the digital control case, and then a discrete LQR problem is solved to produce a set of time-invariant feedback coefficients for use in the simulations and experimental setup.

This system is 24th order including, six actuator positions, six actuator rates, 6 modal amplitudes and 6 modal amplitude rates. A full state feedback (FSF) characteristic gain set is show below along with the corresponding Q and R values used to generate them.

$$\mathbf{K}_{\mathbf{fsf}}^{\mathbf{T}} = \begin{bmatrix}
28.198 & 1.737 & 1.684 & -9.447 & 4.767 & 4.679 \\
1.737 & 28.145 & 1.737 & 4.767 & -9.535 & 4.767 \\
1.684 & 1.737 & 28.198 & 4.679 & 4.767 & -9.447 \\
-3.457 & 1.754 & 1.702 & 22.095 & 4.805 & 4.718 \\
1.754 & -3.509 & 1.754 & 4.805 & 22.007 & 4.805 \\
1.702 & 1.754 & -3.457 & 4.718 & 4.805 & 22.095 \\
-113.246 & -0.000 & 113.246 & -184.863 & -0.000 & 184.863 \\
62.184 & -0.000 & -62.184 & 138.691 & -0.000 & -138.691 \\
-59.488 & -0.000 & 59.488 & -143.504 & -0.000 & 143.504 \\
-65.934 & 131.868 & -65.934 & -106.387 & 212.775 & -106.387 \\
36.449 & -72.898 & 36.449 & 80.139 & -160.278 & 80.139 \\
-34.846 & 69.693 & -34.846 & -82.826 & 165.652 & -82.826 \\
-1.281 & 0.811 & 0.768 & -2.710 & 1.383 & 1.327 \\
0.811 & -1.324 & 0.811 & 1.383 & -2.766 & 1.383 \\
0.768 & 0.811 & -1.281 & 1.327 & 1.383 & -2.710 \\
-2.282 & 1.161 & 1.121 & -3.765 & 2.053 & 2.009 \\
1.161 & -2.322 & 1.161 & 2.053 & -3.810 & 2.053 \\
1.121 & 1.161 & -2.282 & 2.009 & 2.053 & -3.765 \\
-1.527 & 0.000 & 1.527 & -2.467 & 0.000 & 2.467 \\
0.155 & -0.000 & -0.155 & 0.716 & -0.000 & -0.716 \\
-0.650 & -0.000 & 0.650 & -1.665 & -0.000 & 1.665 \\
-0.891 & 1.782 & -0.891 & -1.424 & 2.849 & -1.424 \\
0.086 & -0.172 & 0.086 & 0.405 & -0.810 & 0.405 \\
-0.380 & 0.760 & -0.380 & -0.959 & 1.918 & -0.959
\end{bmatrix} \tag{6.17}$$

$$
\mathbf{R} = \begin{bmatrix} 1 & 0 & 0 & 0 & 0 & 0 \\ 0 & 1 & 0 & 0 & 0 & 0 \\ 0 & 0 & 1 & 0 & 0 & 0 \\ 0 & 0 & 0 & 1 & 0 & 0 \\ 0 & 0 & 0 & 0 & 1 & 0 \\ 0 & 0 & 0 & 0 & 0 & 1 \end{bmatrix} \tag{6.18}
$$

$$
\mathbf{Q} = \left[\begin{array}{cccccccccccc c}
10^3 & 0 & 0 & 0 & 0 & 0 & 0 & 0 & 0 & 0 & 0 & 0 & \\
0 & 10^3 & 0 & 0 & 0 & 0 & 0 & 0 & 0 & 0 & 0 & 0 & \\
0 & 0 & 10^3 & 0 & 0 & 0 & 0 & 0 & 0 & 0 & 0 & 0 & \\
0 & 0 & 0 & 10^3 & 0 & 0 & 0 & 0 & 0 & 0 & 0 & 0 & \\
0 & 0 & 0 & 0 & 10^3 & 0 & 0 & 0 & 0 & 0 & 0 & 0 & \\
0 & 0 & 0 & 0 & 0 & 10^3 & 0 & 0 & 0 & 0 & 0 & 0 & \\
0 & 0 & 0 & 0 & 0 & 0 & 10^6 & 0 & 0 & 0 & 0 & 0 & \\
0 & 0 & 0 & 0 & 0 & 0 & 0 & 10^6 & 0 & 0 & 0 & 0 & \\
0 & 0 & 0 & 0 & 0 & 0 & 0 & 0 & 10^6 & 0 & 0 & 0 & \\
0 & 0 & 0 & 0 & 0 & 0 & 0 & 0 & 0 & 10^6 & 0 & 0 & \\
0 & 0 & 0 & 0 & 0 & 0 & 0 & 0 & 0 & 0 & 10^6 & 0 & \\
0 & 0 & 0 & 0 & 0 & 0 & 0 & 0 & 0 & 0 & 0 & 10^6 & \\
0 & 0 & 0 & 0 & 0 & 0 & 0 & 0 & 0 & 0 & 0 & 0 & 0_{12\times 24} \\
0 & 0 & 0 & 0 & 0 & 0 & 0 & 0 & 0 & 0 & 0 & 0 & \\
0 & 0 & 0 & 0 & 0 & 0 & 0 & 0 & 0 & 0 & 0 & 0 & \\
0 & 0 & 0 & 0 & 0 & 0 & 0 & 0 & 0 & 0 & 0 & 0 & \\
0 & 0 & 0 & 0 & 0 & 0 & 0 & 0 & 0 & 0 & 0 & 0 & \\
0 & 0 & 0 & 0 & 0 & 0 & 0 & 0 & 0 & 0 & 0 & 0 & \\
0 & 0 & 0 & 0 & 0 & 0 & 0 & 0 & 0 & 0 & 0 & 0 & \\
0 & 0 & 0 & 0 & 0 & 0 & 0 & 0 & 0 & 0 & 0 & 0 & \\
0 & 0 & 0 & 0 & 0 & 0 & 0 & 0 & 0 & 0 & 0 & 0 & \\
0 & 0 & 0 & 0 & 0 & 0 & 0 & 0 & 0 & 0 & 0 & 0 & \\
0 & 0 & 0 & 0 & 0 & 0 & 0 & 0 & 0 & 0 & 0 & 0 & \\
0 & 0 & 0 & 0 & 0 & 0 & 0 & 0 & 0 & 0 & 0 & 0 &
\end{array} \right] \tag{6.19}
$$

The actual partial state feedback gain set that was used is as follows.

$$\mathbf{K}_{\mathbf{psf}}^{\mathbf{T}} = \begin{bmatrix} 28.198 & 1.737 & 1.684 & -9.447 & 4.767 & 4.679 \\ 1.737 & 28.145 & 1.737 & 4.767 & -9.535 & 4.767 \\ 1.684 & 1.737 & 28.198 & 4.679 & 4.767 & -9.447 \\ -3.457 & 1.754 & 1.702 & 22.095 & 4.805 & 4.718 \\ 1.754 & -3.509 & 1.754 & 4.805 & 22.007 & 4.805 \\ 1.702 & 1.754 & -3.457 & 4.718 & 4.805 & 22.095 \\ -113.246 & -0.000 & 113.246 & -184.863 & -0.000 & 184.863 \\ 62.184 & -0.000 & -62.184 & 138.691 & -0.000 & -138.691 \\ -59.488 & -0.000 & 59.488 & -143.504 & -0.000 & 143.504 \\ -65.934 & 131.868 & -65.934 & -106.387 & 212.775 & -106.387 \\ 36.449 & -72.898 & 36.449 & 80.139 & -160.278 & 80.139 \\ -34.846 & 69.693 & -34.846 & -82.826 & 165.652 & -82.826 \\ 0 & 0 & 0 & 0 & 0 & 0 \\ 0 & 0 & 0 & 0 & 0 & 0 \\ 0 & 0 & 0 & 0 & 0 & 0 \\ 0 & 0 & 0 & 0 & 0 & 0 \\ 0 & 0 & 0 & 0 & 0 & 0 \\ 0 & 0 & 0 & 0 & 0 & 0 \\ 0 & 0 & 0 & 0 & 0 & 0 \\ 0 & 0 & 0 & 0 & 0 & 0 \\ 0 & 0 & 0 & 0 & 0 & 0 \\ 0 & 0 & 0 & 0 & 0 & 0 \\ 0 & 0 & 0 & 0 & 0 & 0 \end{bmatrix} \tag{6.20}$$

The gain set was derived so that the vibrational control effort was of primary importance, as shown by $Q_{7,7}$ ... $Q_{12,12}$, whereas the global position of the truss was of less significance, as shown by $Q_{1,1}...Q_{6,6}$. Since only partial state feedback (PSF) was implemented the Q values that relate to the rates were set to zero, $Q_{13,13}...Q_{24,24}$. For more information see Section 3.5.1.

The use of zero values in Q, corresponding to the rate terms, minimizes the effect of the rate terms on the optimal control. When the rate gain values are treated as zero, slightly less than optimal control results. This is shown by comparing the values of the optimal cost function, Eq. (3.50), as shown in Table 6.2 for both full state feedback and partial state feedback.

Table 6.2: Cost Function Values for Full State Feedback and Partial State Feedback

Full State Feedback	322480
Partial State Feedback	325250

Figure 6.2 shows two traces of the tip of the slender beam. This spiral plot shows a difference between the full state feedback, K_{fsf} (Eq.(6.17)), case and the partial state feedback, K_{psf} (Eq.(6.20)), case. In the first portion of the plot, the first loop and a quarter, open loop data is shown. At this point control is initiated and the full state feedback case is slightly better that the partial state feedback case.

This also shows that the FSF case is only slightly better than the PSF case. This validates that fact that, if our model is correct, we can achieve good, not quite optimal, control using only the partial state feedback for this control configuration. Therefore the next step is to verify our system model.

6.4 Simulated and Experimental Results

In order to verify the analytical model, open-loop and closed-loop simulated data was compared to experimental data.

The following plots show that there is excellent agreement between the simulated and experimental results. Initial condition displacements were used to provide the slender beam with an input motion. The adaptive truss controls the beam such that the motion is reduced. Different initial condition responses were used to check the

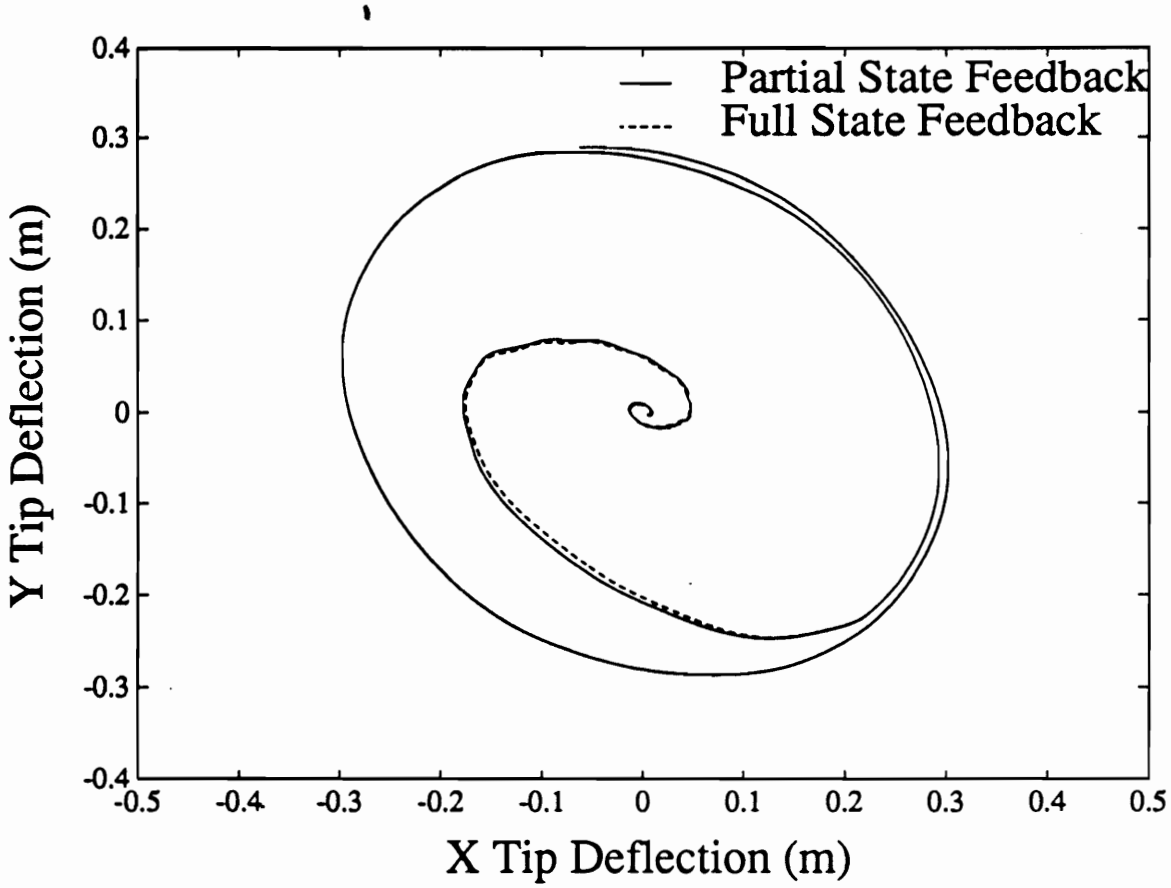

Figure 6.2: Full State Feedback vs. Partial State Feedback

validity of the model. These include; 1-D first mode-like, 1-D second mode-like, and 2-D (spiral first mode-like. As a numerical comparison open and closed loop natural frequencies and damping values were determined and are presented in Table 6.3.

Table 6.3: Slender Beam Comparison

	Open-Loop			Closed-Loop		
	Simulation	Experimental	% error	Simulation	Experimental	%error
	Mode 1					
ω_n	3.11	3.09	0.64	3.20	3.14	1.87
ζ	0.0044	0.0044	0.00	0.2876	0.2746	4.52
	Mode 2					
ω_n	19.56	18.75	3.83	20.30	19.77	2.61
ζ	0.0013	0.0013	0	0.0195	0.0218	-11.79

Figure 6.3 shows simulated and experimental data from a first mode-like deflection. This was accomplished by swinging the beam such that only first mode is excited. The first portion of the plot, approximately 0.9 seconds, shows the open-loop data with the control applied after that. The experimental data was gathered by the control computer. The experimental data was used to determine the initial conditions to be applied to the simulation. The open-loop data verifies that the open loop natural frequency and damping values are correct. The closed-loop data verifies that the rest of the model, how the truss effects the beam and how the actuators effect the truss, is correct. As can be seen from Figure 6.4, the motor voltage is clipped by the controller; also the beam motion does not go completely to zero due to the friction effects in the actuators. Notice in the motor voltage plot that there is a small discrepancy between the two voltage values. On close examination one can see that the trends are very close, the same frequency components are present, there is just a slight magnitude change.

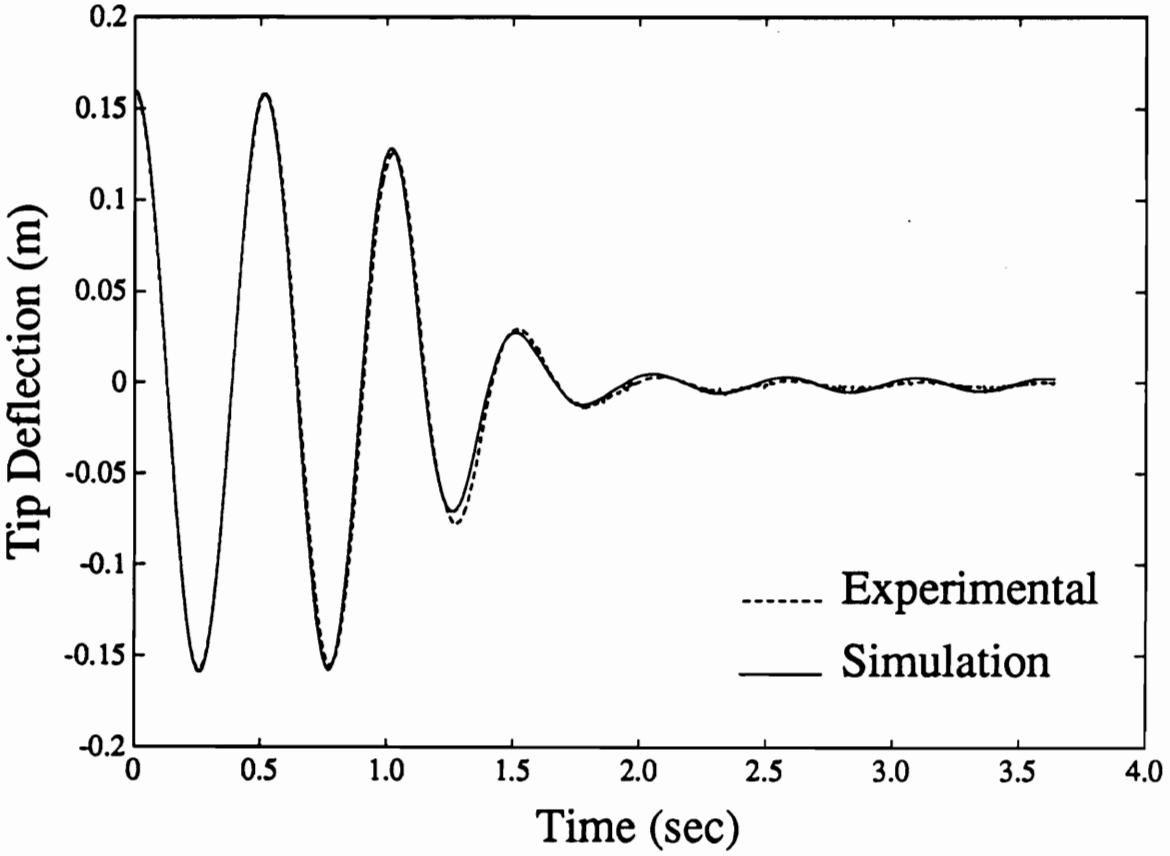

Figure 6.3: First Bending Mode, Controlled Response, Modal Amplitude

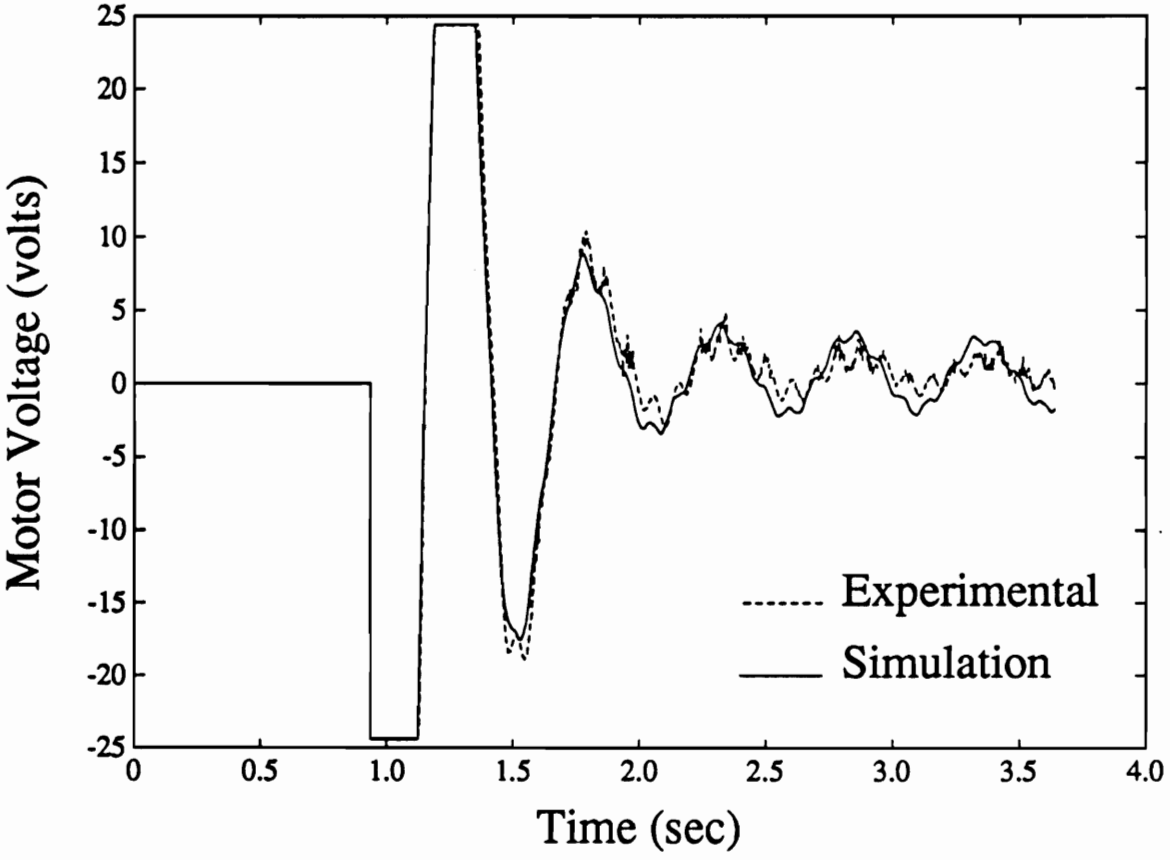

Figure 6.4: First Bending Mode, Controlled Response, Motor Voltage

Figure 6.5 contains second mode-like excitation of the beam, with Figure 6.6 being the corresponding motor voltage. Again we see excellent agreement between the simulated and experimental values. The same procedures used for first-mode comparisons were used for second-mode comparisons; that is, a second mode-like excitation was provided to the beam and simulation.

Figure 6.7 shows the deflection of the tip of the beam given a set of initial conditions. The initial conditions were an initial Y deflection and initial X velocity. This picture is used to visualize how well the truss controls the slender beam in a spatial sence and to see how good the agreement is between simulated and experimental results for 2-D motion. The tip deflection was obtained by summing the three modal amplitudes.

With the excellent agreement between simulated and experimental data it was concluded that the process works. This process includes the modeling procedures, control law development, and the inclusion of friction and saturation in the analysis. The next logical step was to proceed to a more complicated flexible structure.

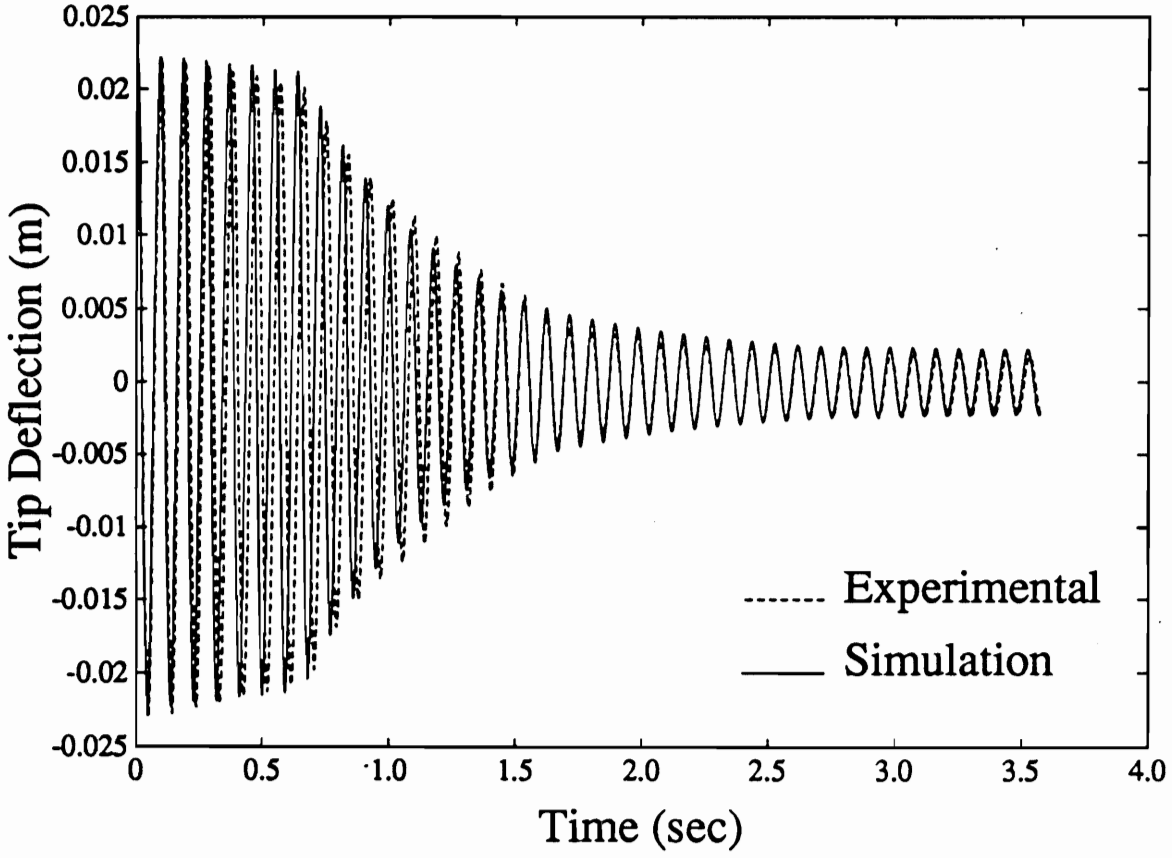

Figure 6.5: Second Bending Mode, Controlled Response, Modal Amplitude

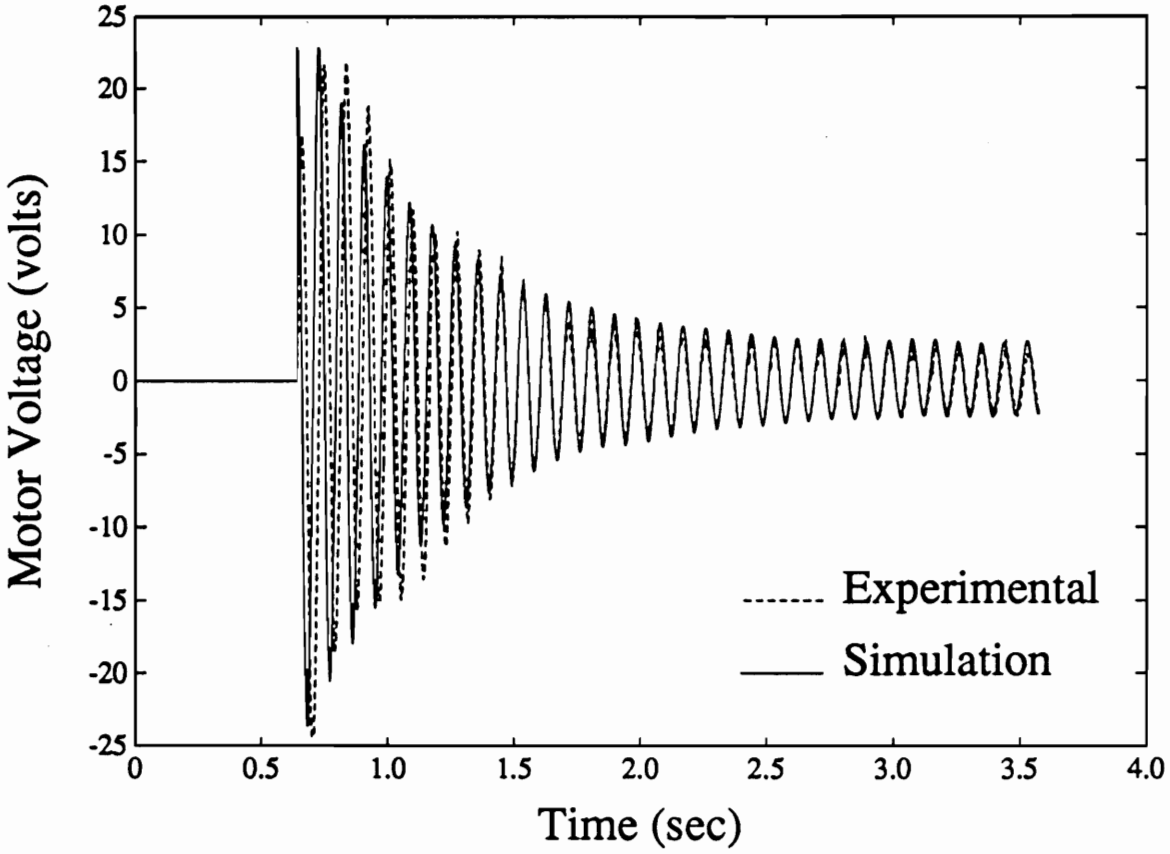

Figure 6.6: Second Bending Mode, Controlled Response, Motor Voltage

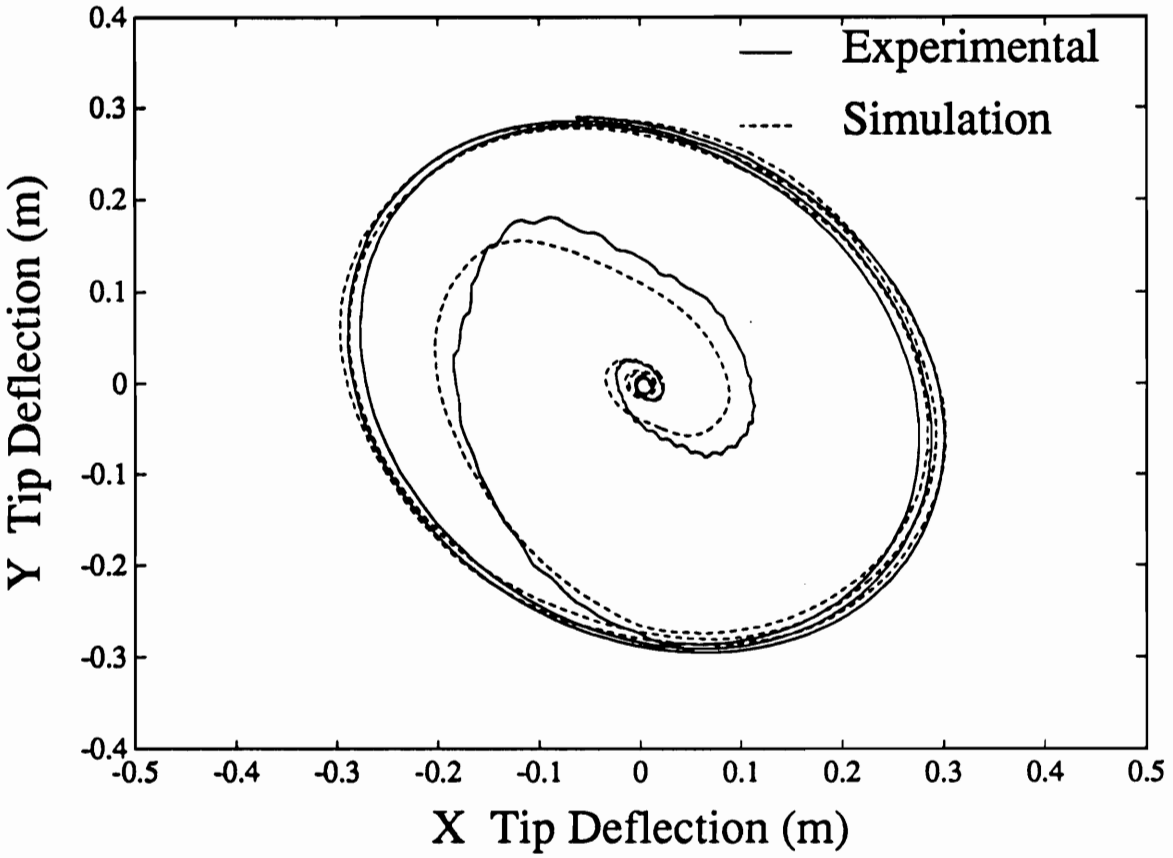

Figure 6.7: Tip Deflection Trajectory

Chapter 7

Specific Flexible Structures, Curved Beams

This chapter presents the control of curved beams using the adaptive truss. The curved beam was chosen as the test article because it is more complicated that the slender beam and because it is a way to approximate an antenna-like structure. NASA Langley Research Center is currently investigating an antenna-like structure that is part of the Evolutionary Model (Newsom, 1990). As a first step a single curved beam was used. This beam could represent one radial stay, a spoke, of the antenna. Second, two curved beams are considered, this adds more complexity to the problem and is one step closer to the antenna. Finally, four curved beams are analyzed, this case actually begins to look like an antenna. From these three cases some conclusions can be drawn about the control of antenna-like structures using an adaptive truss

7.1 A Curved Beam

The beam was cantilevered horizontally from the truss and is curved into a large deflection by the gravitational field; it is represented in Figure 7.1. The beam was

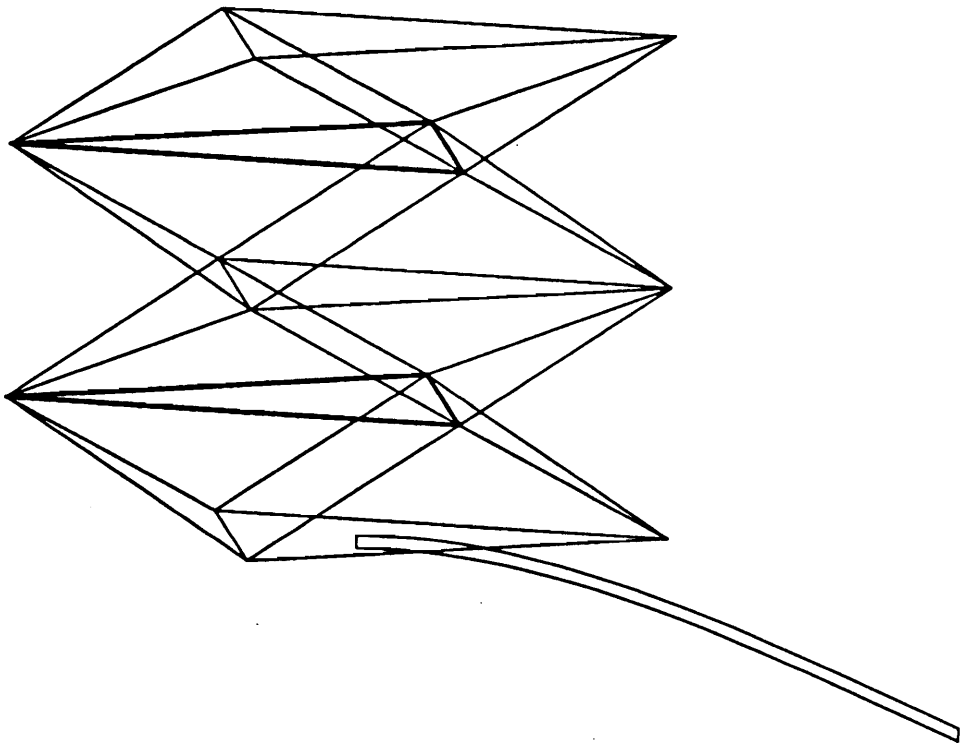

Figure 7.1: Adaptive Truss with A Single Curved Beam Attached

arranged in this manner so that when more beams were added the deflection in each beam would be the same; this provides for the "dish" shape of the antenna. An actual antenna would also have connections between the arms, this is not considered here.

The beam chosen is an aluminum strap $1" \times \frac{1}{16}" \times 57"$. The first attempt at modeling the beam was to use the variational method as presented in Section 3.1.1. However, the position vector that describes the geometric location of a differential mass element on the beam is difficult to pose and operate on because of the large deflections encountered. The curved beam's deflection did not hold to Euler-Bernoulli beam theory, (i.e. the slope was too large), and shortening of the beam was significant. Another theory was needed in order to determine the geometric relationships.

Rohde (1953) first proposed a method for calculating the large deflection of a cantilever beam with a uniform load, see Appendix B for details. Even with this relation the parametric equations of motion become too complex, so the finite element approach, Section 3.1.2, was used.

A finite element model was calculated from the gravity-deflected shape of the cantilever beam (the deflected shape was found using Rohde's equations). An 11-node, free-free model was used producing 66 degrees-of-freedom (DOF). The system was partitioned into 60 unknown DOF's and 6 known DOF's. These partitions were rearranged as in Section 3.1.2 and keeping the first three modes (first bending, first torsion, and second bending) a reduced-order model was produced.

The inclusion of this torsion mode proved to be most troublesome. For a straight beam this mode is normally higher in frequency than the second bending mode; however, due to the large deflection of the beam it is present between the first and second bending modes. Figure 7.2 shows the changes in frequencies of the first three modes as gravity is increased. As stated this mode caused some problems, the major one being that in the slender beam the first three bending modes were transduced with strain gages sensitive to bending and the modal transformation was based on bending modes. Now, a new type of mode needs to be transduced, one torsion gage was placed at the root of the curved beam and its output was used to represent the first torsional mode amplitude, (some calibration was done to determine the correct amplitude). This strain gage actually transduced all torsion modes, so the torsional mode information is slightly corrupted. For a better approximation of the torsion mode more gages could have been added and a (torsion) strain-to-(torsion) modal amplitude transformation developed.

The beam was also instrumented with three bending strain gages. The transformation from bending strain to the first three bending modes was the same type presented in Section 4.2.1. This modal transformation is for a straight beam, but proved to be acceptable.

Obviously, there is room for improvement with this experimental configuration, but it is felt that some useful knowledge has been gained. To expand on this thought different test cases were performed using the single curved beam. Table 7.1 shows a numerical comparison of open and closed loop natural frequencies and damping values for the single curved beam.

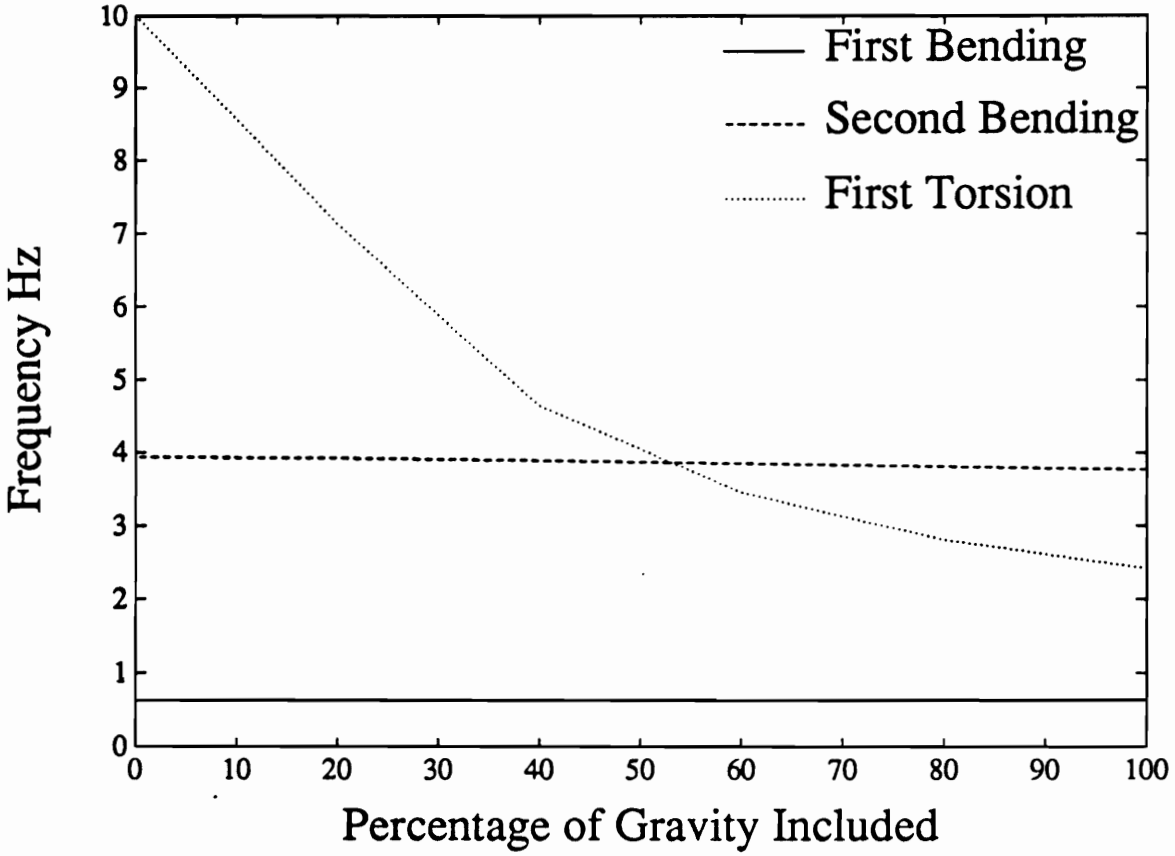

Figure 7.2: First Three Frequencies of a Horizontal Cantilever Beam as Gravity is Increased

Table 7.1: Single Curved Beam Comparison

	Open-Loop			Closed-Loop		
	Simulation	Experimental	% error	Simulation	Experimental	%error
	First Bending Mode					
ω_n	4.5497	4.6109	-1.34	4.5826	4.6223	-0.87
ζ	0.0137	0.0196	43.0	0.3729	0.3212	13.86
	First Torsion Mode					
ω_n	15.077	15.015	0.411	15.333	18.363	-19.76
ζ	0.0016	0.0018	-12.75	0.1110	0.1224	-10.2
	Second Bending Mode					
ω_n	22.757	22.569	0.826	22.832	23.130	-1.30
ζ	0.0081	0.0082	-1.23	0.0273	0.0398	-45.0

Figure 7.3 shows the control of the curved beam given a first mode-like excitation; the control begins at about 1.5 seconds and is shown in Figure 7.4. The high frequency components that are generated in the experimental data in both the modal amplitude and the motor voltage is believed to be from the strain transformation, because the coefficients for a straight beam were used. The simulation seems to have slightly less damping than the experimental case in the open-loop part (before 1.5sec) and slightly more damping in the closed-loop part. Since the damping value in the model is derived from experimental data, the open-loop difference is just an error. The closed-loop discrepancy is not well understood. The motor voltage shows that higher frequency modes exist in the experimental data that in the simulated data, which could explain the closed-loop damping differences; if more energy is in the experimental data than is in the simulated data, the simulated data would have a higher damping ratio.

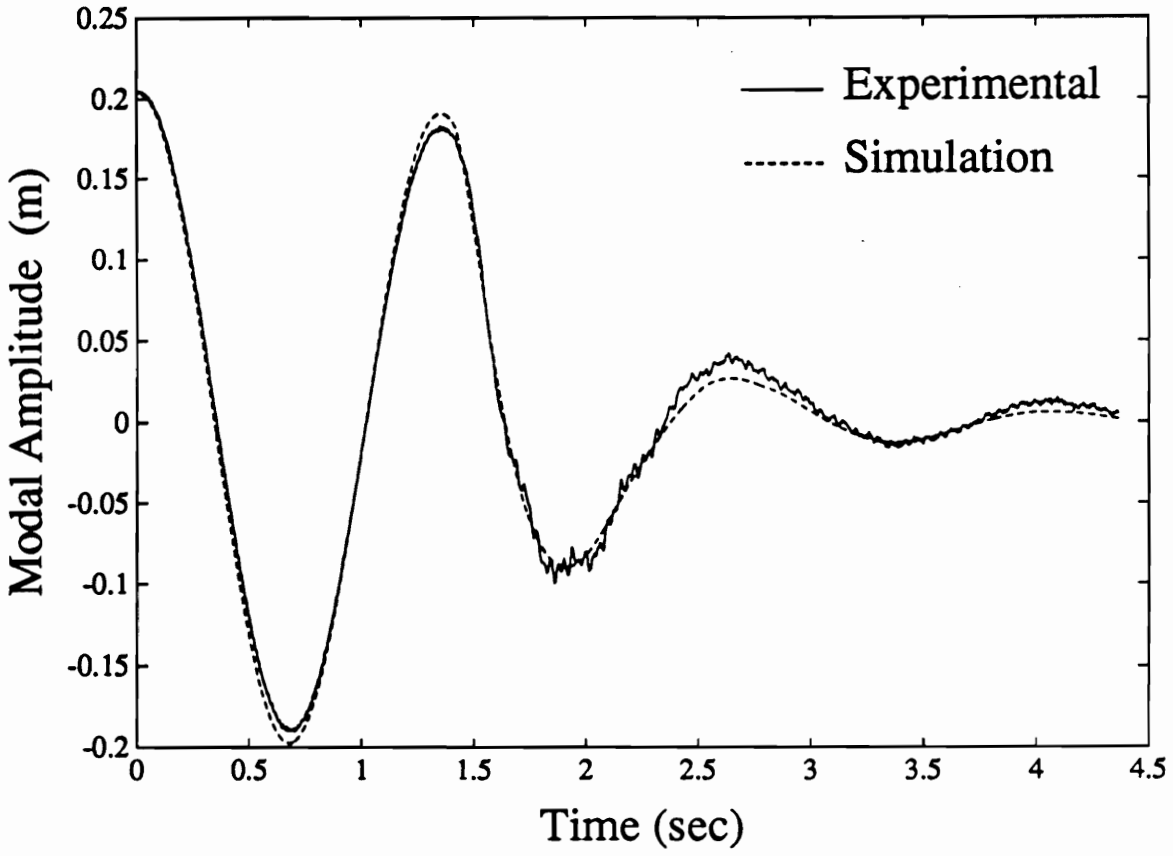

Figure 7.3: One-Beam Case: First Bending Mode, Controlled Response, Modal Amplitude

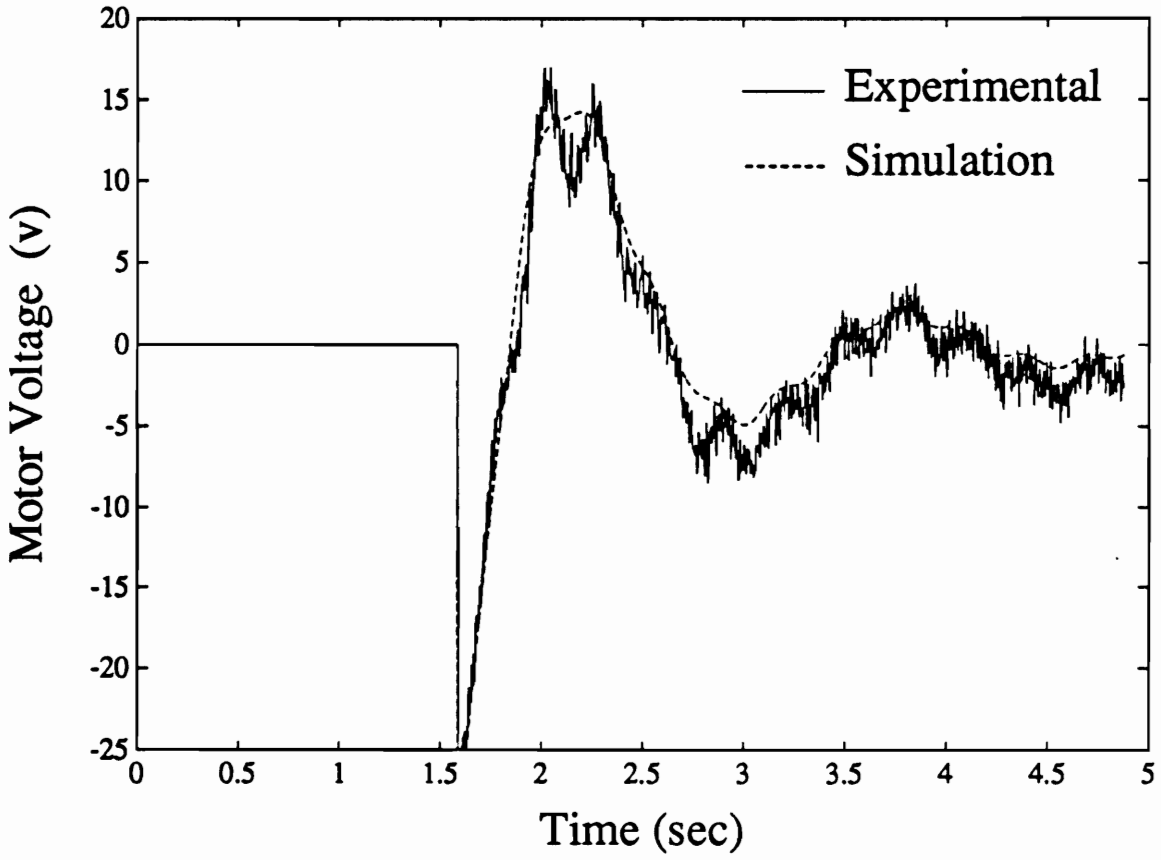

Figure 7.4: One-Beam Case: First Bending Mode, Controlled Response, Motor Voltage

Figure 7.5 shows initial condition control of the first torsion mode of the curved beam. The excellent control capabilities of the adaptive truss can be seen. The differences in the simulated and experimental data are presumed to be due to the single gage strain transformation, discussed above. This is the first occurance in this work where the simulated and experimental data disagree drastically. The motor voltage, Figure 7.6 also shows these differences, which is natural since the voltage is calculated primarily based on the modal amplitudes.

Figure 7.7 presents a third mode (second bending mode) excitation with very good agreement shown. There seems to be some higher frequency components in the second mode amplitude, this indicates that the strain transformation is slightly incorrect, but notice that this only occurs for the closed-loop portion of the data. The transformation was developed for the uncurved beam.

Although the agreement between the simulations and the experiments was not as good for the curved beam as in the slender beam studies, the results were encouraging. The main discrepancies seem to lie in the transformations from strain to modes. Next, the control of two curved beams is discussed.

7.2 Two Curved Beams

Two curved beams were attached to the adaptive truss as shown in Figure 7.9 and a finite-element model developed. The beams have no interaction except through the base of the truss, which, for the analysis, is assumed to not allow this interaction. This interaction was observed to be small in the experimental setup . However, real structures would most likely have other connections between the beams. For exam-

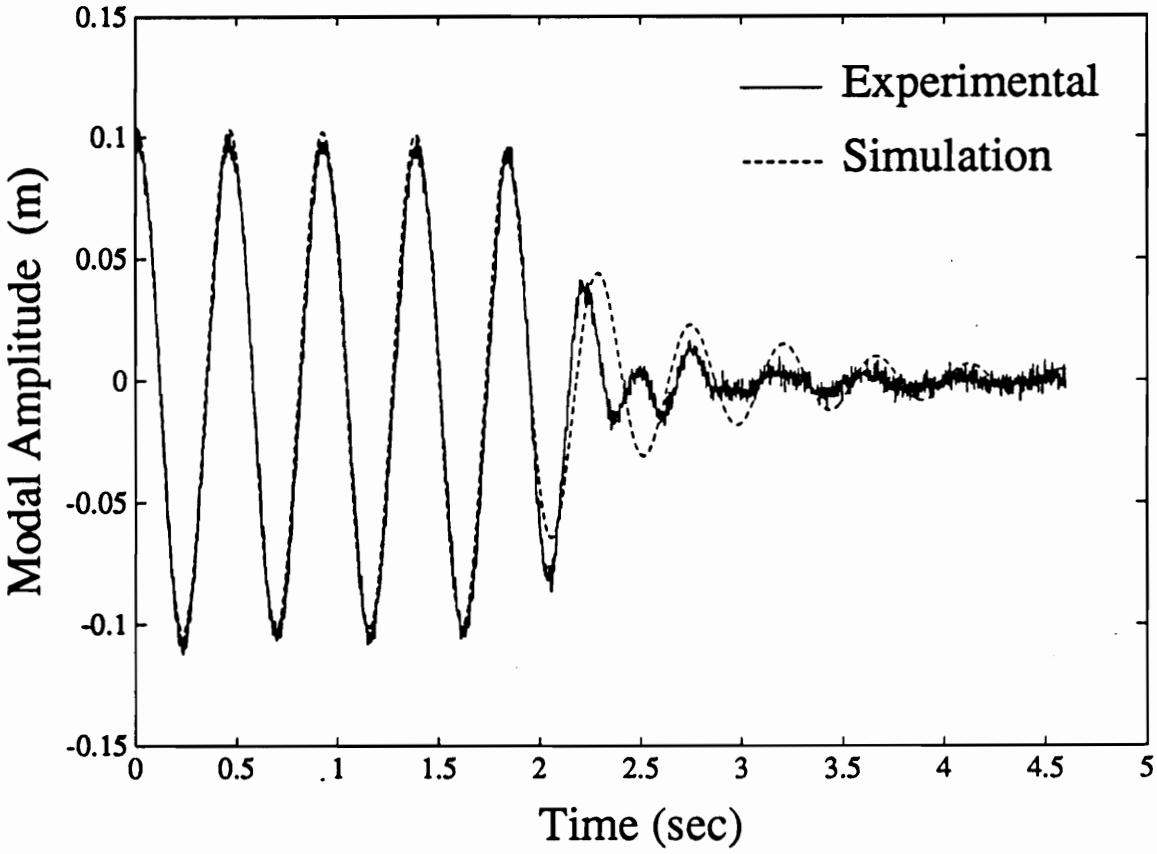

Figure 7.5: One-Beam Case: First Torsion Mode, Controlled Response, Modal Amplitude

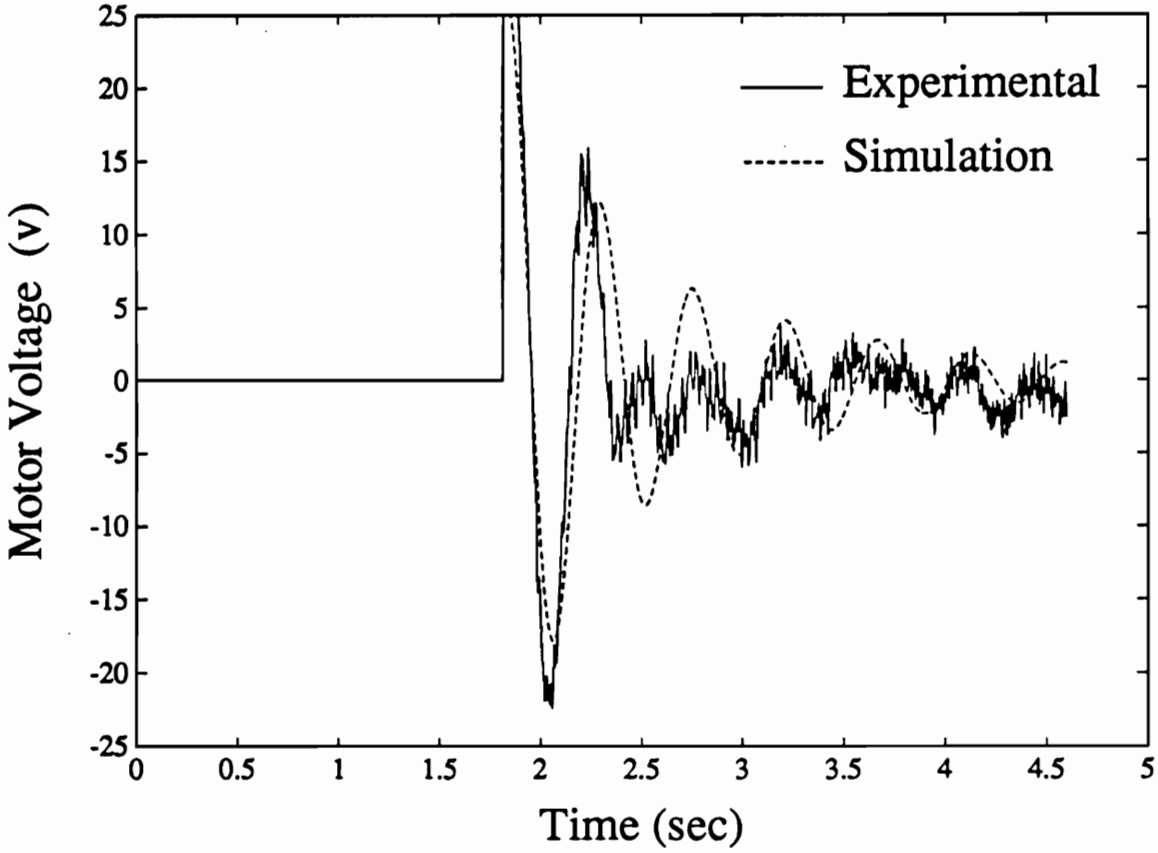

Figure 7.6: One-Beam Case: First Torsion Mode, Controlled Response, Motor Voltage

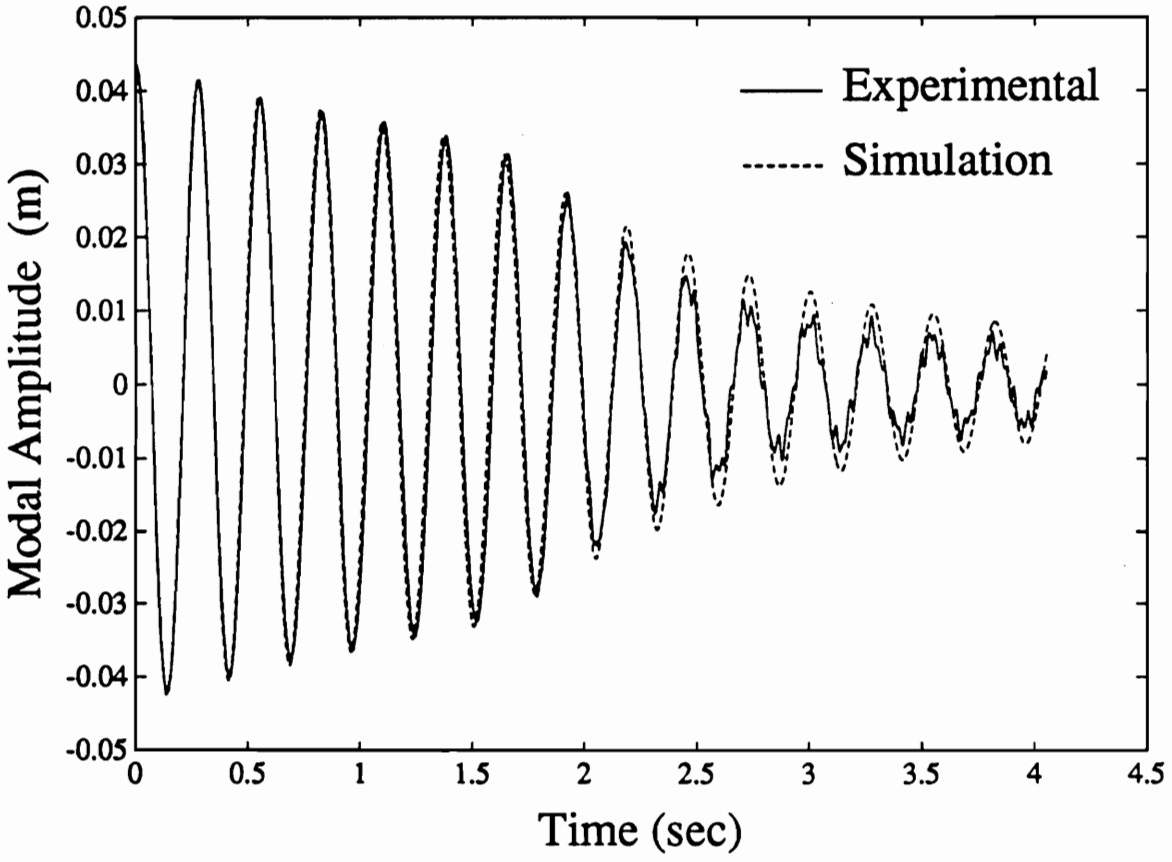

Figure 7.7: One-Beam Case: Second Bending Mode, Controlled Response, Modal Amplitude

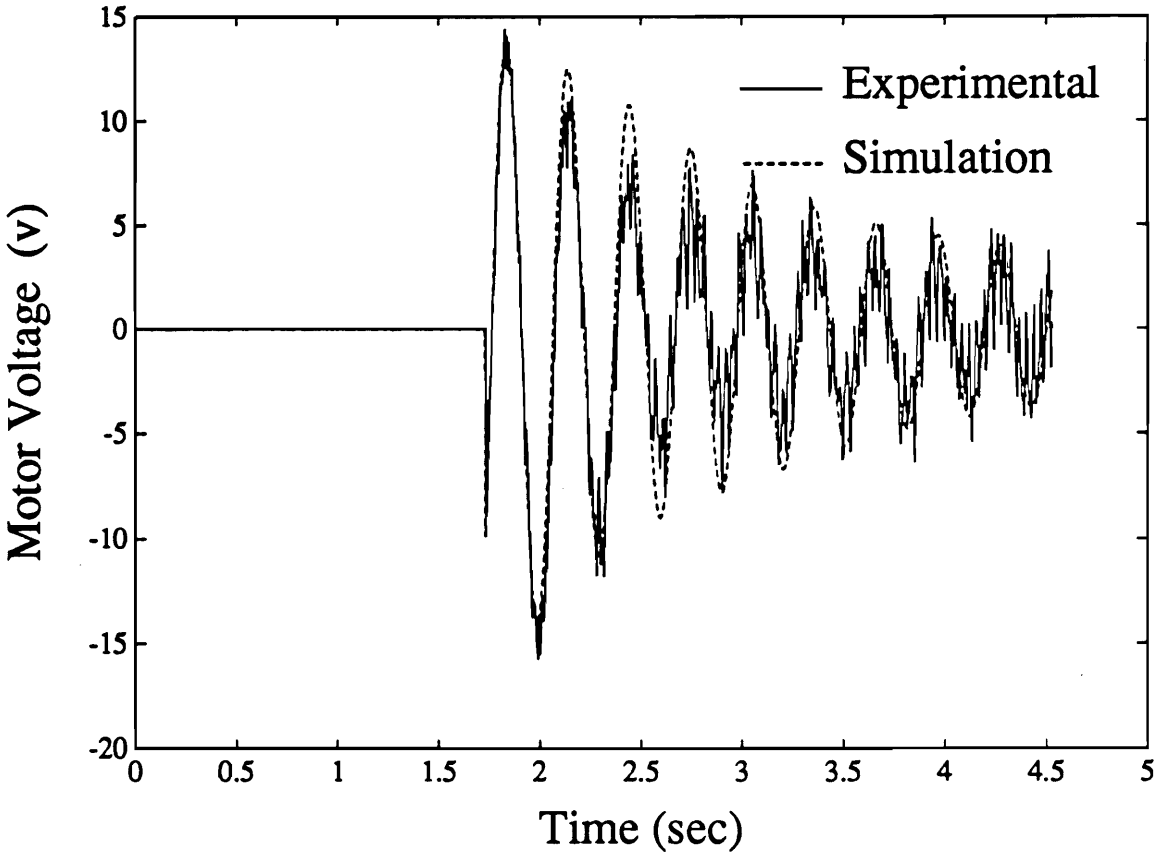

Figure 7.8: One-Beam Case: Second Bending Mode, Controlled Response, Motor Voltage

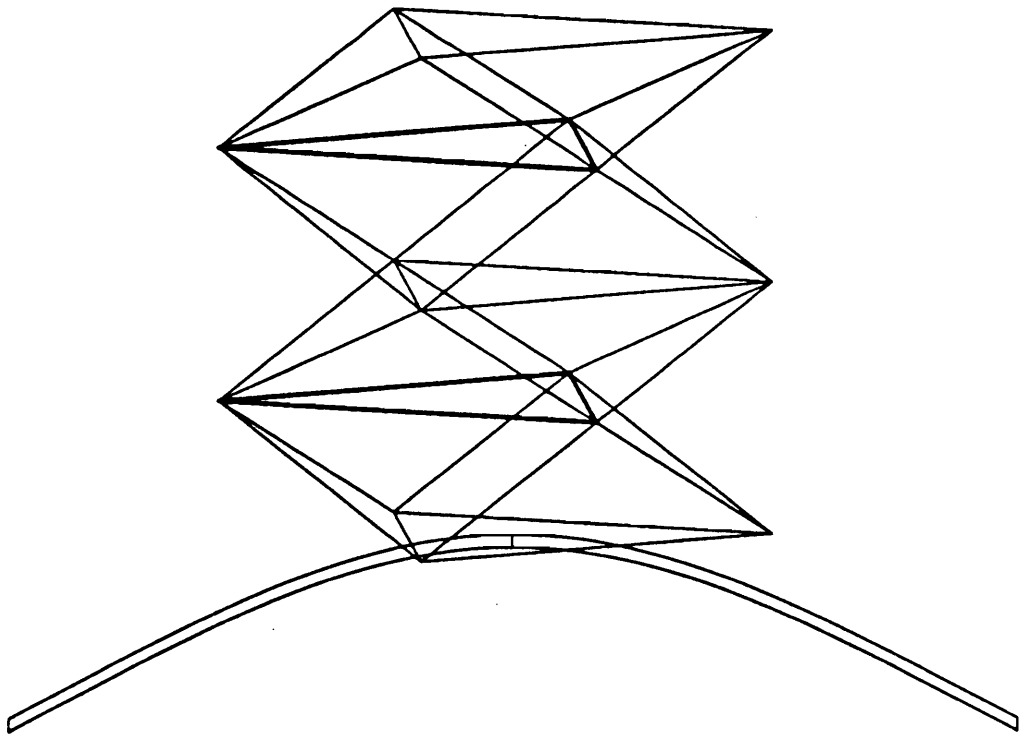

Figure 7.9: Adaptive Truss with Two Curved Beams Attached

ple, the antenna on the Evolutionary Model has wire connections at the tip of the beams. The added connections may make the problem easier to control, because of the coupling. The difficulty with the two-beam case is that the beams are in the same plane and motion to control one beam will cause the second beam to be excited. This is shown in the plots that follow.

Table 7.2 shows a numerical comparison of open and closed loop natural frequencies and damping values for the two curved beam configuration.

Table 7.2: Two Curved Beams Comparison

	Open-Loop			Closed-Loop		
	Simulation	Experimental	% error	Simulation	Experimental	%error
	First Bending Mode Beam 1 in-phase					
ω_n	4.59	4.60	-0.22	4.61	4.91	-6.5
ζ	0.022	0.020	9.1	0.024	0.021	12.5
	First Bending Mode Beam 2 in-phase					
ω_n	4.63	4.61	0.43	4.60	4.59	0.22
ζ	0.020	0.020	0.0	0.027	0.025	7.4
	First Bending Mode Beam 1 out-of-phase					
ω_n	4.59	4.61	-0.44	5.29	5.24	0.95
ζ	0.022	0.022	0.0	0.52	0.48	7.7
	First Bending Mode Beam 2 out-of-phase					
ω_n	4.63	4.64	-0.22	5.47	5.3	3.1
ζ	0.020	0.019	5.0	0.528	0.42	20.5

As in the single-beam studies the system was modeled with a finite-element approach and a partial state-feedback gain set derived with the LQR procedure. The following results were obtained. Figure 7.10 shows the controlled response to in-phase, first-mode deflections; Figure 7.13 shows the controlled response to out-of-phase first-mode deflections of the two curved beams. Figure 7.12 and Figure 7.15 show

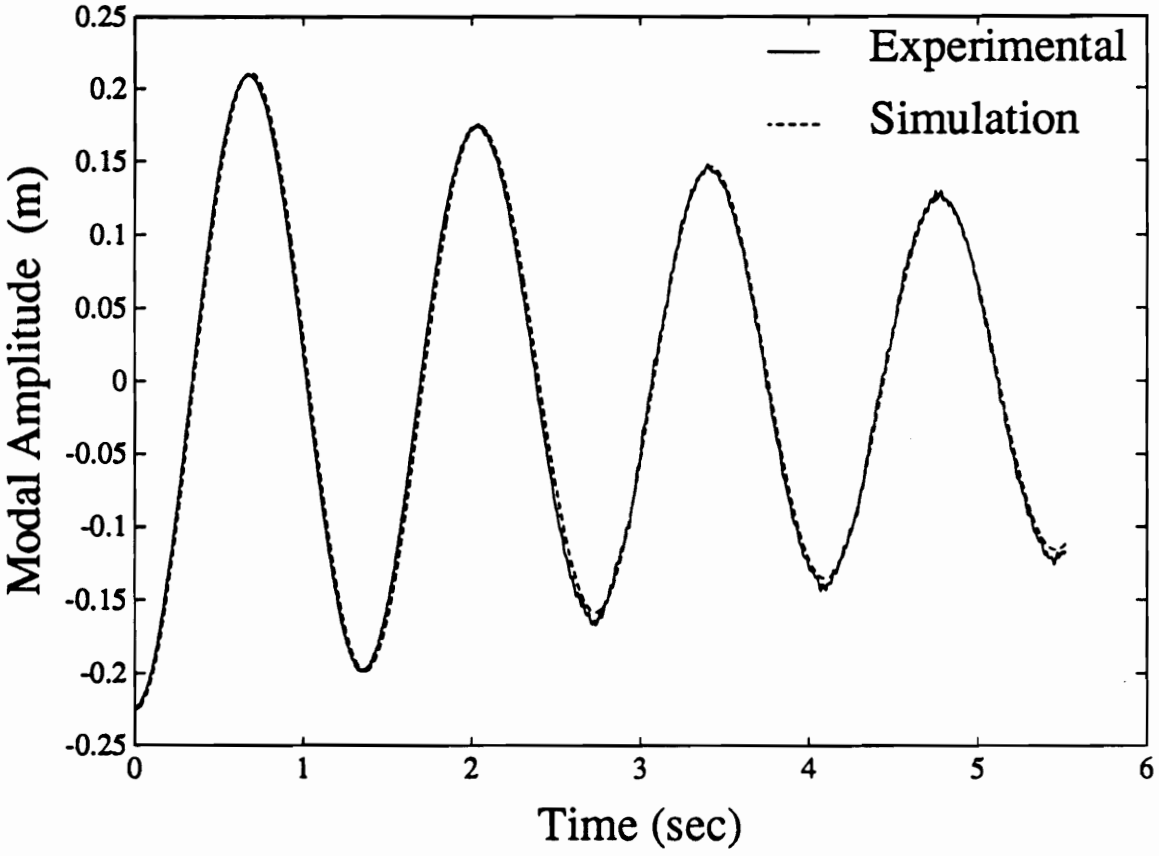

Figure 7.10: Two-Beam Case: First Bending Mode, Controlled Response, Modal Amplitude Beam 1 (in phase)

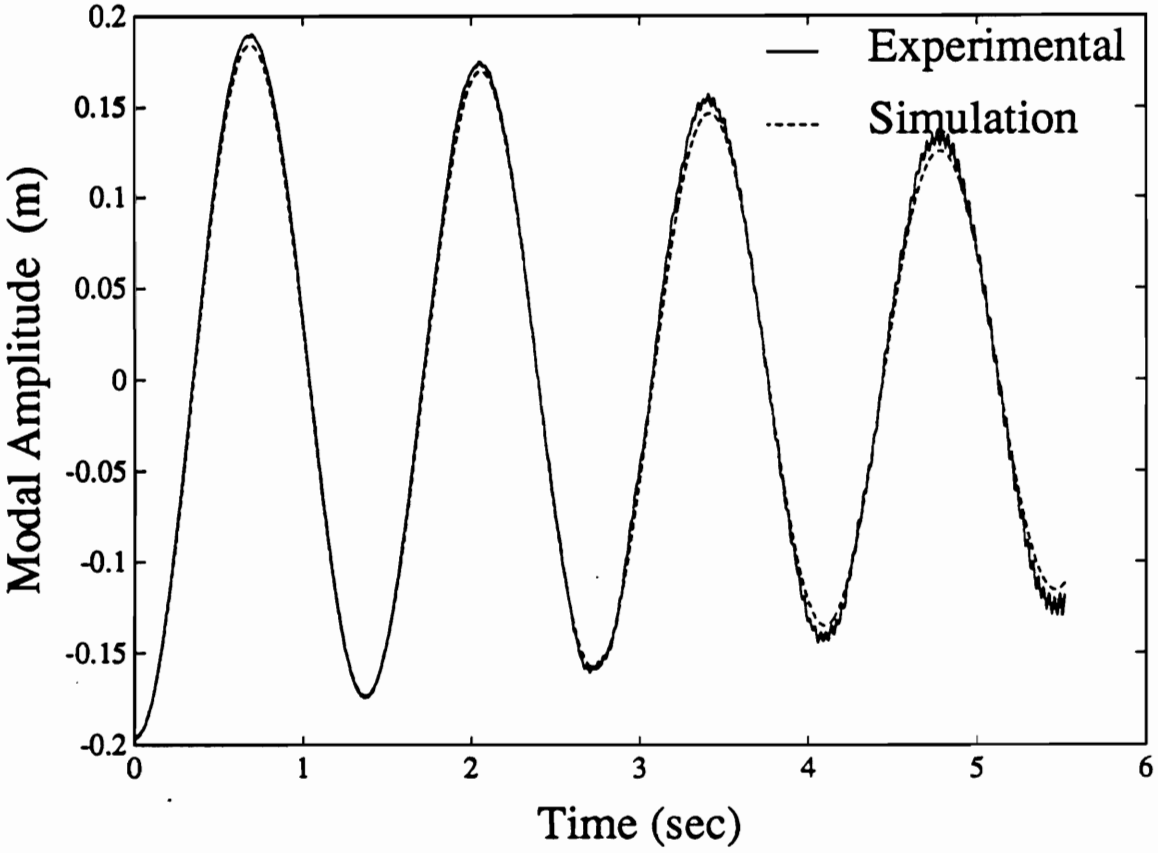

Figure 7.11: Two-Beam Case: First Bending Mode, Controlled Response, Modal Amplitude Beam 2 (in phase)

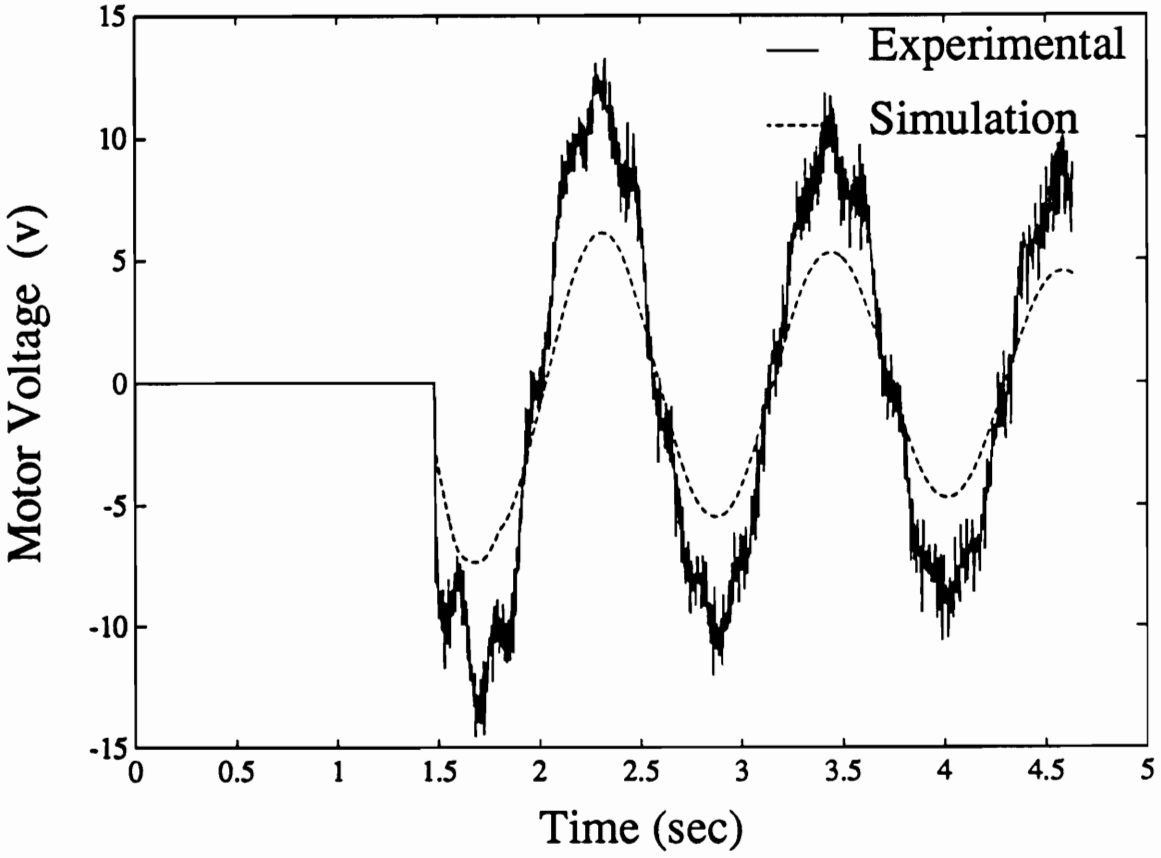

Figure 7.12: Two-Beam Case: First Bending Mode, Controlled Response, Motor Voltage (in phase)

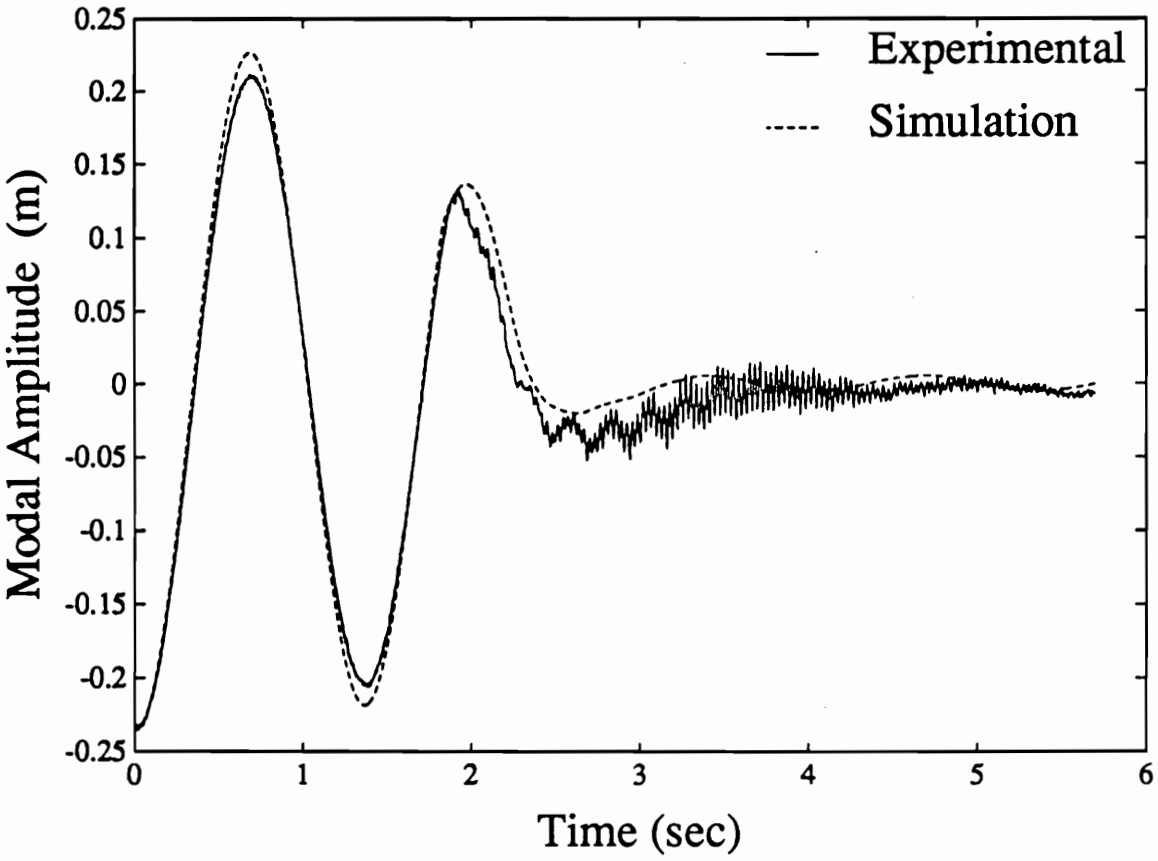

Figure 7.13: Two-Beam Case: First Bending Mode, Controlled Response, Modal Amplitude Beam 1 (out of phase)

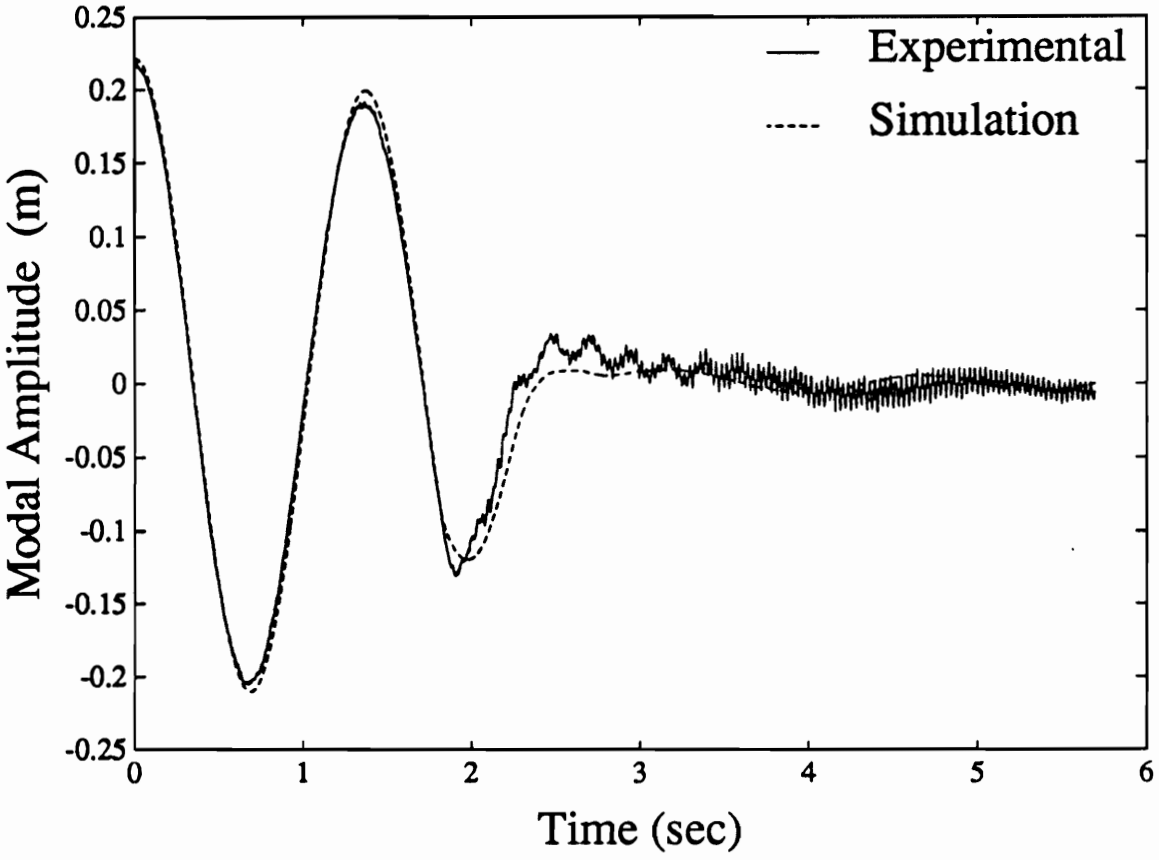

Figure 7.14: Two-Beam Case: First Bending Mode, Controlled Response, Modal Amplitude Beam 2 (out of phase)

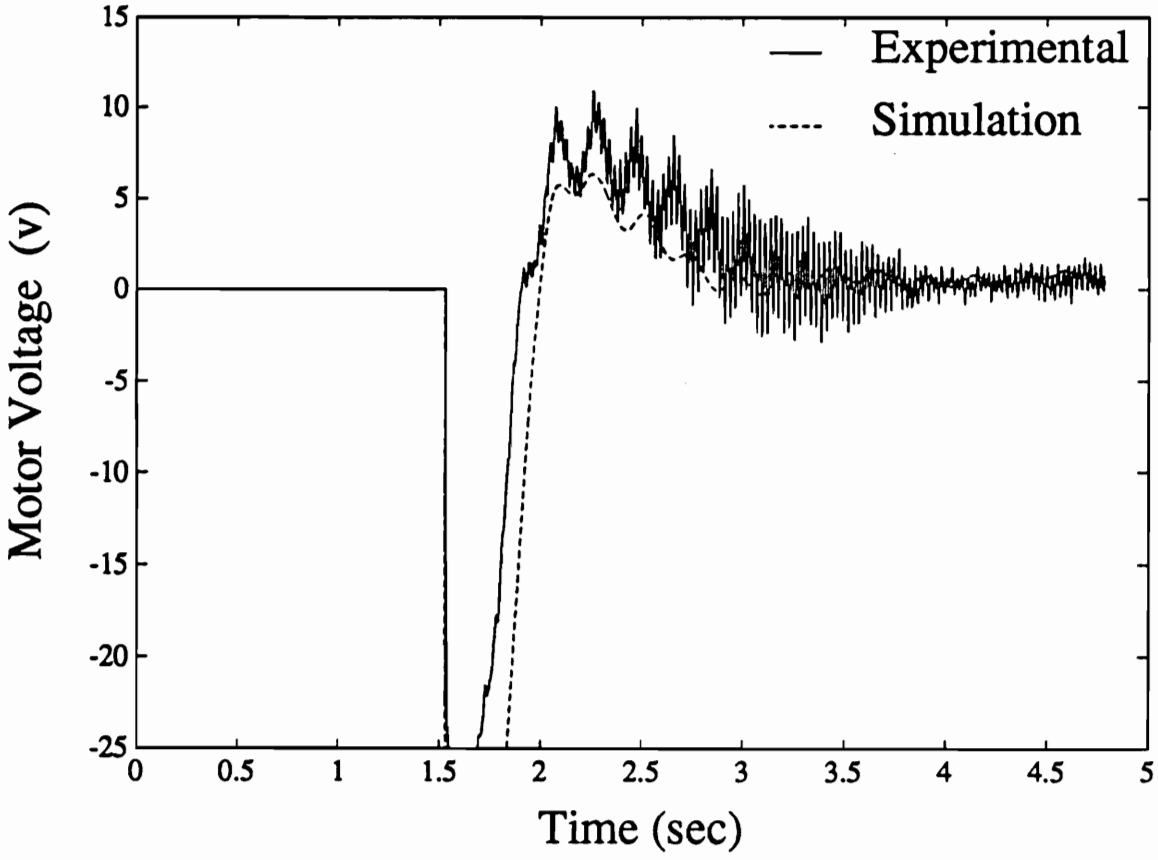

Figure 7.15: Two-Beam Case: First Bending Mode, Controlled Response, Motor Voltage (out of phase)

the corresponding characteristic motor voltages.

There is a significant difference between the ability of the truss to control first mode excitations, for different relative phases between the beams. In the out-of-phase case; the truss primarily rotates about the α axis whereas in the in-phase case the motion is mostly in the z direction. This highlights the different magnitude of mechanical advantages that the adaptive truss has; in the nominal configuration used, the active battens had much more authority over the α motion than the z motion. As in the single beam case some higher frequency components show up in the controlled response of the first modal amplitude. It is more prevalent in the out-of-phase case this is thought to be due to change in the angle of the base of the truss. This causes a more severe change in the modal properties than does the up and down motion of the in-phase case.

Figure 7.16 shows in-phase, second-mode (torsion) excitation of the two beams, Figure 7.18 shows the motor voltage. The truss does a very poor job of controlling this mode. A second mode-like excitation for beam 1 and no initial condition for beam 2 is shown in Figure 7.19. This shows how the adaptive truss puts the energy from one beam into the other while control is being performed. As was seen in single beam study, the torsion mode model is not as accurate as the bending mode models.

The data for the two-beam case seems to be leading us towards some type of conclusion about what type of structures the adaptive truss is capable of controlling. Structures that do not appear to be controllable are those that require γ rotation, torsion mode, and those that require z translation, in-phase bending. As a final

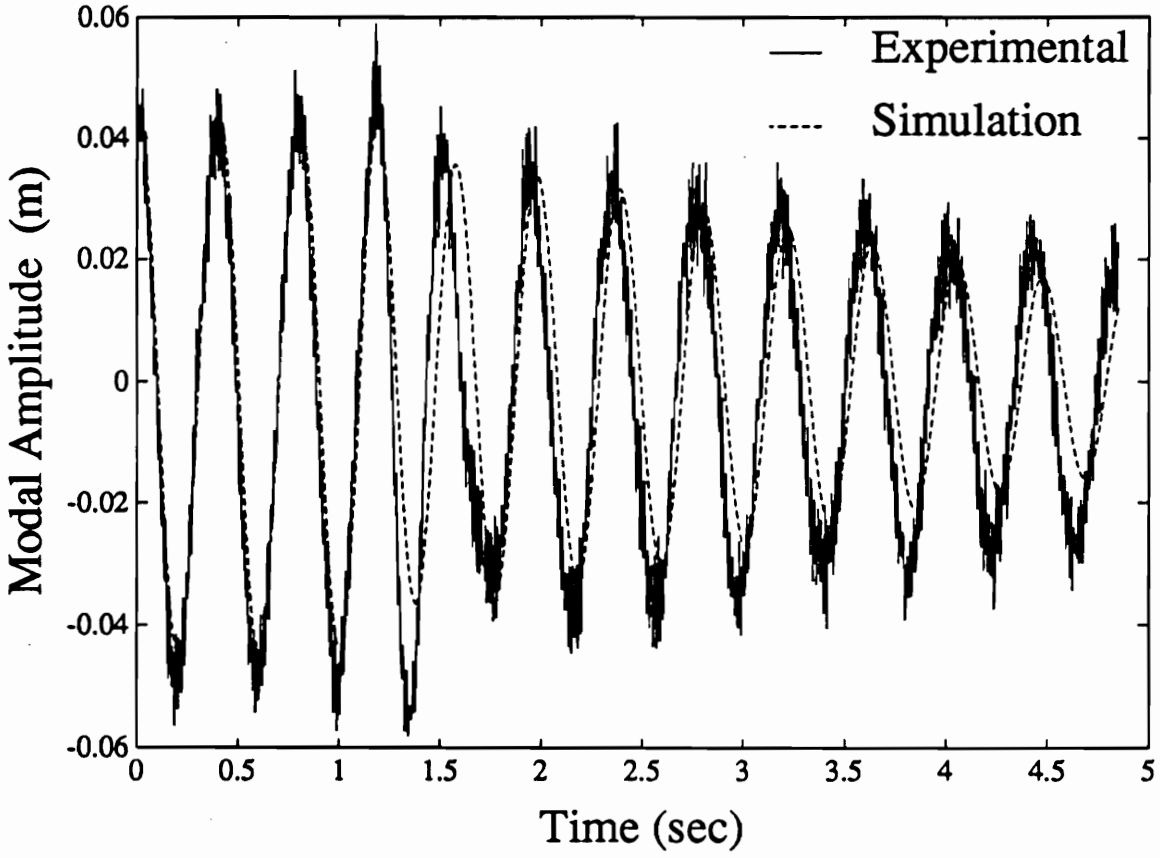

Figure 7.16: Two-Beam Case: First Torsion Mode, Controlled Response, Modal Amplitude Beam 1 (in phase)

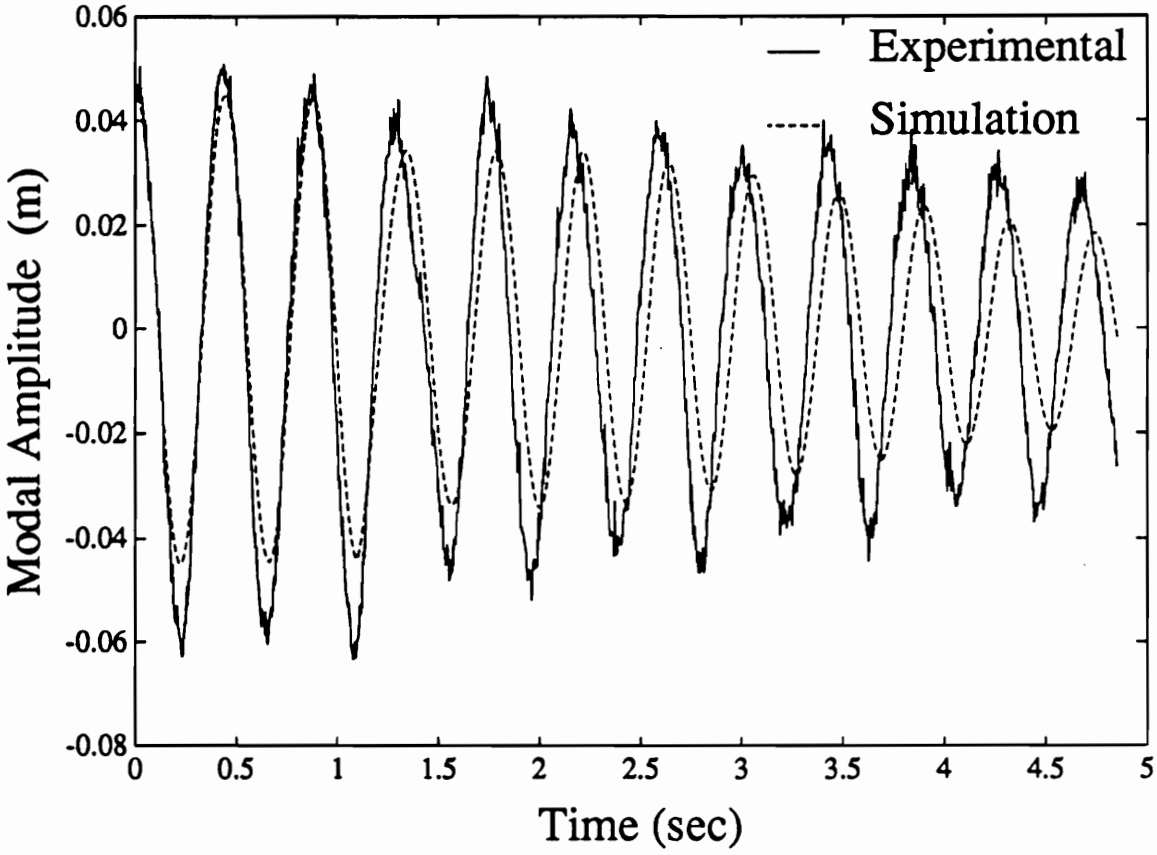

Figure 7.17: Two-Beam Case: First Torsion Mode, Controlled Response, Modal Amplitude Beam 2 (in phase)

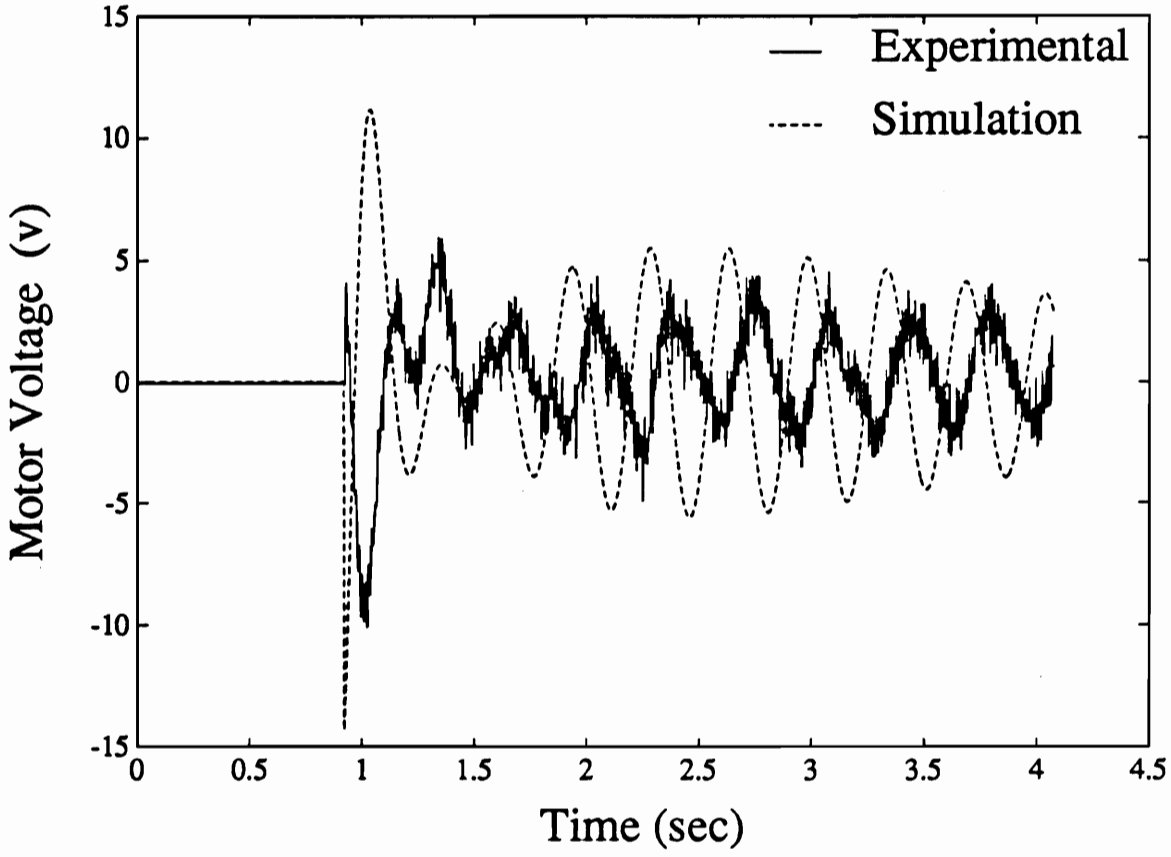

Figure 7.18: Two-Beam Case: First Torsion Mode, Controlled Response, Motor Voltage (in phase)

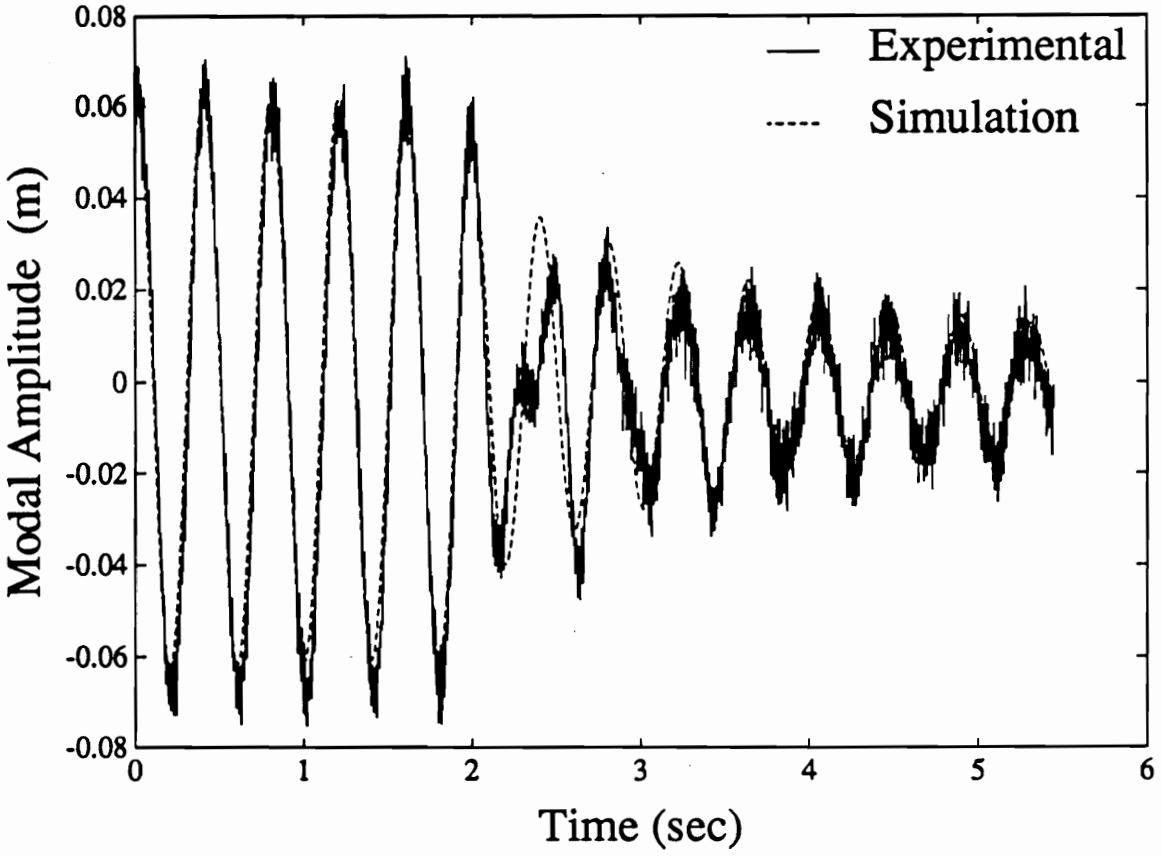

Figure 7.19: Two-Beam Case: First Torsion Mode, Controlled Response, Modal Amplitude Beam 1

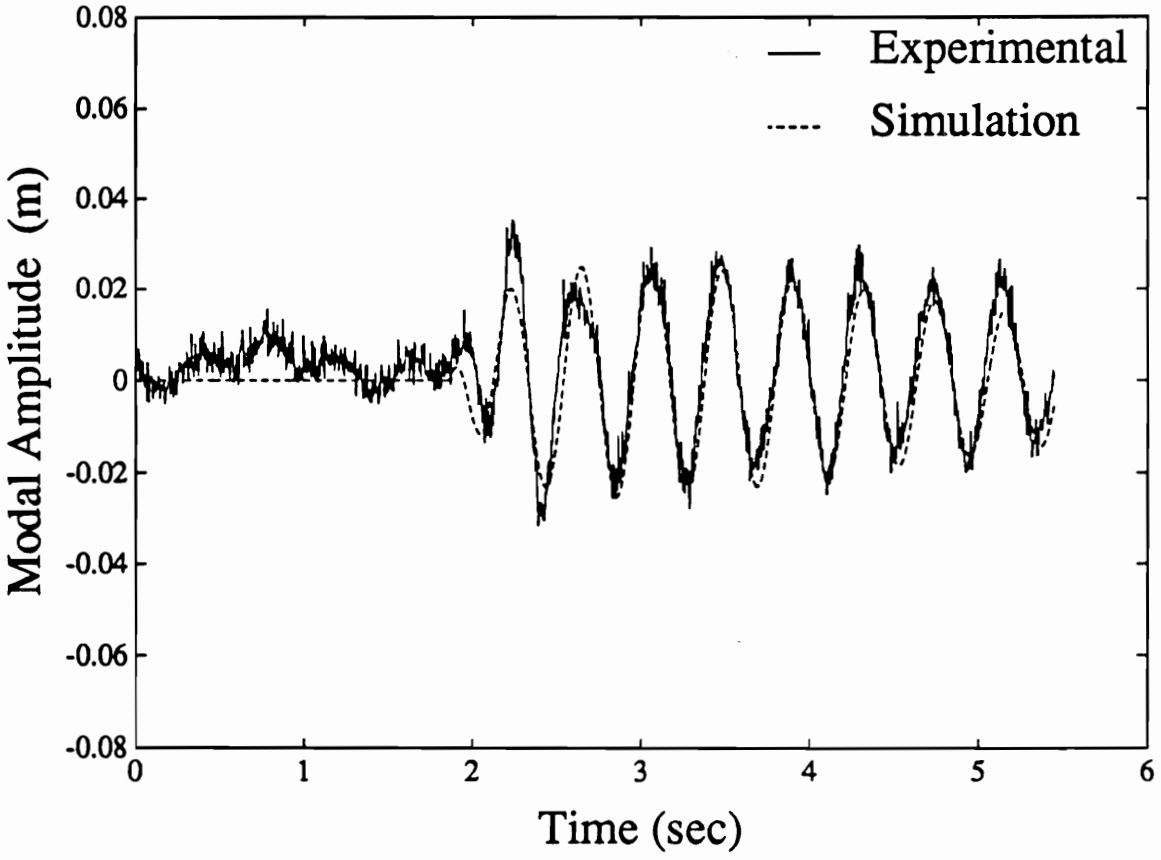

Figure 7.20: Two-Beam Case: First Torsion Mode, Controlled Response, Modal Amplitude Beam 2

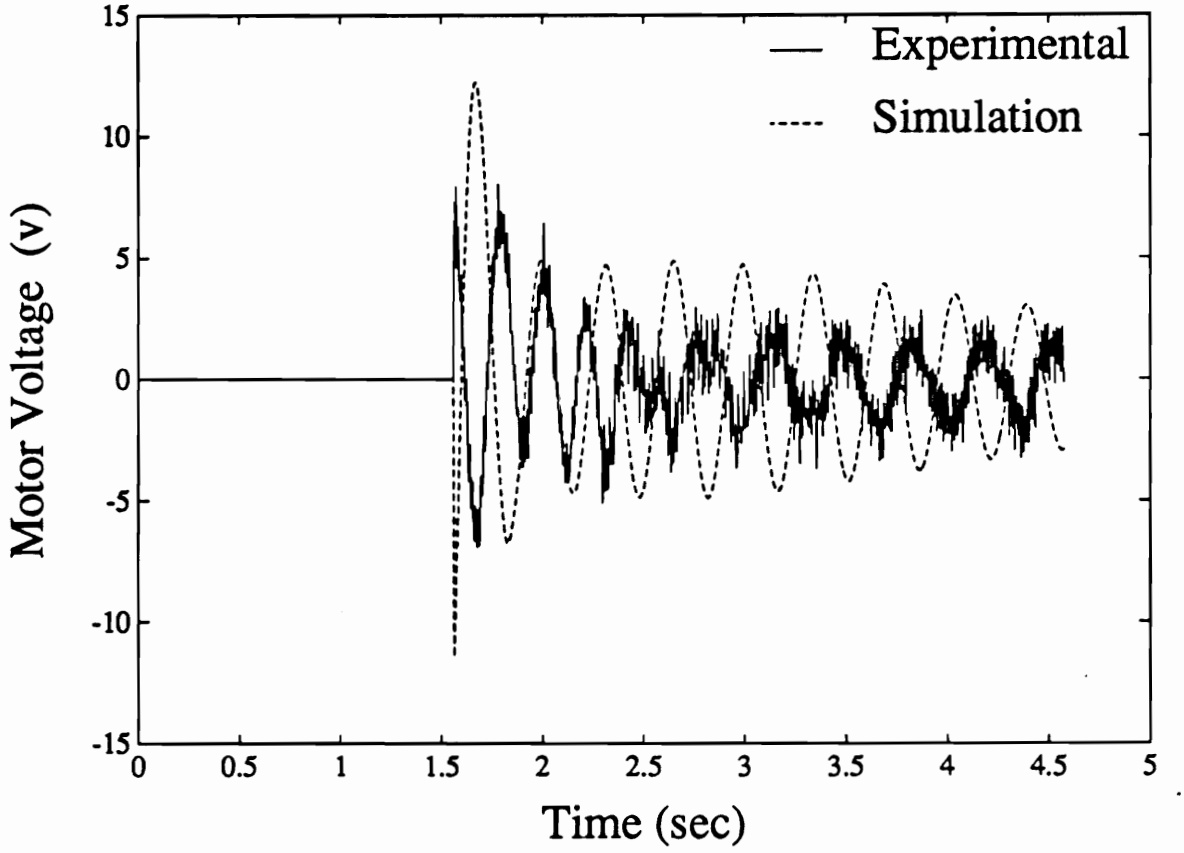

Figure 7.21: Two-Beam Case: First Torsion Mode, Controlled Response, Motor Voltage

check a four-beam case is analyzed.

7.3 Four Curved Beams

A four-beam structure is fairly representative of a antenna-like structure. It possesses the type of modal parameters of interest, "dish" like modes, repeated modes and antisymmetric modes. For these reasons, a four-beam model was derived for an analytical investigation. The model proved to be uncontrollable. This can be seen, intuitively, by imagining a first mode deflection with beams 1 and 3, having a positive deflection (see Figure 7.22 for the numbering scheme), and beams 2 and 4 having the same magnitude, but negative displacement. The only linear control effort that can effect all beams is a z translation, but beams 2 and 4, say, go up while beams 1 and 3 go down; thus causing cancellation of control for a linear analysis.

The uncontrollability of this configuration helps explain what the adaptive truss can and can not control. This insight is discussed in the conclusion chapter.

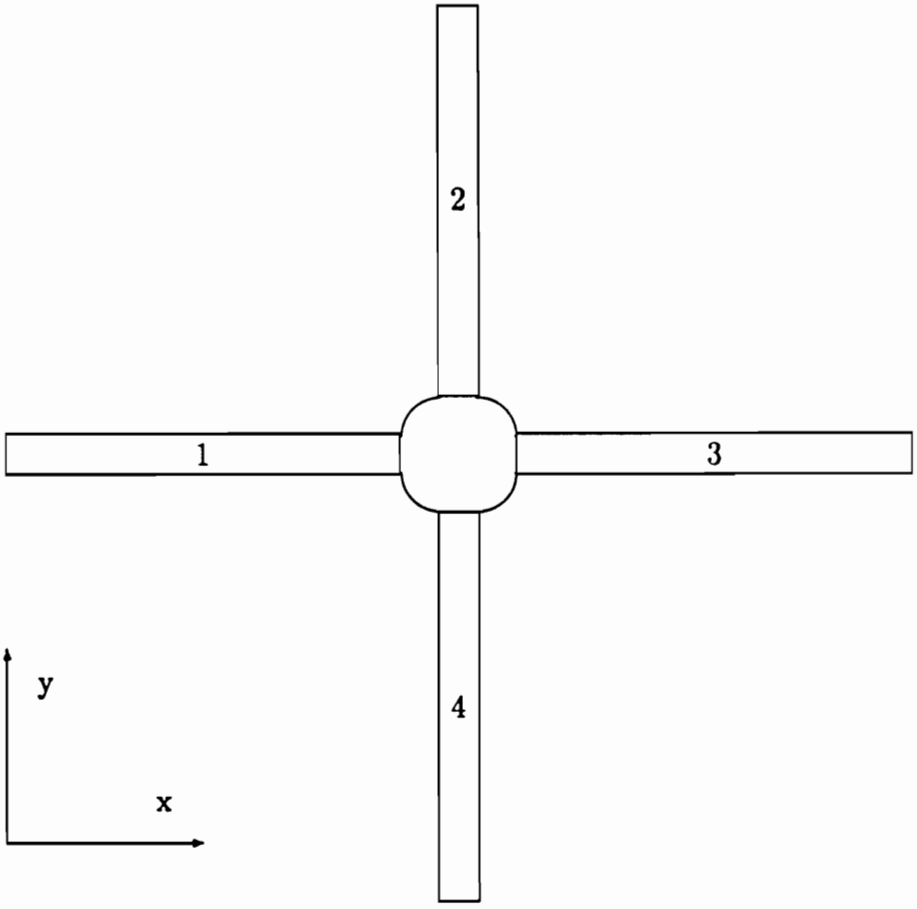

Figure 7.22: Numbering Scheme for Four-Beam Case

Chapter 8

Conclusions

The control of flexible structure vibrations using a cantilevered truss has been demonstrated. The adaptive truss at VPI&SU has been used successfully to control three flexible structures; a slender beam, a curved beam, and two curved beams. Modeling methods, simulation techniques, and experimental concerns that pertain to the adaptive truss have been presented and validated. This work has advanced the state of the art in control of flexible structures using a adaptive truss.

This work has also shown that the adaptive truss is not capable of controlling the four beam configuration. This flexible structure needs more than one actuator location in order to be controllable.

Some improvements could be made to this procedure for the control of flexible structures with the adaptive truss, these include;

- Model the truss dynamics (flexibility and mass), this will only be important if the structure is approximately the same or greater weight as the truss.
- Model the coupling between the truss and the flexible structure. As seen from

the two curved beam problem there is some interaction between the beams that is not shown in the finite-element model.

- Include more (torsional) strain gages for the curved beam case and develop a (torsional) strain to (torsional) mode transformation.

There is much more work that could be done with the adaptive truss; including disturbance rejection, controlling massive structures, slewing and pointing control, as well as robotic tasks. It is believed that this contribution will expand the knowledge of control of flexible structures using a cantilevered adaptive truss and help those fellow engineers who decide to pursue its usefulness.

List of References

1. **Aviation Week & Space Technology**, McGraw-Hill, June 18, 1990

2. Clark, W. W., "A Planar Comparison of Actuators for Vibration Control of Flexible Structures," Masters Thesis, Virginia Polytechnic Institute and State University, May, 1988.

3. Clark, W. W., Robertshaw, H. H., and Warrington, T. J., "A Planar Comparison of Actuators for Vibration Control of Flexible Structures," *Structures, Structural Dynamics and Materials Conference, 30th*, Mobile, AL, April 1989, AIAA Paper 89-1330-CP.

4. Clark,W.W., Robertshaw,H.H., and Warrington,T.J., "A Comparison of Actuators for Vibration Control of the Planar Vibrations of a Flexible Cantilevered Beam," Accepted for the *Journal of Intelligent Material Systems and Structures*, Technomics Press, October 1990.

5. Craig, J. J., **Introduction to Robotics Mechanics and Control,** Addison-Wesley Publishing Company, 1986.

6. Electro-Craft Corporation, **DC Motors Speed Controls Servo Systems,** Library of Congress Card Number 78-61244, 1980.

7. Fanson, J. L., Blackwood, G. H. and Chu, C.-C., "Active Member Control of

Precision Structures," *Structures, Structural Dynamics and Materials Conference,* 30^{th}, Mobile, AL, April 1989, AIAA Paper 89-1329-CP.

8. Hallauer, W. L. Jr., Lamberson, S.E., "Experimental Active Vibration Damping of a Plane Truss Using Hybrid Actuation," *Structures, Structural Dynamics and Materials Conference,* 30^{th}, Mobile, AL, April 1989, AIAA Paper 89-1169-CP.

9. Hurty, W. C., Rubinstein, M. F., **Dynamics of Structures,** Prentice-Hall Englewood Cliffs, New Jersey, 1964.

10. Juang, J.-N., Horta, L. G., Robertshaw, H. H., "A Slewing Control Experiment for Flexible Structures," *Journal of Guidance, Control, and Dynamics*, Volume 9, Number 5, September-October 1986.

11. Kung,H.-F., "Dynamics and Control of a Spatial Truss Actuator", Masters Thesis, Virginia Polytechnic Institute and State University, May, 1988.

12. Laskin, R. A., "A Spaceborne Imaging Interferometer - The JPL CSI Mission Focus," presented an the Third NASA/DOD Controls Structures Interaction Technology Conference, San Diego, CA, Jan 29- Feb 2, 1989.

13. Little, J. N., Laub, A. J., "Control System Toolbox, for use with MATLAB," The MAthworks, Inc., 1896.

14. Lovejoy, V. D., Robertshaw, H. H., Patten, W. W. and Horner, C. G., "Dynamics and Control of a Planar Truss Actuator," *Vibration Control and Active Vibration Suppression*, D.J. Inman, Ed., DE-Vol. 4, ASME, Sept. 1987.

15. Lu, L. Y., Utku, S., and Wadda, B.K., "Location Selection for Vibration Controllers on Space Crane as Adaptive Structures," *Structures, Structural Dynamics and Materials Conference,* 31st, Long Beach, CA, April 1990, AIAA Paper 90-1167-CP.

16. Newsom, J. R., Layman, W. E., Waites, H. B., and Hayduk, R. J., "The NASA Controls-Structures Interaction Technology Program", 41st *Congress of the International Astrotautical Federation* Dresden, GDR, October 6-12, 1990.

17. Popov, E. P. **Mechanics of Materials**, Prentice-Hall Englewood Cliffs, New Jersey, 1976.

18. Preumont, A., Sparavier, M., Dufour, J., "Application of Piezoelectric Actuators to the Active Damping of a Truss Structure," *Structures, Structural Dynamics and Materials Conference,* 31st, Long Beach, CA, April 1990, AIAA Paper 90-0950-CP.

19. Reddy, J. N., **An Introduction to the Finite Element Method**, McGraw-Hill Book Company, 1984.

20. Reinholtz, C. F. ,Tidwell, P. T., Robertshaw, H. H., and Horner, C. G., "Kinematic Analysis of Generalized Adaptive Trusses," accepted for the First Joint US/Japan Conference on Apaptive Structures, November 1990.

21. Rhodes, M.D., and M.M. Mikulas, "Deployable Controllable Geometry Truss Beam," NASA Technical Memorandum 86366, June 1985.

22. Robertshaw, H. H., Wynn R. H.,Jr., Kung, H.-F., Hendricks, S. L., and Clark, W. W., "Dynamics and Control of a Spatial Active Truss Actuator," *Struc-*

tures, Structural Dynamics and Materials Conference, 30^{th}, Mobile, AL, April 1989, AIAA Paper 89-1328-CP.

23. Rohde, F.V., "Large Deflections of Cantilever Beams with Uniformly Distributed Load," *Q. Appl. Math*,11,337-338 (1953).

24. Thomson, W. T., **Theory of Vibration with Applications**, Prentice-Hall Englewood Cliffs, New Jersey, 1981.

25. Wada, B.K., "Adaptive Structures", *Structures, Structural Dynamics and Materials Conference,* 30^{th}, Mobile, AL, April 1989, AIAA Paper 89-1160-CP.

26. Warrington, T. J., Horner, C. G., "Flexible Beam Control Using an Adaptive Truss," Proceedings of the 1990 American Controls Conference, Vol. 1, pp 340-349.

27. Warrington, T. J., Clark, W. W., Robertshaw, H. H., and Horner, C. G., "The Analysis and Contol of Large-Angle Slewing of a Flexible Beam Using an Adaptive Truss,", submitted to the *Structures, Structural Dynamics and Materials Conference,* 32^{nd}, Baltimore, MD, April 1991.

28. Wynn, R. H.,Jr., Robertshaw, H. H., and Horner, C. G., "An Analytical Study of a Six Degree-of-Freedom Active Truss for Use in Vibration Control," *Structures, Structural Dynamics and Materials Conference,* 31^{st}, Long Beach, CA, April 1990, AIAA Paper 90-1164-CP.

Appendix A

Integrals for Slender Beam

$$I_i = \int_0^L \phi_i{}^2\, dx \qquad i = 1, ..., 6$$

$$I_7 = \int_0^L \phi_1\, \phi_2\, dx = 0$$

$$I_8 = \int_0^L \phi_2\, \phi_3\, dx = 0$$

$$I_9 = \int_0^L \phi_1\, \phi_3\, dx = 0$$

$$I_{10} = \int_0^L \phi_4\, \phi_5\, dx = 0$$

$$I_{11} = \int_0^L \phi_5\, \phi_6\, dx = 0$$

$$I_{12} = \int_0^L \phi_4\, \phi_6\, dx = 0$$

$$I_{i+12} = \int_0^L \phi_i\, dx \qquad i = 1, ..., 6$$

$$I_{i+18} = \int_0^L x\, \phi_i\, dx \qquad i = 1, ..., 6$$

$$I_{25} = \int_0^L \phi_1\, \phi_4\, dx$$

$$I_{26} = \int_0^L \phi_1\, \phi_5\, dx = 0$$

$$I_{27} = \int_0^L \phi_1\, \phi_6\, dx = 0$$

$$I_{28} = \int_0^L \phi_2\, \phi_4\, dx = 0$$

$$I_{29} = \int_0^L \phi_2\, \phi_5\, dx$$

$$I_{30} = \int_0^L \phi_2\, \phi_6\, dx = 0$$

$$I_{31} = \int_0^L \phi_3\, \phi_4\, dx = 0$$

$$I_{32} = \int_0^L \phi_3\, \phi_5\, dx = 0$$

$$I_{33} = \int_0^L \phi_3\, \phi_6\, dx$$

$$I_{i+33} = \int_0^L [\phi_i'']^2\, dx \qquad i = 1, ..., 6$$

$$I_{40} = \int_0^L \phi_1''\, \phi_2''\, dx = 0$$

$$I_{41} = \int_0^L \phi_2''\, \phi_3''\, dx = 0$$

$$I_{42} = \int_0^L \phi_1''\, \phi_3''\, dx = 0$$

$$I_{43} = \int_0^L \phi_4''\, \phi_5''\, dx = 0$$

$$I_{44} = \int_0^L \phi_5''\, \phi_6''\, dx = 0$$

$$I_{45} = \int_0^L \phi_4''\, \phi_6''\, dx = 0$$

$$I_{46} = \int_0^L \int_0^s [\phi_1'(x)]^2\, dx ds$$

$$I_{47} = \int_0^L \int_0^s [\phi_2'(x)]^2\, dx ds$$

$$I_{48} = \int_0^L \int_0^s [\phi_3'(x)]^2\, dx ds$$

$$I_{49} = \int_0^L \int_0^s [\phi_4'(x)]^2\, dx ds$$

$$I_{50} = \int_0^L \int_0^s [\phi_5'(x)]^2\, dx ds$$

$$I_{51} = \int_0^L \int_0^s [\phi_6'(x)]^2\, dx ds$$

$$I_{52} = \int_0^L \int_0^s \phi_1'\, \phi_2'\, dx ds$$

$$I_{53} = \int_0^L \int_0^s \phi_2'\, \phi_3'\, dx ds$$

$$I_{54} = \int_0^L \int_0^s \phi_1'\, \phi_3'\, dx ds$$

$$I_{55} = \int_0^L \int_0^s \phi_4'\, \phi_5'\, dx ds$$

$$I_{56} = \int_0^L \int_0^s \phi_5'\, \phi_6'\, dx ds$$

$$I_{57} = \int_0^L \int_0^s \phi_4'\, \phi_6'\, dx ds$$

Appendix B

Large Deflection Of A Uniformly Loaded Cantilever Beam

The classical approach to defining the deflection of a cantilever beam due to a uniform load is to use the Euler-Bernulli beam theory. This theory states that the bending moment at any point of a beam is proportional to the corresponding curvature:

$$M = EI\frac{d\theta}{ds} = EI\frac{\frac{d^2w}{dx^2}}{\left[1+\left(\frac{dw}{dx}\right)^2\right]^{\frac{3}{2}}}, \tag{B.1}$$

where:

M is the bending moment
θ is the normal slope
w is the transverse deflection
EI is the flexural rigidity of the beam.

In most applications of this equation the slope of the beam is small, so the squared term is neglected. Which leads to the classical equation

$$M = EI\frac{d^2w}{dx^2}. \tag{B.2}$$

In cases where the slope is not small some other approach must be used.

Rohde (1953) proposed an approach which starts with a curvature definition for a uniformly loaded beam.

$$\frac{1}{\rho} = \frac{d\theta}{ds} = \frac{M}{EI} \tag{B.3}$$

$$\frac{dM}{ds} = EI\frac{d^2\theta}{ds^2} \tag{B.4}$$

With the coordinate system at the free end the moment as a function of s is

$$M(s) = -ws\cos(\theta). \tag{B.5}$$

Expand θ in a power series

$$\theta = \sum_{n=0}^{\infty} a_n s^n, \quad \frac{d\theta}{ds} = \sum_{n=1}^{\infty} n a_n s^{n-1}, \quad \frac{d^2\theta}{ds^2} = \sum_{n=2}^{\infty}(n-1)n a_n s^{n-2}. \tag{B.6}$$

Applying the boundary conditions at $s = 0$ (the free end) $\theta = \alpha$, $\frac{d\theta}{ds} = 0$. Substitute into the power series, $a_0 = \alpha$, $a_1 = 0$.

$$\theta = \alpha + T, \tag{B.7}$$

where:

$$T = \sum_{n=2}^{\infty} a_n s^n.$$

Then expand $\cos(\theta)$

$$\cos(\alpha + T) = \cos(\alpha)\cos(T) - \sin(\alpha)\sin(T) \tag{B.8}$$

$$\frac{d^2\theta}{ds^2} = -\frac{ws}{EI}(\cos(\alpha)\cos(T) - \sin(\alpha)\sin(T)). \tag{B.9}$$

Expanding $\cos(T)$ and $\sin(T)$ in a Taylor's series and equating coefficients produces Table (B).

Table B.1: Large Deflection Coefficients

a_3	=	$\frac{-w\cos(\alpha)}{6EI}$
a_6	=	$\frac{wa_3\sin(\alpha)}{30EI}$
a_9	=	$w\frac{2a_6\sin(\alpha)+A_3^2\cos(\alpha)}{144EI}$
		etc.

Thus

$$\theta = \alpha + \sum_{k=1}^{\infty} a_{3k}S^{3k}. \tag{B.10}$$

Since $\frac{dy}{ds} = \sin(\theta)$,

$$y = \int_0^s \sin(\theta)ds = \int_0^s \sin(\alpha + \sum_{\infty}^{k=1} a_{3k}S^{3k})$$

$$= T_1\sin(\alpha) + T_2\cos(\alpha) \tag{B.11}$$

$$T1 = \int_0^s \cos(\sum_{\infty}^{k=1} a_{3k} S^{3k})$$

$$= s - \frac{a_3^2 s^7}{14} - \frac{a_3 a_6 s^{10}}{10} - \cdots \tag{B.12}$$

$$T2 = \int_0^s \sin(\sum_{\infty}^{k=1} a_{3k} S^{3k})$$

$$= \frac{a_3 s^4}{4} + \frac{a_6 s^7}{7} - \frac{(a_9 - \frac{a_3^3}{6}) s^1 0}{10} + \cdots \tag{B.13}$$

Similarly,

$$x = T_1 \cos(\alpha) - T_2 \sin(\alpha) \tag{B.14}$$

Rohde arbitrarily chooses α the end angle; however, if α is chosen to be the same as if an Euler-Bernoulli equation with small slope. From Popov (1976) the equation for the slope at zero is

$$\theta(0) = \frac{q_0 L_3}{6EI} \tag{B.15}$$

therefore

$$\alpha = \arctan(\frac{wl^3}{6EI}). \tag{B.16}$$

The results of these equations were found to be in excellent agreement with experimental data for the aluminum beam in question.

Vita

Robert H. Wynn, Jr was born in Cookeville, Tennessee on November 7, 1961. He grew up in Hixson, Tennessee, where he graduated from Hixson High School in 1980. He returned to Cookeville to attend Tennessee Technological University. He received a Bachelor's degree in Mechanical Engineering 1984 and Master's degree in 1986. After teaching for a year at the University of Tennessee at Chattanooga he enrolled at Virginia Polytechnic University & State University. In September 1990 he graduated with a PhD in Mechanical Engineering. Upon graduation he will accept a one year appointment as an Assistant Professor at VPI&SU. He and his wife, Carol J. Wynn, will stay in Blacksburg until she receives her PhD in Mechanical Engineering in 1991.